

**Spatial and Timing Regulation of Upper-Limb Movements in
Rhythmic Tasks**

by

Robert William Nickl

A thesis submitted to The Johns Hopkins University in conformity with the
requirements for the degree of Doctor of Philosophy of Biomedical Engineering.

Baltimore, Maryland

March, 2018

© Robert William Nickl 2018

All rights reserved

Abstract

Rhythmic movement is vital to humans and a foundation of such activities as locomotion, handwriting, and repetitive tool use. The spatiotemporal regularity characterizing such movements reflects a level of automaticity and coordination that is believed to emerge from mutually inhibitory or other pattern generating neural networks in the central nervous system. Although many studies have provided descriptions of this regularity and have illuminated the *types* of sensory information that influence rhythmic behavior, an understanding of *how* the brain uses sensory feedback to regulate rhythmic behavior on a cycle-by-cycle basis has been elusive.

This thesis utilizes the model task of paddle juggling, or vertical ball bouncing, to address how three types of feedback—visual, auditory, and haptic—contribute to spatial and temporal regulation of rhythmic upper-limb movements. We use a multi-level approach in accordance with the well-known dictum of Marr and Poggio. The crux of this thesis describes a method and suite of experiments to understand how the brain uses visual, audio, and haptic feedback to regulate spatial or timing regularity, and formulate a cycle-by-cycle description of this control: to wit, the nature

ABSTRACT

and algorithms of sensory-feedback guided regulation. Part I motivates our interest in this problem, by discussing the biological “hardware” that the nervous system putatively employs in these movements, and reviewing insights from previous studies of paddle juggling that suggest how the “hardware” may manifest itself in these behaviors.

The central experimental approach of this thesis is to train participants to perform the paddle juggling task with spatiotemporal regularity (in other words, to achieve limit-cycle behavior), and then interrogate how the brain applies regulates closed-loop performance by perturbing task feedback. In Part II, we review the development of a novel hard-real-time virtual-reality juggling simulator that enabled precise spatial and temporal feedback perturbations. We then outline the central experimental approach, in which we perturb spatial feedback of the ball at apex phase (vision), and timing feedback of collision- (audio and haptic) and apex-phase events to understand spatial and timing regulation.

Part III describes two experiments that yield the main research findings of this thesis. In Experiment 1, we use a sinusoidal-perturbation-based system identification approach to determine that spatial and timing feedback are used in two dissociable and complementary control processes: spatial error correction and temporal synchronization. In Experiment 2, a combination of sinusoidal and step perturbations is used to establish that these complementary processes obey different dynamics. Namely, spatial correction is a proportional-integral process based on a one-step memory of

ABSTRACT

feedback, while temporal synchronization is a proportional process that is dependent only on the most recent feedback.

We close in Part IV with a discussion of how insights and approaches from this thesis can lead to improved rehabilitation approaches and understanding of the physiological basis of rhythmic movement regulation.

Readers: Noah J. Cowan, Sridevi V. Sarma, Adrian M. Haith, Lawrence P. Schramm

Acknowledgments

The research in this thesis was enabled or enhanced by several people I have been privileged to know over my undergraduate and graduate life. I wish to express my deepest gratitude to the following:

- My advisor, Dr. Noah Cowan. His scientific curiosity and high standards have been an inspiration to me. I cannot quantify what I have learned under his mentorship.
- My thesis committee: Dr. Sridevi Sarma, Dr. Adrian Haith, and Dr. Lawrence Schramm. My interactions with them have played a critical role in my scientific development.
- Past and present members of the Locomotion in Mechanical and Biological Systems (LIMBS) Lab: Abhinav, Alican, Amanda, Erin, Ismail, Manu, Mert, Ned, Nicole, Radha, Ravi, Sarah, Sean, Shahin L., and Shahin S. My time as a graduate student has been enriched by my relationships and interactions with them.

ACKNOWLEDGMENTS

- Faculty and researchers throughout the Laboratory for Computational Sensing and Robotics (LCSR), many of whom have become good friends. I specifically thank Anton, Gowtham, Jon, and Simon for helpful discussions as I was programming and updating the hard-real-time juggling system. I am grateful to the many students that volunteered to take part in pilot tests.
- Previous mentors at undergraduate and graduate levels that were formative in my development as a researcher. My abilities as an engineer-scientist are the product of my educational experiences in and outside of the classroom. At the University of Pittsburgh, I benefited as an undergraduate research assistant from the tutelage of Dr. Bob Boston and Dr. Marlin Mickle. At Johns Hopkins, I had the privilege of learning under many great instructors, including Dr. Cowan, Dr. Louis Whitcomb, Dr. Marin Kobilarov, and Dr. Reza Shadmehr. Dr. Shadmehr's Learning Theory course in particular was an influence on the theoretical modeling done in this thesis. Although he was not one of my instructors, Dr. Scott Paul helped me learn to be a better teacher myself by giving me the opportunity to guest lecture in his Introduction to Rehabilitation Engineering course for the past three years.
- Dr. Amy Bastian, Dr. Pablo Celnik, and Dr. Vikram Chib, as well as their students, for allowing me to participate in their lab meetings and discussions for the past two and a half years. I am grateful to Dr. Bastian for allowing me

ACKNOWLEDGMENTS

to train to record muscle electrophysiology, and for lending me equipment to apply these techniques to my juggling system.

- The Link Foundation and National Science Foundation, which supported me via student fellowships during the first and last years of this thesis research.
- My care providers during my medical leave and re-integration into graduate school.
- Deans Peter Espenshade and Peter Maloney for helping me to transition back to the Johns Hopkins community.
- Most importantly, my immediate family—Harry, Susan, and Joseph Nickl—for their love and support.

Dedication

To my family.

Contents

| | |
|---|------------|
| Abstract | ii |
| Acknowledgments | v |
| List of Tables | xiv |
| List of Figures | xv |
| List of Acronyms | xx |
| Introduction and Organization of Thesis | 1 |
| Part I: Background | 4 |
| 1 Rhythmic Movements: Definitions and Biological Bases | 6 |
| 1.1 Biological and Health Motivation | 7 |
| 1.2 Distinctive Features | 8 |
| 1.2.1 Kinematics | 8 |
| 1.2.2 Rhythmic motions are not tilings of discrete | 9 |

CONTENTS

| | | |
|----------|--|-----------|
| 1.2.2.1 | Information-theoretic arguments | 9 |
| 1.2.2.2 | Dynamic arguments | 11 |
| 1.3 | Coordination of Rhythmic Movements | 12 |
| 1.3.1 | Theoretical dynamics | 13 |
| 1.3.2 | Biological substrates of rhythmic primitives | 15 |
| 1.4 | Modulation of Coordination Patterns | 16 |
| 1.4.1 | Sensory influences | 17 |
| 1.4.2 | Motor timekeeping | 18 |
| 1.4.2.1 | Properties | 18 |
| 1.4.2.2 | Neural substrates | 19 |
| 1.5 | Summary | 21 |
| 2 | Juggling and Rhythmicity | 23 |
| 2.1 | Scientific and Health motivation | 23 |
| 2.2 | Juggling Dynamics and Definitions | 26 |
| 2.2.1 | Hybrid dynamical ball bouncing model | 26 |
| 2.2.2 | Discrete-time state-space model of juggling | 28 |
| 2.3 | Previous Juggling Studies | 29 |
| 2.3.1 | Nonlinear dynamics of repeated impacts | 30 |
| 2.3.2 | Control hypotheses and robotic experiments | 31 |
| 2.3.2.1 | Closed-loop control | 32 |
| 2.3.2.2 | Open-loop control | 35 |

CONTENTS

| | | |
|--------------------------------------|--|-----------|
| 2.3.2.3 | Switched control | 35 |
| 2.3.3 | Human behavior | 36 |
| 2.3.3.1 | Spatiotemporal coordination | 38 |
| 2.3.3.2 | Feedback control | 39 |
| 2.4 | Summary | 43 |
| Part II: Experimental Methods | | 49 |
| 3 | Paddle Juggling Infrastructure | 50 |
| 3.1 | Motivation for Hard-Real-Time Processing | 50 |
| 3.2 | Hardware | 51 |
| 3.3 | Software | 52 |
| 3.4 | Validation | 61 |
| 3.5 | Summary | 63 |
| 4 | Experimental Approach | 71 |
| 4.1 | Perturbation-based Identification | 71 |
| 4.2 | General Experimental Structure | 74 |
| 4.2.1 | Training protocol (Session 1) | 75 |
| 4.2.2 | Perturbation design considerations | 76 |
| 4.3 | Summary | 78 |
| Part III: Experiments | | 80 |

CONTENTS

| | | |
|----------|---|------------|
| 5 | Separability of Spatial and Timing Control | 82 |
| 5.1 | Introduction | 82 |
| 5.2 | Model and Hypothesis | 83 |
| 5.3 | Experiment | 88 |
| 5.4 | Data Analysis | 90 |
| 5.5 | Results | 94 |
| 5.6 | Discussion | 98 |
| 6 | Dynamics of Spatial and Timing Control | 103 |
| 6.1 | Introduction | 103 |
| 6.2 | Experiment | 104 |
| 6.3 | Methods | 105 |
| 6.4 | Results | 112 |
| 6.5 | Discussion | 117 |
| | Part IV: Conclusions and Appendices | 125 |
| 7 | Conclusions and Future Directions | 126 |
| 7.1 | Interplay of Spatial and Timing Control | 128 |
| 7.2 | Significance and Future Work | 131 |
| 7.2.1 | Physiology | 131 |
| 7.2.2 | Rehabilitation | 133 |
| 7.3 | General conclusion | 135 |

CONTENTS

| | |
|---|------------|
| App. A: Task Dynamics and Transfer function. | 141 |
| App. B: Software Infrastructure | 146 |
| App. C: Derivation of EKF model of ball juggling | 154 |
| Bibliography | 170 |

List of Tables

| | | |
|-----|--|----|
| 2.1 | Task States and Parameters for Ball Bouncing (Paddle Juggling) . . . | 27 |
|-----|--|----|

List of Figures

| | | |
|-----|--|----|
| 1.1 | (A) Areas of the brain implicated in the control of rhythmic timekeeping and vision. Adapted from https://msu.edu/~protect/unhbox/voidb@xpenalty@M\{}brains/brains/human/sagittal/0152_mri.html | 22 |
| 2.1 | Paddle juggling in the time-domain (A) and phase-plane (B). Cycle peak numbers are labeled for cross referencing between panels. (A) Simulation using a naive proportional controller. (B) Phase plane of juggling, showing hybrid dynamics (i.e. jump discontinuity at $b = p = 0.1$ [m]). S : Poincaré section | 46 |
| 2.2 | Pilot experiment on ball and hand position stability during paddle juggling under 4 feedback conditions ($n = 1$ juggler, on apparatus described in Chapter 3). (A) Ball apex position over cycle number (left), and probabilistic distribution of states over height (right). (B) The same data, for paddle position. | 47 |
| 2.3 | Juggling setups: (A) Spatial juggler, similar to MIT Direct-Drive Serial-Link Arm (Aboaf et al. 1988) and Bueghler (Rizzi et al. 1991-1996). (B) Two-degree of freedom planar juggler (Buehler et al. 1988-1994). (C) Pendulum juggler as an example of blind juggling without spatial tracking [1] (D) Pantograph setup, used in Schaal (1993, 1996), Sternad (2001); (E) Freely moving paddle setups (i) with audio only [2], (ii) coupled with pulley or solenoid braking systems to provide haptic feedback [3]. The panels are derived from the following original source material with permission: Panel A is adapted from Fig. 1 of [4] (Copyright IEEE 1991); Panel B is reprinted from Fig. 1 in [5] (Copyright IEEE 1989); Panel C is adapted from Fig. 1 in [1] (Copyright IEEE 2011); Panel D is adapted from Fig. 4 of [6]. Panel E is adapted from Fig. 2 of [7] and Fig. 2 of [3] | 48 |

LIST OF FIGURES

3.1 Overview of experimental setup. (A) Conceptual drawing of experiments. Subject holds haptic paddle and moves handle up and down (1 dimension vertically), generally by combination of wrist, elbow, shoulder rotations. (B) Information flow between task and juggler. 64

3.2 Overview of paddle juggling software architecture, showing interfacing between ROS (Robot Operating System) and OROCOS (Open Robot Control Software). Each block is a separate subprogram (“node” or “component”). Message threads connecting each subprogram, and their directionality of data flow, are shown as arrows. Callback and data transfer rates are presented in Hertz (Hz) 65

3.3 User interface (text-based) for experiments 66

3.4 Logic flow of each experimental trial (embodied in MAIN node from Fig. 3.2. 67

3.5 Histogram of timing jitters measured during experiments. 68

3.6 Timing perturbation validation. (A) Representative perturbation conditions for one participant (S8). (B) Box plot of timing perturbation accuracies. 69

3.7 Overview of frame rate testing: (A) Bar code scanner, with circuitry facing out. When facing monitor, topology is reflected about vertical midline (axis intersecting source and ground symbols). The circuit is a current divider, with a photodiode and resistor in each branch. Bar patterns are read as on/off bits measured at the nodes V_n . (B) Example bit pattern. 70

4.1 Paddle juggling task. The bias is subtracted from both signals, so that they are centered around 0. (A) Overview of paddle juggling task. Participants bounced a virtual ball on a monitor by moving a handle (haptic paddle) up and down, and received sensory cues at different phases of each ball bouncing cycle. (B) Example task kinematics (ball and paddle heights) and hand kinematics (velocity and position) from a typical experiment. For all experiments, virtual paddle position was clamped, while virtual paddle velocity was computed from veridical hand movements. 79

5.1 Overview of Experiment 1. (A) Perturbation schema (spatial, and event timings). Block diagram represents general information flow between juggler (G) and task (H) dynamics. (B) Experimental structure. Session 1 was a training session (see Chapter 4). Sessions 2 and 3 included sinusoidal perturbations with equal numbers of spatial and timing perturbations per session. (C,D) Example perturbations of spatial (C) or timing (D) feedback. 100

LIST OF FIGURES

5.2 Time-domain responses to spatial and temporal perturbations. Data in panels A, B, and D is averaged across 5 trials for 1 juggler (mean ± 1 s.e). Perturbations in all panels are shown in dashed black lines. All frequencies are in perturbation cycles per juggling cycle. (A) Visual feedback of ball peak height relative to goal (sinusoidal perturbation, 2/40). (B) Actual ball height for perturbation stimuli of frequencies 2/40 (left) and 7/40 (right). (C) Paddle (hand) velocities for timing response. For plotting, velocity curve is partitioned around peak velocities for each cycle, rotated, and lined by increasing cycle number along the x axis to form a contour plot (D). (D) Velocity contour is ridged where haptic and audio (i.e. timing) feedback is applied. Red curves show location of maximum hand velocity relative to collision time for perturbation frequencies 2/40 (left) and 7/40 (right). 101

5.3 Experiment 1: Frequency-domain analysis of perturbation responses. (A, B) Magnitude spectra of spatial and timing responses to spatial or timing perturbations (black stems). Responses are averaged over all participants (n = 10; bars are ± 1 s.e. estimated by statistical bootstrap). (A) Magnitude spectra of visual perturbation and actual ball position. (C, D) Spectral coherence between spatial (C) and timing (D) stimuli and both ball position and paddle timing responses. . . . 102

6.1 Overview of Experiment 2. (A) Ball position (spatial feedback) or event times (timing feedback) of the paddle juggling task are perturbed with offsets varying either sinusoidally or as a step function over cycle number. Block diagram represents general information flow between juggler (G) and task (H) dynamics. (B) Experimental structure. Session 1 is as discussed in Chapter 4 (*: trials varied in number based on juggler skill, but continued until end of session). Sessions 2 and 3 consisted of equal mixes of sinusoidal and step perturbations of spatial feedback in one session, or timing feedback in the other (order counterbalanced across subjects). 120

6.2 (A, B) Model selection plots for spatially based (A) and timing based (B) controllers. Plots show tradeoff between model accuracy (y-axis) and inter-person model reliability (x-axis) for various controllers, labeled in terms of number of control model parameters (M zeros, N poles of controller transfer function). Boxed data points show the models optimally balancing accuracy (y-axis) and reliability (x-axis). 121

LIST OF FIGURES

6.3 Time- and frequency-domain behavior of spatial- and timing-based controllers. (A, B) Step responses of spatial controller (A, $n = 16$) and timing controller (B, $n = 6$). Perturbations are shown in red. Black curves are averages across jugglers ± 1 s.e. Equivalent controllers (blue) are least-squares fits based on models selected in Fig. 6.2. (C, D) Frequency-response plots of spatial and timing controllers, determined from sinusoidal perturbations. Black curves are averaged across jugglers (C, D; $n = 16$). Shaded areas represent total ranges of magnitude and phase responses. Best-fit models are shown in blue lines. 122

6.4 Distributions of parameter fits for spatial (A) and timing (B) controller models. Blue dots are bootstrap estimates of inter-juggler averages (200 resamples). Red crosses show individual juggler best fits. 123

6.5 Cross-validation of parametric models in frequency and time domains for four representative jugglers. Each row represents one individual. (A) Closed-loop models of spatial control. (B) Closed-loop model of timing compensation. All frequency-domain plots (left column) show data in black (mean; range in shaded area), and best-fit models as blue lines. All time-domain plots show data in black (mean ± 1 s.e.), best-fit model in blue, and perturbation in red. 124

7.1 Average paddle accelerations at collision times across 5 trials for each subject (using Experiment 2, $n = 16$). Data is taken between pre-perturbation and early ramping periods. Shown are 95% confidence intervals (shaded red), and mean acceleration for entire subject (solid red), with reference to the passive stability threshold of 0 ms^{-2} , negative values being necessary for passive control (A) Lowest-frequency and (B) highest-frequency perturbations. 137

7.2 Average paddle accelerations at collision times across 5 trials for each juggling participant (data from Experiment 2, $n = 16$). Data is as described in Fig. 7.1, but for timing perturbation trials under the lowest- (A) and highest-frequency (B) perturbations. 138

7.3 Relationships between timing perturbations and temporal (paddle shift) and spatial (change in ball height) behavior under both perturbation modalities studied. (A, C) Spatial perturbations. Because the ball is displayed artificially higher or lower than actuality, the following collision timing cue would be perceived earlier or later than expectation (“T perturb (effective)”). Juggler time shifts are anti-correlated to this effective perturbation (A). Time shifts, however, correlate with spatial corrections (C). (B, D) Timing perturbations. Here, collision (and apex) event cues are directly manipulated to be later or earlier than actuality. Paddle timing shifts positively correlate with perturbations as expected from Experiments 1-2 (B), but not with ball position (D). 139

LIST OF FIGURES

| | | |
|-----|--|-----|
| 7.4 | Extension of hard-real-time juggling system to allow recording of EMG signals. During experiments (right monitor), EMG signals are recorded and displayed online on a separate monitor in a software environment (<code>rosqt</code>) that can be inspected privately in (soft) real-time by the experimenter. | 140 |
|-----|--|-----|

List of Acronyms

ADL Activities of daily living

ANOVA Analysis of variance

CPG Central pattern generator

DAQ Data acquisition

DFT Discrete Fourier transform

EEG Electroencephalography

FRF Frequency response function

HKB Haken–Kelso–Bunz

I/O Input/output

IRB Institutional review board

OROCOS Open Robot Control Software

ACRONYMS

ROS Robot Operating System

SMA Supplementary motor area

SCT Synchronization-continuation task

Introduction and Organization of Thesis

Motor tasks are generally classed as discrete or rhythmic, based on the types of movements required to perform them. Rhythmic movements are characterized by their regularity in space and time, which is theorized to emerge from interactions between oscillatory networks of neurons throughout the motor system (such as central pattern generators, or CPGs), as well as from the coupling between neural and mechanical systems. The mechanisms whereby rhythmic movements are regulated are not well understood. The object of this thesis is to use a model rhythmic task—paddle juggling, or vertical ball bouncing—to study closed-loop feedback control about limit cycles.

Part I reviews the state of knowledge about the biological basis of rhythmic movements, and introduces juggling as a simple task that can yield insight into how the brain executes and regulates coordinated rhythmic movements. Chapter 1 surveys current views about how rhythmic movements are defined, and the biological sub-

INTRODUCTION AND ORGANIZATION

strates that may be involved in their assembly and modulation. Chapter 2 discusses rhythmic features of paddle juggling, including prior art of robotic and human performance studies. Research has generally proceeded along three directions: global (nonlinear) dynamics; robotics, as a testbed for hypothetically valid controllers; and human behavioral studies, to observe the actual signatures of rhythmic coordinative control in biology. Insights from these studies will be related to the contexts established in Chapter 1.

To rigorously investigate spatial and temporal control in paddle juggling, I developed a virtual reality, hard-real-time simulator and a set of perturbation experiments, which I describe in Part II. This simulator is controlled by a Stanford Haptic Paddle [8], and is an extension of previous setups used in [9] and [10]. It includes several innovations, including the flexibility to alter task dynamics, and the ability to apply precise temporal perturbations to investigate the effects of timing on rhythmic motor control along the lines of previous studies in my laboratory [11, 12] (which were in turn influenced by [13]). Chapter 3 reviews the design of this experimental apparatus. Chapter 4 outlines the basic paradigm (perturbation-based system identification) of experiments, along the lines of previous studies in my laboratory to infer closed loop control of behavior [14–18].

Part III discusses two experiments I conducted on the simulator to investigate how people rhythmically move their arms in response to perturbations of spatial cues (displayed ball peak) and timing cues (haptic and audio pulses at collisions; onset of

INTRODUCTION AND ORGANIZATION

ball flashes at apices). Chapter 5 evaluates the hypothesis that spatial and timing cues are used to inform spatial control. Ultimately, this hypothesis is falsified, in favor of an alternative hypothesis of separable spatial and timing control. Chapter 6 is a follow-up study in which the dynamics of these two processes are investigated at a cycle-by-cycle level.

In closing (Part IV, Chapter 7), I speculate on how insights and approaches from this study can be applied to understand—and possibly leverage—how the brain uses spatial and timing information in other coordination tasks.

Part I: Background

The following two chapters discuss prior knowledge of rhythmic movement. Chapter 1 begins by reviewing defining characteristics of rhythmic movements, followed by a treatment of the dynamics and hypothetical biological substrates underlying them. It concludes with a discussion of cortical areas that may influence these movements through efferent signaling. Our desire to characterize and dynamically model this cortically mediated sensory control is the impetus behind the methods and experimentation in this thesis.

Chapter 2 introduces the experimental paradigm of vertical ball juggling. We begin by discussing the rhythmic dynamics of this task. The simplicity and rhythmicity of this task have inspired a number of studies in robotics and human behavior, which will be discussed and related to concepts in the preceding chapter. Together, these chapters scientifically motivate the development of a hard-real-time paddle juggling system and perturbation experiments that are the subject of Part II.

PART I: BACKGROUND

Dissemination

Portions of Chapters 1 and 2 are abstracted from my NIH F31 proposal and a commentary I published in the Journal of Neuroscience [19].

Chapter 1

Rhythmic Movements: Definitions and Biological Bases

Biological movements encompass a range of activities from eye saccades and directed reaching, to chewing and full-body locomotion. The literature classes the former two movements as discrete, and the latter two as rhythmic (or continuous). Discrete movements are the basis of a cohesive and relatively mature body of knowledge [20]. Such detailed mechanistic knowledge lacks for rhythmic movements. This may reflect the absence of a task paradigm as insightful as reaching or saccading have been for discrete motor control, or be the result of fundamental distinctive traits of rhythmic behavior that are only now beginning to be rigorously analyzed [21].

This chapter reviews prior knowledge of rhythmic movements, beginning with a discussion of their kinematics, which reflect a degree of automaticity that seems

CHAPTER 1. RHYTHMIC MOVEMENTS

to be fundamentally different from discrete movements. We follow by discussing a prominent dynamical model of rhythmic movement, as well as biological substrates of rhythmic movement primitives, thus laying out a descriptive generative framework of how larger scale rhythmic behaviors are constituted. In closing, we discuss potential ways that cortical signaling may influence rhythmic movement: a knowledge gap that will be pursued in following chapters.

1.1 Biological and Health Motivation

Rhythmic movements are ubiquitous: canonical examples include arm and leg cycling, tapping, circle drawing, swimming, and legged locomotion (running and walking). While the focus of this thesis is limb movement—specifically of the arm—we acknowledge that the term “rhythmic” has been applied to autonomic behaviors (e.g. peristalsis, swallowing, heartbeat) and fine motor control (speech, handwriting, tremor), and that many of the concepts discussed below may be applicable to these and other behaviors vital for survival.

1.2 Distinctive Features

1.2.1 Kinematics

Discrete and rhythmic movements are distinguished by their temporal and spatial properties. Discrete movements, such as unidirectional reaches, are start-and stop (“single-shot”) and exhibit a bell-shaped velocity pattern [22]. This pattern reflects biphasic acceleration, which is a signature of distinct propulsion and braking phases (Fig. 1 in [23]). It has been explained by an optimal control model in which humans program their movement trajectories to maximize smoothness in a mean-squared-jerk sense [22]. Rhythmic movements, on the other hand, are oscillatory. Widespread examples are found in the movements of distal and proximal joints relative to the body’s midline: wrist velocities in the drawing of ellipsoids [24]; finger velocities in a back-and-forth tapping task (Fig. 2 in [23]); elbow angle in back-and-forth *repetitive* reaching [25]; and femoral angle during walking [26].

Taxonomy between rhythmic and discrete movements is defined more rigorously in a paper by Hogan and Sternad [21]. Their formulation defines the critical feature of discrete movements to be the presence of “postures”: phases of (approximate) absence of movement. The interchangeable use of the terms “rhythmic” and “continuous” reflects a lack of such poses. Hogan and Sternad further show that the minimum-jerk optimal movement without postures is indeed sinusoidal. Based on this characterization, they propose a two-fold rubric for describing movements: jerk

as a measure of optimality, and harmonicity as a measure of rhythmicity [21, 27].

1.2.2 Rhythmic motions are not tilings of discrete

In practice, Hogan and Sternad acknowledge that static “postures” are a fuzzy concept, as very few segmented discrete movements come to complete stops [21]. It is logical to ask whether rhythmic movements are simply concatenations of discrete: a question that has been considered in a study by Guiard of back-and-forth arm movements between two endpoints, which were performed discretely and rhythmically [27]. The study, perhaps unsurprisingly, found that the kinematics of discrete movements were categorically different at end points, reflecting additional motor control required for initiating and terminating movement segments. Such a notion that rhythmic movements exhibit a degree of automaticity absent from discrete has been investigated separately in a body of experiments, and is one reason why the older literature often calls them “preprogrammed” movements.

1.2.2.1 Information-theoretic arguments

In the 1950s and 60s, Paul Fitts and colleagues studied human performance on a back-and-forth tapping task between two horizontally spaced targets of varying width. While this task is essentially the same as that considered by Guiard [27], Fitts’s interest lay more directly in the upper limits of human capacity to make voluntary movements rapidly. Fitts framed this as an information processing problem,

CHAPTER 1. RHYTHMIC MOVEMENTS

defining the ratio of movement extent (distance) and precision (dispersion of endpoint location) as an “Index of Difficulty” and claiming it to be a surrogate of information channel capacity.¹ The intuition behind this analogy is that more stereotypically accurate movements (reflected by lower endpoint dispersion) reflect more efficient information processing by the motor system and hence higher capacity for making such movements.

Fitts compared point-to-point whole-arm tapping movements under two conditions— “continuous” (as fast as possible) [29] and “discrete” (with breaks) [30]— with fixed target width and distance. For both movement classes, comparable changes in target configuration led to comparable changes in task difficulty (providing a consistency check). The overall movement time for continuous movement was less than for discrete. Dividing both classes of movement into planning and execution times, however, Fitts consistently found a cognitive difference: rhythmic movements took longer to execute but seemingly required less explicit planning time. These characteristics seemed endemic to rhythmic movements, as practice did not shorten movement or planning times.

Do these regular differences in planning persist across muscle groups? Smits-Engelsman and colleagues replicated Fitts’s experiments using target configurations that effectively localized the muscles engaged to the fingers and wrist [23]. For the rhythmic task, they found that as the joints involved in movement became more

¹Channel capacity C , defined by communications theorist Claude Shannon [28], is of the form $C = f(\frac{S}{N})$, where S is the power of a “meaningful” signal, and N is the power of noise

CHAPTER 1. RHYTHMIC MOVEMENTS

proximal (as in the transition from fingers to wrist), velocity and accuracy (thus informational “capacity”) of movements was categorically improved. This finding suggests that in rhythmic movements, increasing muscle coordination (by recruiting more motor neuron pools to be involved in a task) has a unique additive effect for motor performance. Such overall improved performance with increased muscle recruitment has also been observed in the continuous tasks of handwriting and circle drawing [24].

1.2.2.2 Dynamic arguments

Continuous movements also exhibit a degree of autonomy, as revealed in perturbation studies on primates and humans. In the 1970s Brooks and colleagues conditioned monkeys to rapidly make wrist movements between two targets without visual feedback, but with audio cues [31]. Post-training, they had the monkeys perform wrist cycling, but suddenly withdrew the audio cue at random. Surprisingly, the resultant behavior depended on how many zero crossings the wrist made during each flexion–extension cycle. When one zero crossing per cycle was observed—indicating harmonicity—movements were relatively unaffected; however, when multiple zero crossings were exhibited—a symptom of more segmented, discrete movements—cue withdrawal tended to be more disruptive to wrist cycling, particularly to amplitude [32].

Feldman conducted a similar experiment on humans, training them to oscillate

CHAPTER 1. RHYTHMIC MOVEMENTS

their elbow in the horizontal plane against a spring-mass system [25]. When these harmonic movements were perturbed by the removal of this resistance, the overall rhythmicity of the movement (including amplitude) was unaffected. The influence of perturbations only manifested as a change in the midpoint of oscillation.

Others have noted unique kinematic features of rhythmic movements that seemingly arise out of their harmonicity, such as the two-thirds power law [33] and anchoring, a phenomenon in which variability over cycles is minimized at movement extrema [34]. Such studies combined with [23] suggest that rhythmic movements exhibit automaticity and self-sustainment that categorically differ from discrete movements, an idea that has been pursued in studies of coordination dynamics.

1.3 Coordination of Rhythmic Movements

A framework for understanding the organic basis of rhythmic movements is Bernstein's degrees-of-freedom problem [35]: how can spatially and temporally regular rhythmic movements emerge from the complex interactions of motor units, each with their own dynamics and constraints? Scientists in the dynamics and motor control communities have sought explanation for the "preprogrammed" nature of rhythmic movements through the concept of motor synergies and their self organization [36].

1.3.1 Theoretical dynamics

A model of how rhythmic movements are generated in the musculoskeletal system should describe how muscles (which are viscoelastic elements [37]) synergize into stable oscillatory movements of entire limbs [25, 31, 38]. Such a synergistic model should further be capable of accounting for behavioral entrainment that has been observed between separate oscillating limbs [38, 39], potentially through the nonlinear coupling of separate oscillatory circuitry [39].

The influential Haken–Kelso–Bunz (HKB) model [40, 41] is one such descriptive model. The overarching idea is that coordinative behavior can emerge from a series of coupled oscillators that are controlled by a phase variable ϕ , which is associated with a potential V that the nervous system is motivated to reduce². For example, the original presentation of this model focuses on the behavior of finger oscillation between hands [39], and illustrates how entrainment between the fingers can be reproduced by a system of nonlinearly coupled van der Pol oscillators with a potential $V(\phi)$ that penalizes deviations from mirror symmetry. Haken’s van der Pol oscillator model has been argued to be a generally valid for within-limb movements, and predicts an inverse relationship between movement amplitude and frequency that has been validated in other studies [38, 40, 42, 43]. It has even been explored as a possible framework for studying the learning of motor coordination in rhythmic skills [44, 45], including juggling [46].

²Which has stability connotations similar to the Lyapunov function in systems theory.

CHAPTER 1. RHYTHMIC MOVEMENTS

Seemingly, the HKB model has greatest validity for movements that are relatively unconstrained and do not place demands on conscious control. For instance, a study of preferred frequency in a vertical elbow swinging task showed that volunteers self-selected frequencies in a manner that was consistent with a HKB-like oscillator [43]. In contrast, studies have shown that whenever a task has an element of spatial accuracy (implied or explicit), people modulate their joint stiffness actively throughout a movement, as shown in a targeted elbow oscillation task [47]. Another experiment on a Pong-like ball-bouncing task found that wrist stiffness was likewise modulated, but over the span of multiple movements and in service of regulating locational accuracy of the ball [48].

Notably, this idea of the dynamical assembly of oscillatory primitives to generate movement—which we have thus far described in terms of upper limb movements—bears similarities to the template–anchor hypothesis of another rhythmic behavior: locomotion [49]. This hypothesis parallels our discussion, in that it supposes that a fundamental physical model (or *template*, like the oscillatory primitives described above) accounts for basic movement, and that this dynamical framework can be modified by an *anchor* model of the constraints of an animal’s body (or in our discussion, like the introduction of task-related physical or cognitive constraints).³

³Prospective control architectures that may accomplish such dynamical body–task couplings are shown in Fig. 7 of [49].

1.3.2 Biological substrates of rhythmic primitives

As discussed in the previous section, rhythmic arm movements have been commonly viewed as manifestations of oscillatory primitives. What might be the biological basis for the organization of muscles into rhythmic movement on a larger scale?

Since the early 20th century, it has been thought that rhythmic movement is largely driven by reciprocal inhibition of muscle groups, which manifests in alternating patterns of flexions and extensions [50]. A logical assumption is the involvement of central pattern generators (CPGs), oscillatory networks that are self exciting and sustaining [51]. CPGs are usually modeled as half-centers: neuronal networks that rhythmically coordinate muscle activities via alternating periods of inherent activation and external inhibition from other half-centers. CPGs are characterized by the ability to sustain rhythmic behavior in the absence of feedback (i.e. limit cycle dynamics), signs of which we have noted in human and primate arm movements [25, 31, 39]. As such, they are obvious candidates for the biological substrates of rhythmic motor control [37, 52–54].

It has been proposed that CPGs are embedded in the spinal cord [51]. A clear demonstration of CPG existence is in the lamprey, where swimming in intact specimens parallels electrical patterns (“fictive” motions) elicited in isolated spinal cords [55, 56]. Decerebrate cats also manifest fictive movements, which can be modified by cutaneous and proprioceptive input [57]. In humans, CPGs are evidenced in patients with spinal injury [58] and in newborns that “airstep” [59]—conditions where

corticospinal pathways are transected or undeveloped.

On balance, however, CPGs should be viewed with a skeptical eye. As noted by Delcomyn [60], false positive evidence of CPGs in larger animals may have resulted from an inability to truly isolate spinal cord circuitry from sensory ganglia or descending efferents from the brain. Delcomyn cites an extensive study (even by today's standards) of 28 deafferented toads, many of which after transection still showed autonomous spinal activity only "some of the time" [61].

1.4 Modulation of Coordination Patterns

Rather than arguing the existence of self-sustaining CPGs that are capable of implementing rhythmic movements on their own, it may be more fruitful to take the more general position that the spinal cord contains pools of recurrently connected neurons that are actively influenced by the periphery and cortex: even nondescript timing signals [60]. In dynamics language, rhythmic movement circuitry may be a parametric oscillator that is pumped by some feedback and modulated by others. We note that at least one juggling study has also mentioned this possibility [62], and that human motor task performance has been modeled as emergent from the dynamical interactions between human movement and task dynamics, both in an abstract sense [63] and as a specific instantiation of coupled oscillator models [49].

1.4.1 Sensory influences

Studies have shown that spinal rhythmicity is modulated by peripheral feedback [57, 58, 64] and audio signaling (although the latter may have been due to a startling effect) [65]. In Section 1.3.1, we noted that planning and intention appear to modulate rhythmic movements away from sinusoidal kinematics, in a manner that appears related to cognitive task demands [27, 47, 48]. These modifications may be due to co-contractions to regulate limb inertia or posture [25, 47].

One model of how descending efferents modulate CPG-like circuitry is the “common core hypothesis”: that the cortex and brainstem modulate CPG-like circuits in the human upper and lower limbs [66, 67] (see [68] for an earlier version of this concept). Recent findings that cyclical arm movements can modulate lower spinal excitability purport to be evidence of such a core timing mechanism [69–71]. Such a model of bi-directional spinal and cortical interactions may be a suitable context for understanding how sensory feedback controls rhythmic movements. For example, arm coordination may be driven by CPG-like circuitry that can be modified and reset cortically by visual, audio, or haptic feedback [66], or alternatively by frontal signalling related to executive planning.

1.4.2 Motor timekeeping

Consider that timing is vital to rhythmicity, and that animals have a remarkable ability to keep time both with and without cues. Whether for dancing, making music in a group, playing sports, or communicating with another, animals (especially humans) often seamlessly detect environmental cues, cognitively analyze them, and coordinate outward behavior to their temporal structure with great precision.

Motor (or mental) timekeeping is believed to underlie the ability for humans (and some animals) to synchronize motor activities to external cues (such as tapping a surface in time to a light or sound signal) [76], as well as the ability to maintain such periodicity even after these external cues are extinguished (in a synchronization–continuation task, or SCT) [77].

1.4.2.1 Properties

Computationally, mental timekeeping may be analogous to running a stopwatch. It likely involves enumerating events (such as neural spikes), in a manner that can be started, stopped, or reset with respect to a criterion or reference value stored in memory [72]. It has been suggested that such a timer can be implemented by neuronal accumulators operating as a thresholded drift-diffusion process [12, 74, 75]. Accumulator neurons, prevalent in the decision-making literature [73] are intuitively appealing as a candidate mechanism, as they allow us to interpret action initiation as a decision process predicated on the passage of time relative to an event.

CHAPTER 1. RHYTHMIC MOVEMENTS

Given that some tasks (such as juggling) are themselves rhythmic, an interesting possibility is that feedback influences human rhythmic movements by helping motor timekeeping circuitry to establish its own clock on which to act.

1.4.2.2 Neural substrates

Timekeeping in the brain is diverse and widespread, and a number of brain structures have been implicated in timekeeping, depending on context (Figure 1.1). An imaging study from an SCT task shows that sensory and motor cortices are constantly engaged in both metronome synchronization and rhythm continuation phases (after the metronome is turned off), with additional recruitment of the supplementary motor area (SMA), cerebellum, and midbrain during continuation [78].

The SMA may be a key nexus between motor planning and execution stages [77]. An imaging study of rhythmic hand movement shows increased activity in this area, which is known to be involved in movement sequencing [87]. Merchant and colleagues provide multiunit evidence from monkeys [88] that SMA and pre-SMA may be the site of neural accumulator circuitry that strongly correlates with behavioral timing. As the monkeys tapped to an external cue, a subpopulation of neurons was observed that rate coded the time elapsed since a tapping cue and apparently maintained activity even when this cue was extinguished. Another group of neurons, which was tuned to the duration of inter-stimulus intervals, also predicted errors in tapping behavior, and whether these errors were anticipative or late.

CHAPTER 1. RHYTHMIC MOVEMENTS

The cerebellum and basal ganglia are believed to be critical to proper action timing, largely through patient and virtual lesion studies showing timing impairment [79,80]. The importance of the cerebellum is especially clear: cerebellar patients show accuracy deficits when making rhythmic arm circling movements that are punctuated by discrete events [81], and the cooling of dentate cerebellum in monkeys has been shown to impair rhythmic wrist movement [82].

In the basal ganglia, the striatum, which is associated with action selection, may communicate dopaminergically with the prefrontal cortex to generate a relevant timing threshold in working memory, as in the Striatal Beat Frequency model [84]. Duration-tuned neurons have likewise recently been found in the frontal areas [85,86]. It is possible that the basal ganglia are a relay between decision making (threshold setting for accumulator neurons) in the frontal cortex and the gating of motor activity in the SMA [83].

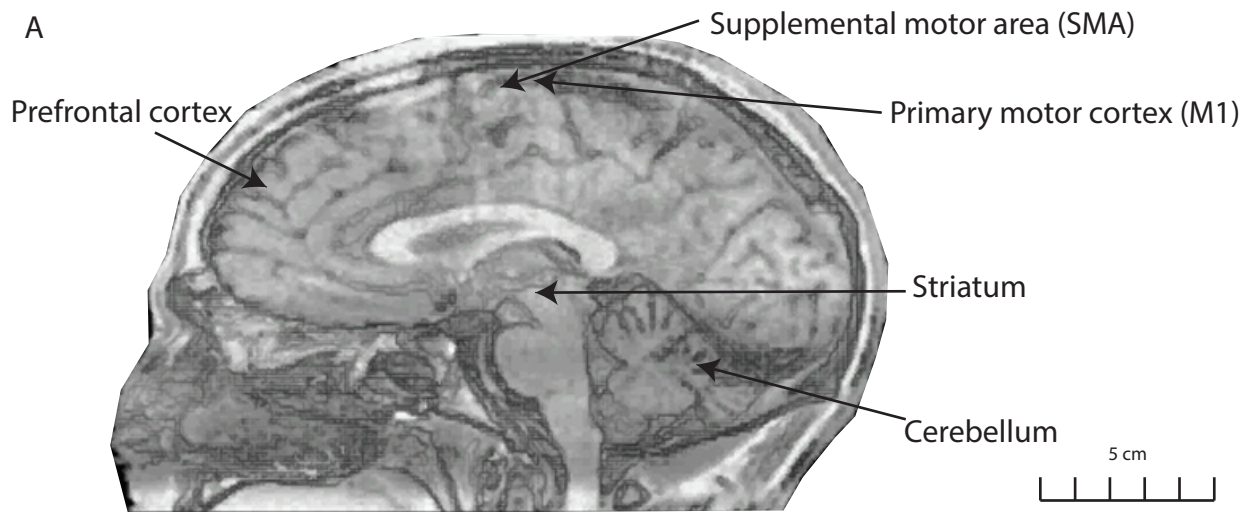
While timekeeping networks in the brain are still not functionally well understood, a variety of affiliated regions implicated in executive planning and sensory processing evidently converge in the movement planning area of SMA, which has been shown to have a direct connection to the spinal cord and thus may exert a direct influence on CPG-like networks [89].

1.5 Summary

In this chapter we outlined the biological significance of rhythmic movements, and highlighted distinctions from discrete movements (such as point-to-point reaching). Among these is that rhythmic movements exhibit more spatiotemporal regularity, while requiring less direct planning. Rather, they are characterized by automaticity that can be modulated by external goals, an emergent property of the interplay between dynamics implicit in the body and an external task or mechanical system.

While the implementation of rhythmic movements is fairly well understood at the hardware layer, our knowledge of how sensory feedback is used to control them is sparser. This goal of the experiments within this thesis is to enlighten our understanding of what (and how) feedback modalities influence movement control about average rhythmic behavioral patterns (or limit cycles). In studying the closed-loop dynamics of this control, we hope to contribute to the identification and algorithmic description of rhythmic motor control per the holistic approach to understanding neuroscience advocated by Marr and Poggio [90]. Chapter 2 follows with a presentation of our motor task of interest: paddle juggling.

CHAPTER 1. RHYTHMIC MOVEMENTS



Adapted from https://msu.edu/~brains/brains/human/sagittal/0152_mri.html

Figure 1.1: (A) Areas of the brain implicated in the control of rhythmic timekeeping and vision. Adapted from https://msu.edu/~brains/brains/human/sagittal/0152_mri.html.

Chapter 2

Juggling and Rhythmicity

We begin by discussing our motivations for studying juggling, and proceed to define by way of a state-space model the specific type of juggling that will be the object of further research in Parts II and III: vertical–high-bounce–paddle juggling.

Following exposition of the juggling dynamics, we outline previous juggling research. Where appropriate, we relate some of the related findings to our knowledge of rhythmic behavior in humans (Chapter 1).

2.1 Scientific and Health motivation

As discussed in Chapter 1, the manner in which the body solves Bernstein’s coordination problem—to organize disparate spinal and brain circuitry with many individual degrees of freedom into rhythmic movements with spatial and temporal regularity—

CHAPTER 2. JUGGLING AND RHYTHMICITY

is a matter of debate. Research from coordination dynamics and spinal physiology seems to suggest a degree of self-organization of CPG-like circuitry. However there is also evidence that the brain actively controls this rhythmicity to meet dynamic and cognitive demands and affordances dictated by a task at hand. This view—that motor behavior is fundamentally intertwined with task dynamics inferred by feedback—is often called the action-perception, or ecological, view of motor behavior [63, 91, 92]. An understanding of both the biological and ecological aspects of behavior is vital if we are to understand health and disease in motor control, or to create therapies to improve movement pathologies.

Continuous behaviors are pervasive throughout biology, including such life-essential acts as locomotion, mastication, and communication (written and verbal). How the brain uses sensory feedback to regulate such rhythmic behaviors is poorly understood. Transformative progress can be made by identifying a simpler quintessential task, similar to how reaching and saccading have elucidated the brain’s control of discrete movements [20].

Juggling embodies several dynamic features that will be explained in the next section by way of introducing a mathematical model. It is a hybrid-dynamical task [93] and is arguably the simplest non-trivial example of one [94]. This feature is significant to biology and health because a number of locomotor behaviors (walking, running) share this nature.

The implications of juggling behavior on walking are enticing [6, 95, 96], considered

CHAPTER 2. JUGGLING AND RHYTHMICITY

by such notable scientific figures as Claude Shannon,¹ himself a juggling hobbyist, and Marc Raibert, a father of legged robotics [95]. It would be overly reductionistic to claim that juggling directly leads to walking insight—walking possibly has at least 100 times as many degrees of freedom [97]—but it could help shed light into how therapists can better coordinate subcomponents of walking that have direct benefit to activities of daily living (ADL) or long-term health. For example, many motor disorders manifest themselves as disorders of managing collision timing between the foot and the floor (such as foot drop in ataxia, or shuffling in Parkinson’s disease or ataxia).

The hybrid dynamics of juggling render it interesting in other less directly health-related aspects. The first is that juggling is an intermittently controlled arm task (also noted by [96]): it requires the user to act within a specific time window (in this case, to loft a ball), and also to allow enough time to reset the states of the arm between consecutive ball contact phases (a “refractory period”). The second is that certain juggling actions can result in dribbling regimes that can make control difficult (e.g. Zeno behavior, described in Section 2.3.1 [93]), making for a possibly interesting paradigm for studying recovery of stability after fumbling [96] or tripping.

¹See reference in Chapter 1 to Shannon’s role in communications theory and Fitts’s analytical approach

2.2 Juggling Dynamics and Definitions

Juggling evokes images of tossing numerous objects (balls, rings, clubs) to achieve a specific spatial pattern, whether in a figure eight shape spanning both hands (“cascade juggling”), or linear up-and-down paths (“vertical juggling”) within a single hand. Jugglers not only obey spatial constraints to achieve these patterns, but temporal constraints that govern when to catch and release each ball, embodied in a juggling theorem attributed to Claude Shannon.² [98,99]

Juggling thus implies the properties of spatial and temporal regularity characteristic of rhythmic movement. Mathematically it is a *repeated impacts process* [100,101] that has been used as a model task in robotics and human motor control to study behaviors involving intermittent interactions with dynamic objects [96].

2.2.1 Hybrid dynamical ball bouncing model

Essentially juggling is bouncing a ball off a surface in a prescribed spatial trajectory. Our specific task of interest is the one-ball-vertical-paddle juggle, which entails ricocheting the ball in the up-down dimension off a rigid surface with high elasticity, such that collisions are effectively instantaneous. With the notation in Table 2.1, we can construct the following dynamic model for the position of the ball during a cycle

²Shannon’s (juggling) theorem describes a constraint for how the durations that a ball is airborne (“flight time”), that the ball occupies a hand (“dwell time”), and that a hand is empty (“vacancy”) must be allocated during a juggling cycle: (flight time + dwell time) \times (# hands) = (vacancy + dwell time) \times (# balls). Claude Shannon was mentioned in Chapter 1 in his indirectly related capacity as a founder of information theory

CHAPTER 2. JUGGLING AND RHYTHMICITY

n (Eqn. 2.1).

| Symbol | Definition | Units |
|------------------------------|--|---------------------|
| $p(t)$ | Paddle position as function of time | [m] |
| $p[n]$ | Paddle position (at collision of cycle n) | [m] |
| $b(t)$ | Ball position as function of time | [m] |
| $b[n]$ | Ball apex position (at apex of cycle n) | [m] |
| $\dot{b}_n^-, \dot{b}^- [n]$ | Ball collision velocity | [ms ⁻¹] |
| $\dot{b}_n^+, \dot{b}^+ [n]$ | Ball launch velocity | [ms ⁻¹] |
| $t_{a,n}$ | Ball ascent time | [s] |
| $t_{d,n}$ | Ball descent time | [s] |
| $t_{b[n]}$ | Time of n^{th} ball collision | [s] |
| \dot{p}_n | Paddle velocity at collision n | [ms ⁻¹] |
| g | Acceleration | [ms ⁻²] |
| α | Coefficient of restitution | [] |
| g | Gravitational acceleration (= -9.81) | [ms ⁻²] |

Table 2.1: Task States and Parameters for Ball Bouncing (Paddle Juggling)

$$\dot{b}(t) = \begin{cases} \dot{b}_n^+ + g(t - t_{b[n]}), & b(t) > p(t) & \text{Flight} \\ \alpha \dot{b}_n^- + (1 + \alpha)\dot{p}_{n+1}, & b = p & \text{Collision} \end{cases} \quad (2.1)$$

The hybrid dynamics of juggling comprise a Flight regime with continuous dynamics (in terms of time in seconds), and a Collision regime with discrete dynamics (in terms of time in cycle number). The dynamic regime—hence the influence of the human on the ball’s movement—is determined by the relative distance between the ball and the paddle, termed a threshold function or a guard. Figure 2.1 shows these concepts by way of a phase-plane representation.

The Collision dynamics are also called a collision map (or *reset map*). This map describes how the impending ball velocity on cycle n *jumps* to a ball launch velocity

CHAPTER 2. JUGGLING AND RHYTHMICITY

on cycle $n + 1$ via the coefficient-of-restitution (α) and velocity of the paddle (forcing function $\dot{p}_n = \dot{p}[n]$). The parameter α is akin to the “elasticity” of the ball and maps (isomorphically) to the kinetic energy lost in the collision (see Appendix A).

Aside from being hybrid dynamical, paddle juggling is rhythmic, as can be proved by showing the existence of a set of (nominal) states that define a limit cycle in terms a spatial goal height, h (see Appendix A). As we noted in our discussion of rhythmic arm and wrist cycling in Sections 1.2 and 1.3, such limit cycle behavior is a key signature of rhythmic arm and wrist movement in humans and primates.

2.2.2 Discrete-time state-space model of juggling

As mentioned in Appendix A, we can analyze juggling rhythms by studying the evolution of states cycle-by-cycle at a particular phase (Poincaré section) of the dynamics. Selecting this phase to be the ball apex instant of each cycle (defined by the surface S in Fig. 2.1) we can express the paddle juggling physics in discrete-time state-space form:

$$\begin{aligned} b[n + 1] &= p[n] + \dot{b}^+[n]t_a[n] + \frac{1}{2}gt_a^2[n] && \text{(Ball ascent)} \\ p[n] &= b[n] + \frac{1}{2}gt_a^2[n] && \text{(Ball descent)} \\ \dot{b}^+[n + 1] &= -\alpha\dot{b}^-[n] + (1 + \alpha)\dot{p}[n] && \text{(Collision)} \end{aligned} \tag{2.2}$$

We adopt the common convention that the paddle–arm inertia far exceeds that of

ball, such that paddle velocity does not change at the moment of collision ($p^+[n+1] = p[n]$ and $\dot{p}^+[n+1] = \dot{p}^-[n]$). We also assume that the vertical positions where ball-paddle collisions occur is approximately invariant, which is observed in skilled juggling behavior [98]. This “high bounce” assumption, which is mathematically equivalent to stating that the positions of the juggling surface are locked, has been the foundation of most analytical studies of bouncing control ([6, 102–104] are but a few examples).

We observe that this simple model can be extended to more general juggling settings. For example, inelastic collisions with non-infinitesimal dwell times that are more representative of juggling with the hands can be accommodated by adding an additional ball-in-hand dynamic regime covering the dwell time, and replacing the single collision map with two threshold functions governing flight-to-dwell and dwell-to-flight transitions. The general m ball juggling case can be accommodated by adding additional spatial degrees of freedom for each ball; however the analysis quickly becomes cumbersome and has been a barrier to dynamic modeling [105, 106].

2.3 Previous Juggling Studies

As apparent from the previous section and Appendix A, rhythmic juggling performance relies crucially on the control of paddle movement at collision instants, subject to dynamics specified by gravity and ball-paddle elasticity. Juggling and more generally ball bouncing have drawn research interest in three primary domains: (1)

theoretical dynamics, to understand global behavior (i.e. not restricted to limit-cycle neighborhoods); (2) robotics, to develop hypothetical control policies for sustained ball bouncing; (3) human behavior, to describe natural movements.

2.3.1 Nonlinear dynamics of repeated impacts

Juggling, as a repeated impacts process, has often been cited as an example of rich dynamics that can arise in even simple nonlinear hybrid systems [93, 107, 108].

One of the earliest bodies of dynamical research on repeated impacts processes was driven by the desire to understand and model the behavior of vibrating contacts in industrial settings, such as loose joints [101] or objects riding conveyor belts [100]. Studies focused on dynamics under specific forcing functions (of which paddle velocity $\dot{p}[n]$ in our model is an example). Veitz considered 2-dimensional forcing under horizontal and vertical sinusoidal excitations (of equal frequency), while Wood considered approximately Gaussian excitations [101].

Early on, it was acknowledged that solutions to these stochastic problems could only be characterized probabilistically, and only guaranteed under specific relationships between excitation variables (amplitude, frequency) and parameters (gravity and α). Researchers observed that unpredictable or non-periodic ball trajectories would appear under certain elasticity conditions (specifically increase of vertical excitation frequency ω relative to gravity) [100, 102]. This is a signature of chaotic

behavior, the existence of which was formally proved by Holmes [102].³

Another property of juggling that has been of theoretical interest is the existence of Zeno behavior, characterized by the occurrence of a boundless number of discrete transitions in a given time [93, 109]. In juggling, this corresponds to the state where the ball comes to rest on the paddle (the so-called “sticking solution” [6]).

2.3.2 Control hypotheses and robotic experiments

Robotic jugglers emerged in the mid-to-late 1980s as a result of an interest in intermittent control. Roboticians were partly motivated by an interest in extending robotic manipulation beyond the traditional continuous-contact setting. The relative analytical tractability of [local] juggling dynamics was expedient to the design and implementation of such controllers.

The control of juggling from both the robotics and human motor control perspectives has focused (with various degrees of explicitness) on the timing and velocity of paddle movement at collisions. These studies have addressed juggling from the standpoint of feasibility: (1) what sensory feedback is [theoretically] sufficient to initiate a rhythmic pattern and (2) how long can this behavior be sustained?

³Holmes does this by proving the existence of a dynamical flow in the shape of a “Smale horse-shoe”, a sufficient condition for chaos.

2.3.2.1 Closed-loop control

Due perhaps in part to the complexity of global juggling dynamics, control problems have traditionally focused on local analysis about a set of nominal states (the existence of which we showed in Appendix A). The majority of studies have been in parameter regimes where chaos is not a major issue.

Early robot designs assumed that vision was necessary and sufficient for juggling. Atkeson and colleagues considered spatial (3-dimensional) juggling to study whether multipurpose robots could be taught to perform complex tasks with only high-level control policies that did not explicitly account for task dynamics. Initial attempts focused on hitting a ball to a target height using a policy that simply compensated for the most recent error, reasoning that this was a self-evident way that humans would correct their behaviors online.⁴ Their testbed was a three-degree-of-freedom arm equipped with a square plywood paddle (similar but not identical to Fig. 2.3A). This simple policy had limited success, unable to sustain juggling for more than a few bounces on average and tending to fail because the ball’s landing position was laterally unstable [110]. Failures were attributed to limitations in the accuracy of modeling the robot’s dynamics in order to determine control output. Arguably, although the guiding approach may have been rooted in intuition about behavior, the absence of a task-related internal model is essentially juggling without a cerebellum [111].

Attempting to make their policy more adaptive, Atkeson and colleagues next

⁴The gain of this policy was dependent on the desired theoretical convergence properties of the robot’s closed-loop transfer function as determined by pole placement.

CHAPTER 2. JUGGLING AND RHYTHMICITY

incorporated a generalization layer; the robot was taught to adjust where on the paddle to hit the ball based on a “knowledge” of which sections of the paddle were likelier to sustain ball movement [110]. This involved rigorously priming the robot by having a (human) teacher repeatedly drop the ball on the paddle so that a lookup table could be programmed. Ultimately, this proved to be an unnatural and inefficient juggling method: generalization functions for one ball landing were not applicable for other landings, and the robot tended to drop the ball within 30 cycles [112], unable to surpass novice skill [113].

Later studies used more ecological approaches incorporating greater knowledge of task physics. Koditschek and colleagues had greater success by introducing task models, beginning with the more analytically tractable case of planar juggling (Fig. 2.3B). In so doing, they considered the design problem as one of determining the appropriate schedule of actions: hitting the ball at a desired velocity given a collision time. That is, akin to coordination dynamicists, they conceived of the robotic controller as implementing a “motor program” [5, 114].

In early experiments with the planar (2-dimensional) juggler, Buehler and colleagues attributed shortcomings in accuracy and robustness to limitations in the ability of hardware to sense the timing of collisions. Buehler proposed a provably stable controller that entailed programming the angle of the paddle to track the angle of the ball trajectory in a proportional-derivative manner. Called the Mirror Algorithm for this reason, it eliminated the need to measure timing directly by shifting responsibility

CHAPTER 2. JUGGLING AND RHYTHMICITY

to the subtasks of continuously tracking ball position and estimating the ball’s energy at all times [105]. The Mirror Algorithm was undeniably successful, able to sustain juggling for several minutes. Subsequent work by Rizzi extended the mirror law to the spatial case [4, 106].⁵ Additional improvements, which included augmenting the tracking algorithm to include a predictive (Kalman filtering) stage that accounted for ball shape, enabled juggling to persist for well over 1 hour. Two-ball juggling was demonstrated, provided that collisions for each ball were separated far enough in time [105, 106, 115]. In what was presented as an incidental detail, Rizzi embedded a microphone into the paddle as an impact detector [116] to assist in resetting states for visual servoing. We note that the two-ball spatial juggling problem under purely visual control (and visual detection of collisions) has also been approached using non-linear optimal control approaches [117], but has not achieved the longevity of Rizzi’s design and seemingly experiences the same lateral instability issues as early spatial jugglers without explicit task models [110].

Closed-loop blind control

Only recently has the ability to juggle without visual feedback been investigated in robots that juggle “blindly”, such as the pendulum juggler of Figure 2.3C). Designs have achieved stable juggling by sinusoidally moving the “paddle” continuously, subject to phase shifts based on the detected impacts of the ball (typically using mi-

⁵The robot is called the Yale Spatial Juggler or the Buehler, named after Buehler. The configuration is similar to Fig. 2.3A

CHAPTER 2. JUGGLING AND RHYTHMICITY

crophones as sensors) [1, 118]. This approach is analogous to basing control on touch or proprioception.

2.3.2.2 Open-loop control

While closed-loop juggling has been remarkably successful, the most successful robots have placed significant burden on vision-based control and estimation. Inspired by work in passively stable walkers [119], a set of open-loop frameworks have been proposed, whereby stability could be imposed by virtue of robot-task dynamics rather than active control [115]. On one hand, this is appealing because it relies less on continuous feedback regulation. On the other hand, this is limited to task-actor couplings that have guaranteed stability (for example, through the existence of a Lyapunov function [94] or by engineering the robot’s contact surface [115, 118, 120]).

2.3.2.3 Switched control

By virtue of juggling’s chaotic dynamics, a third, intermediate control strategy is possible: that of intermittently applying active control. Chaotic control implies that a juggler should bounce the ball passively, and then “ride” the chaotic dynamics until the ball reaches a point in phase space that is close to a limit cycle. The juggler should then actively control the ball if it will result in a ball state that is within the region of attraction to a limit cycle, where the ball can again be juggled passively [121]. This approach requires a detailed model of the task’s global dynamics, but has been

a recent area of interest in robotic juggling, particularly in the vertical high bounce case [122, 123].

2.3.3 Human behavior

In the previous section, we reviewed the prior art of juggling control in the context of robotics. While the most successful robots have implicitly assumed that vision is a necessary requirement for juggling, we have also seen the success of blind jugglers that rely on collision detection only in a primitive form of touch feedback. Although knowledge of rhythmic behavior and robotics is informative from theoretical perspectives, the approaches the human brain uses for juggling (and thus rhythmic movement) regulation must ultimately be assessed by controlled human experiments [124].

Human Paddle Kinematics and Control Variables

Studies of human vertical juggling have been conducted on platforms ranging from one-degree of freedom robots such as the pantograph in (Fig. 2.3D), to setups that more thoroughly emulate paddle juggling with freely moving physical paddles (Fig. 2.3E).

Hand-paddle movement shows spatiotemporal regularity and is quasi-sinusoidal, as typical for rhythmic tasks (see e.g. [2, 3, 94]). Specifically, many studies have shown a systematic anti-correlation between hand (paddle) amplitude and task frequency, varied either by manipulating target height or gravitational acceleration [6, 94, 125],

CHAPTER 2. JUGGLING AND RHYTHMICITY

despite the fact that the peak-to-peak amplitude of the paddle is not directly task relevant [125]. Such findings are in agreement with predictions of the HKB model [38], supporting a theory of rhythmic arm movement as being driven by neuronal oscillators that are CPG-like.

Similar neural oscillatory behavior apparently manifests in the more general case of spatial cascade juggling. Beek and Beek illustrate how the phase portrait of a skilled juggler's hand can be decomposed into dynamic phases that correspond to viscoelastic oscillators (of van der Pol type) predicted by HKB theory [46].

A departure from HKB predictions

Although amplitude generally varies with cycle period, a handful of studies show that it also varies in an inverse manner with coefficient of restitution α [7, 126]. Because ball-paddle elasticity would not impact ball cycle period, all other variables remaining equal, this behavior is not directly predicted from HKB theory. This departure could potentially be explained within the framework of descending modulation of rhythmic behaviors (see Chapter 1): decreasing elasticity (by lowering α) causes greater energy dissipation from collisions, which may require active control to compensate.

2.3.3.1 Spatiotemporal coordination

Given that arm movement in juggling across platforms and settings is consistent with a neural oscillator of the HKB type, it is reasonable to ask how else rhythmic coordination manifests in paddle and other juggling behaviors.

Evidence for emergent coordination patterns has traditionally been sought by recording time series data throughout the body (including axial postural, head orientation, and respiratory variables [127]), and analyzing them in the frequency domain for signs of nonlinear (subharmonic) coupling [39].

There seems to be clear evidence that jugglers control their behavior based on information flow from ball arcs. In spatial juggling, it has been argued that the spatial trajectories of ball movement are a central reference to which jugglers appear to pace their movements [128].⁶ Juggling studies have also considered timing, albeit at a coarse level (averages over several cycles). Shannon’s juggling theorem [98,99] has provided a guidepost for looking at phase relationships between balls (or hands) [113]. However, to the extent that timing has been evaluated, these studies have considered the average scheduling of relative ball flight–dwell timing (i.e. the process of “tiling” of movement phases to satisfy Shannon’s theorem) rather than on closed-loop processes for cycle-to-cycle timing regulation [62].

Juggling skill is typically measured by the number of consecutive balls that can be sustained without losing rhythmicity, whether the object of study be a robot or a

⁶The use of “clock” in the title is used figuratively to refer to a pacemaker, rather than as a literal timekeeper [72]

CHAPTER 2. JUGGLING AND RHYTHMICITY

human [105,110,129]. In humans, juggling skill seems to develop with a progression in coordination, beginning with learning to phase lock to the ball, followed by reducing variability in task-relevant parameters such as ball-hand location and timing [129] or hand acceleration at impacts [2,3]. This in turn could reflect a process wherein skilled jugglers reorganize their arm and spinal coordination patterns to optimize performance [44,45,130]. Long-term studies of learning suggest that this reorganization comes from an increasing recruitment of central muscle groups involved in posture [127,131].

2.3.3.2 Feedback control

Multiple senses are qualitatively implicated in juggling, but their functional roles in accomplishing limit cycle behavior and sustaining it remain open questions. A major weakness in the above studies of overall coordination is that they describe steady-state nominal behavioral tendencies, but not in a manner that describes closed-loop control in a detailed fashion.

Like their robotic counterparts, human jugglers have traditionally been presumed to depend crucially on visual information. The main evidence that ball juggling is primarily spatially guided arises from correlations in paddle juggling between ball height and paddle kinematics [7,132]. A second line of evidence has been from simulations. Ronsse and colleagues showed that a juggling model relying only on visual observations to estimate ball descent time, and then optimizing paddle movement

CHAPTER 2. JUGGLING AND RHYTHMICITY

energy and ball accuracy within this finite horizon, qualitatively produced paddle movements that matched human behavior under various changes in juggling dynamics (here, ball gravity) [104]. A more recent study suggests that an oscillator system driven by spatial control is sufficient to replicate human behavior [133].

While vision is sufficient for juggling, the plurality of human evidence suggests it is not necessary—or at least employed in object tracking as assumed by robotic and many analyses of human behavior. Although [132] claims that juggling is almost entirely visually controlled, this conclusion was drawn from correlation analysis with much unexplained variability (i.e. low r^2 values). That vision is much less vital than [132] implies is supported by the common observation that many jugglers can perform with their eyes closed [98]. Even jugglers that cannot juggle blindly do not appear to require much spatial information, with estimates in controlled studies ranging from a flash at the ball peak [134], to a 80-200 ms interval per cycle [135]. The latter study suggests that jugglers also appear to be fairly insensitive to the exact phase when visual feedback occurs. Despite claims that jugglers use descending ball movement to gauge time to contact [132], [135] found that jugglers do not exhibit a strong preference about whether visual feedback is provided during ascending or descending phases—only that it is near the apex. Other studies find that skilled jugglers often gaze at distant space [113], and that visual tracking is reduced as a person becomes a more experienced juggler [136]

The use of alternative feedback sources has been an interesting and relatively

CHAPTER 2. JUGGLING AND RHYTHMICITY

unexplored avenue in juggling studies. While haptic [3, 126] and audio feedback [2] has been part of virtual paddle juggling systems for years, their main avowed purpose seems to be to improve realism [126]. The functional roles of touch and sound have been relatively unexplored; but the limited evidence suggests that their importance to date has been underestimated, particularly in light of biological evidence of their impact on rhythmic movement (see Chapter 1).

An interesting study by Sternad and colleagues showed that juggling in the presence of haptic feedback only (with eyes shut) did not materially differ from juggling in the presence of vision only [6]. This result is qualitatively supported by data collected on the juggling apparatus described in Chapter 3 (Fig. 2.2). Ankarali and colleagues found that haptic feedback may even have an augmentative effect on visually-controlled juggling performance by increasing jugglers' streakiness within a goal range (i.e. increasing metastability) [10].

The active control debate

As noted in our discussion of robotics, passive control strategies that involve open loop control are instinctively appealing because they seemingly assure stability without feedback correction. The earliest paddle juggling studies used passive stabilization as a null hypothesis for human control. Work by Schaal and Sternad [6, 94] on pantograph jugglers (Fig. 2.3) concluded that humans obeyed this strategy because they satisfied a key prediction: their average paddle accelerations at impact were negative.

CHAPTER 2. JUGGLING AND RHYTHMICITY

However, this is not to say that humans exclusively used passive stability, as the acceleration confidence intervals in these studies clearly include positive values (in some cases as many as 20% [6]). Nor do these studies argue convincingly that jugglers seek or converge to passively stable solutions.

The evidence for passive stabilization as a guiding motor control principle is not altogether compelling. First, learning to be passively stable would likely involve not only extremely detailed internal modeling of nonlinear global juggling dynamics (see Section 2.3.1), but also some reinforcement learning process [117]. It is difficult to conceive how both steps could be accomplished in the approximately 5 minute period that subjects were reported to be able to learn to paddle juggle [10, 94]. Indeed, attempts to teach subjects to exploit passive stability using reinforcement learning methods have been mixed at best [137]. Secondly, it is entirely possible that the observed signatures of passive stability (slightly negative paddle accelerations at collisions) are a coincidence of swinging the paddle upward during collisions, combined with natural variability between jugglers. This is supported by two lines of evidence. First, Katsumata et al. showed that as paddle-ball collisions became more inelastic (α was decreased), jugglers adopted positive paddle accelerations at collisions [138], violating passive stability [94]. In addition, Wei et al. suggest via a factorial analysis—and Ankarali et al. through time-series stability analysis—that human paddle accelerations vary largely by juggling cycle and by individual, with multiple people averaging

passively *unstable* solutions [10, 126].⁷

An alternative to passive stabilization is the notion that humans constantly regulate their arm movements using active corrections about the passive stable regime [7, 132]. This idea has strong flavors of the “switched control” paradigm discussed earlier in the context of control in chaotic dynamics, which suggests that a flexible juggler should still tactically use active correction. This is evidenced in perturbation studies, which showed both that (1) subjects make excursions to the active control regime during compensation, and that (2) convergence back to limit cycle behavior was faster than predicted from passive dynamics alone [3, 126]. This reliance on active control has been shown in perturbations to coefficient of restitution [126] and in the phase coupling between jugglers and task feedback through artificially induced hardware delays [2].

2.4 Summary

We have reviewed how juggling is a simple yet sufficiently dynamically rich model system for studying rhythmic behavior. In our review of robotics and human behavioral studies, we discussed how researchers from both communities have prevalently assumed that vision is a necessary component. While simple and intuitively appeal-

⁷It has also been argued that negative accelerations may simply be an artifact of non-causal filtering during post analysis, as collision points are near regions where paddle haptic feedback would impose a strongly negative acceleration that can bleed into earlier values [10]. While this may be a concern in later studies (e.g. [126]), this was presumably not an issue in original studies of Schaal and Sternad, as they used causal Butterworth filtering [6, 94]

CHAPTER 2. JUGGLING AND RHYTHMICITY

ing, this gives us an incomplete understanding. Rather than solving explicitly for the timing of motor actions, robots have relied on elaborate visual computations which are brittle and computationally intensive. We can fairly definitively say humans can regulate juggling with minimal visual information [6, 134, 136].

A gap is the role of timing information. Both the robotics community [96, 139] and movement researchers alike [125] have considered the goal of executing juggling to be the establishment of a motor program: a schedule of actions at a sequence of specific times. Essentially, this describes an intermittent controller that applies paddle velocities \dot{p}_n at times t_n . Researchers across robotic and human motor disciplines have tended to ignore the direct problem of estimating timing, and instead assume that vision is dominant. Yet timing appears essential: it is interesting that the most successful robotic designs have incorporated collision detection (microphones) [116, 122], while many other designs show that vision is unnecessary. In human behavior, timing—as embodied in Shannon’s juggling theorem—has been implicitly appreciated, if not explicitly understood [98]. Space and time have even been considered as separate control problems [134], although this is not a prevailing school of thought.

On a more behavioral level, we do not know how rhythms are controlled and maintained on a cycle-by-cycle level. Nor do we know how visual control or timing control manifest, and the degree of overlap between the two. On one hand, rhythmic interactions with the environment or a task may be based on an accurate internal model [96, 112]. On the other, they may be based more directly on the time-domain

CHAPTER 2. JUGGLING AND RHYTHMICITY

properties of the sensory cues given off by the environment or task (the notion of *direct control* within ecological psychology [63, 92]).

The core results of this thesis focus on a set of experiments to elucidate the roles of sensory feedback to regulate rhythmic movements, as well as the general closed-loop algorithms the brain applies to achieve this regulation. Our central approach is to measure the response of human jugglers to sensory perturbations across multiple modalities.

In Part II we outline the design of infrastructure for a paddle juggling experiment with high temporal precision to achieve these perturbations (Chapter 3), followed by a discussion of the perturbation paradigm (Chapter 4).

CHAPTER 2. JUGGLING AND RHYTHMICITY

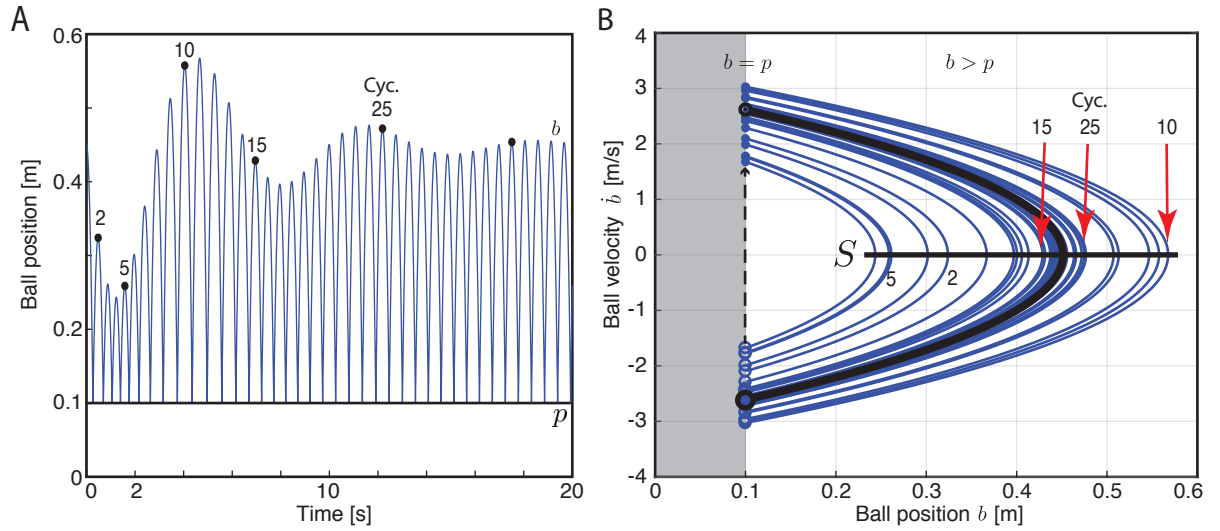


Figure 2.1: Paddle juggling in the time-domain (A) and phase-plane (B). Cycle peak numbers are labeled for cross referencing between panels. (A) Simulation using a naive proportional controller. (B) Phase plane of juggling, showing hybrid dynamics (i.e. jump discontinuity at $b = p = 0.1$ [m]). S : Poincaré section

CHAPTER 2. JUGGLING AND RHYTHMICITY

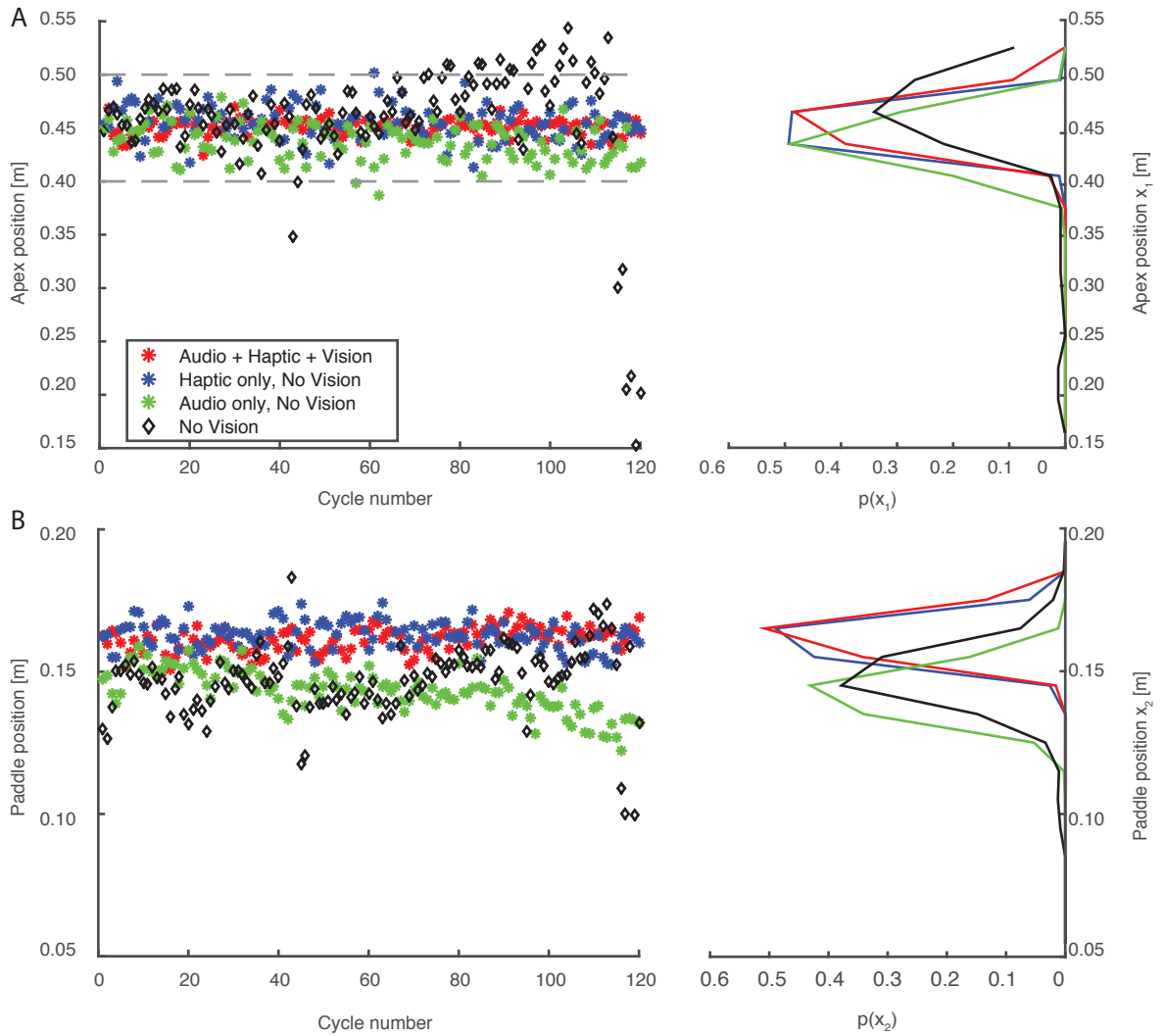


Figure 2.2: Pilot experiment on ball and hand position stability during paddle juggling under 4 feedback conditions ($n = 1$ juggler, on apparatus described in Chapter 3). (A) Ball apex position over cycle number (left), and probabilistic distribution of states over height (right). (B) The same data, for paddle position.

CHAPTER 2. JUGGLING AND RHYTHMICITY

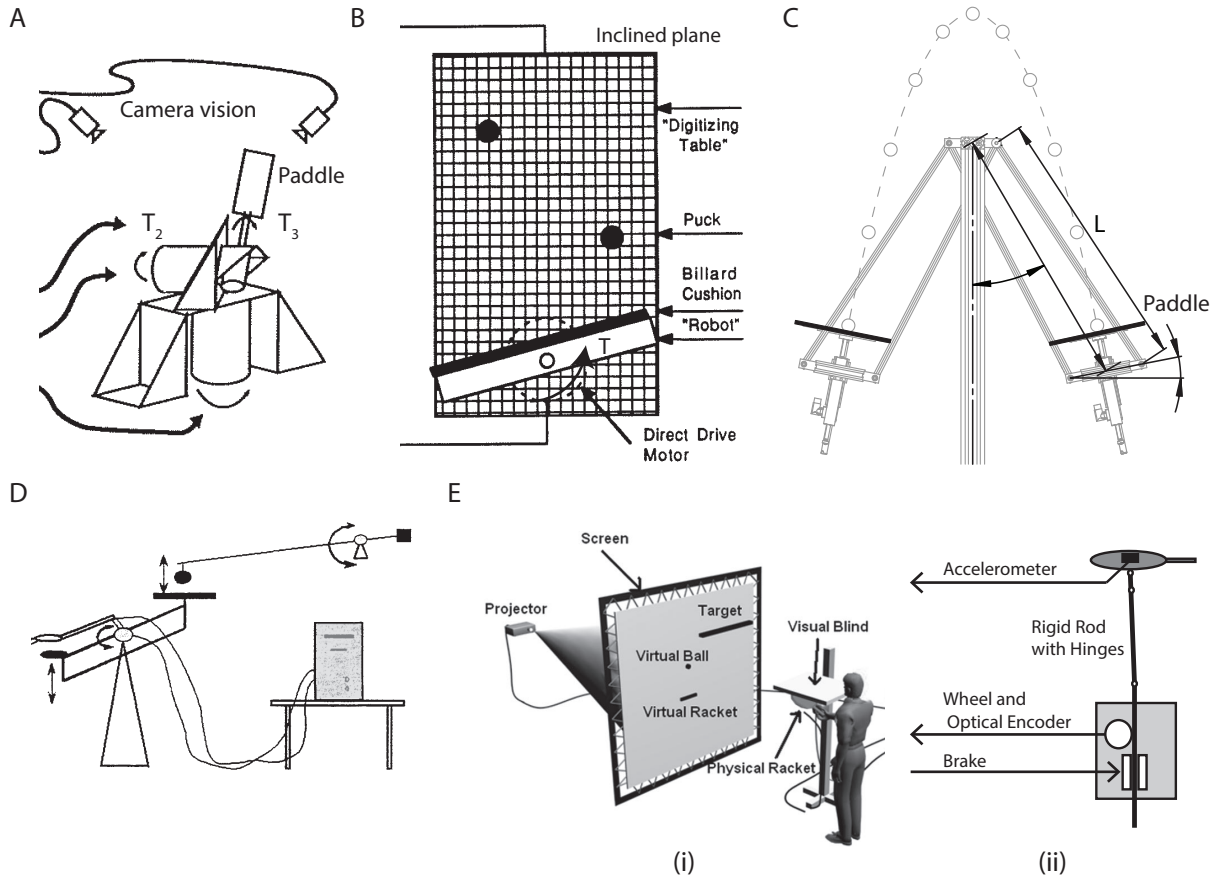


Figure 2.3: Juggling setups: (A) Spatial juggler, similar to MIT Direct-Drive Serial-Link Arm (Aboaf et al. 1988) and Bueghler (Rizzi et al. 1991-1996). (B) Two-degree of freedom planar juggler (Buehler et al. 1988-1994). (C) Pendulum juggler as an example of blind juggling without spatial tracking [1] (D) Pantograph setup, used in Schaal (1993, 1996), Sternad (2001); (E) Freely moving paddle setups (i) with audio only [2], (ii) coupled with pulley or solenoid braking systems to provide haptic feedback [3]. The panels are derived from the following original source material with permission: Panel A is adapted from Fig. 1 of [4] (Copyright IEEE 1991); Panel B is reprinted from Fig. 1 in [5] (Copyright IEEE 1989); Panel C is adapted from Fig. 1 in [1] (Copyright IEEE 2011); Panel D is adapted from Fig. 4 of [6]. Panel E is adapted from Fig. 2 of [7] and Fig. 2 of [3]

Part II: Experimental Methods

In the following chapters, we discuss a virtual-reality apparatus and perturbation experiments to investigate how visual, audio, and haptic feedback are involved in cycle-by-cycle regulation of rhythmic arm movement. Chapter 3 details the development of the hard-real-time hardware and software platform (that did not exist before) to implement a juggling task with convincing and accurate perturbations; additional details are in Appendix B. Chapter 4 outlines the general experimental approach that is the basis of Part III.

Chapter 3

Paddle Juggling Infrastructure

This chapter, together with the companion Appendix B, describes the development of a hard-real-time virtual reality juggling system that runs on the Linux operating system, which did not exist prior to this thesis research.

Fig. 3.1A (modified from [9]) conceptualizes the elements of the task. The block diagram in Fig. 3.1B outlines the information flow desired by such a system, with the infrastructure covered in this chapter boxed in red.

3.1 Motivation for Hard-Real-Time Processing

The purpose of hard-real-time scheduling is to reduce the latency between the calls to and execution of computer processes. The notion of “hardness” expresses the

level of accuracy with which timing constraints are obeyed.

The hard-real-time juggling system was preceded in my laboratory by non-real-time juggling experiments conducted on a Windows platform [9, 10]. The general thrust of these non-real-time experiments was to study the dynamics of freely running juggling in the presence and absence of haptic feedback [10]. In order to run the perturbation experiments—particularly to perturb event feedback timing—a switch to a higher performance platform with more flexibility and greater timing accuracy was required.

3.2 Hardware

Experiments were implemented on a Dell OptiPlex 980 Dual Core (4-thread) computer.¹ Signals were exchanged between the computer and hardware via an input-output (I/O) card (National Instruments PCI-6229) daisy-chained to a connector block (National Instruments SCB-68A), both capable of hard-real-time performance. The connector block serves as the switchboard whereby the operator’s movements of a control device (haptic paddle) are input to the computer, and some types of sensory feedback are output.

The user interacts with the virtual reality task by moving the handle of a haptic paddle that was based on a design developed at Stanford University (introduced in [8];

¹Earlier versions were implemented on a Dual-Core 2-thread pentium, and read encoder counts on a Sensoray 626 IO counter. No significant difference in performance was noted.

CHAPTER 3. INFRASTRUCTURE DEVELOPMENT

first use in our laboratory discussed in [9]). The haptic paddle has 1 rotational degree of freedom and is capstan driven.² Movements of the handle were sampled with an encoder (CUI-103), the outputs of which were connected to a set of pins on the I/O card that were configured to be a counter. The capstan and encoder were mounted on opposite sides of a motor attached to the paddle armature (A-max 26 Series-110170; Maxon Precision Motors, Fall River, MA). The motor shaft acted as a common axis about which force could be applied to the operator’s hand, and hand kinematics could be passively recorded.

The juggling hardware allows three types of feedback. Visual feedback is displayed on a 144 Hz monitor (VG248QE; Asus, Taipei, Taiwan). Haptic feedback is provided by commanding the I/O assembly to send a DC voltage pulse to the motor. Audio feedback is provided similarly by sending a pulse to a standard 3500 Hz buzzer.

3.3 Software

To overcome difficulties noted in under the Motivation section, a hard real-time software interface was needed. This entailed both a hard-real-time kernel, and software that enabled process-level control to greater depth than the default Linux distribution. We focus the ensuing discussion on software, and reserve discussion of kernel configuration for Appendix B.

²Because capstan drives are prone to cable slippage, I also tested timing-belt-and-gear drive. However, because the feasible gear ratios between handle and encoder were much lower, the capstan design was deemed better because its movements felt more natural and more precise.

CHAPTER 3. INFRASTRUCTURE DEVELOPMENT

Because we wished to precisely control the timing of all events, we developed a virtual-reality system on a computer run by a hard-real-time Linux Xenomai kernel, chosen for its state-of-the-art low-latency properties [140]. Custom software was developed based on an open-source robotic control platform with specific hard-real-time capability [141, 142]. This allowed all data collection and experimental events to rigorously occur at a rate of 1000 Hz, and the duration of all feedback displays to be controlled at 1 ms resolution, with errors never exceeding 40 microseconds (see Fig. 3.5).

Our software platform of choice for process-level control was the Robot Operating System (ROS)³ [141], whose versatility, support, and wide array of introspection, validation, and control tools has made it a standard choice for robotics developers. As ROS was not capable of the hard-real-time standards required for precisely applying our perturbations and event-time feedback, we used a hard-real-time control library that was embeddable within the ROS architecture (OROCOS Real-Time-Toolkit). This interfacing is explained further in Appendix B. All coding was done in C++.

As ROS is an operating system, the experimental software is encapsulated in a collection of processes (or “nodes” / “components” in ROS / OROCOS parlance), which mutually interact through a series of threads that are governed by control policies that can be set by the user (see Appendix B). The workflow of the experimental system in schematic form is in Fig. 3.2, with components identified in capital face.

³ROS version Fuerte as of initial development; ROS version Hydro as of rebuild.

An overview of each component follows.

User interface: `juggle_UI.exe`

In order to reduce user burden, a text-based frontend was developed. Running the executable `juggle_UI` opens a menu-driven user interface (Fig. 3.3). The main functionalities are (1) to automate the set up of a file structure for storing experimental data, (2) to allow on-the-fly customization of experimental conditions, and (3) to enable the experimenter to control experiment flow without needing ROS literacy.

The main options are:

1. **Enter Subject Info:** This information is output to a file of extension `*.info`.
The date and the name (first and last) of the participant are used to compose an identifier for the experiment, which is used to generate a folder system for data storage.
2. **Run Trial:** Entry of a trial number causes input of a corresponding trial schedule file extension `*.expt` (generated beforehand in Matlab / Octave).
The user then enters a mode to specify the feedback to be made available—1: Haptic only; 2: Audio only; 3: Audio and Haptic only; 4: Visual only; 5: Visual and Haptic only; 6: Visual and Audio only; 7: Visual, Audio, and Haptic.
3. **Review / Change Parameters:** This allows the experimenter to specify a

CHAPTER 3. INFRASTRUCTURE DEVELOPMENT

mode for the experiment. Defaults are loaded from an XML file.⁴ These can be confirmed or overwritten for the current experimental session only, through the menu interface.

4. **Quit:** Exits to Linux terminal.

Run Trial begins the experiment once a trial and mode number are entered. As this depends on the existence of a trial file `*.expt` and an experiment dossier, its prerequisites are the generation of a subject dossier and file system (via **Enter Subject Info**) and of a set of trial schedules for an experiment (by running a Matlab / Octave script described in Appendix B).

Once a trial commences, the `UI_Component` process is activated while `juggle_UI` remains in suspension, either until the trial completes or is interrupted by the user. In either case, `UI_Receiver` will signal `juggle_UI` to reactivate it.

UI component

This node interfaces with the hard-real-time (OROCOS) partition of the software on behalf of the user interface. Its main functions are to (1) parse the entries of `juggle_UI` and to forward them to the appropriate components, (2) activate components on start of the trial, and (3) shut down components if an interrupt command is issued by the experimenter (i.e. if the user enters “q” or “Q” in the “Experiment Running” submenu of Fig. 3.3).

⁴File `params /defparams.yaml`

Main component

This contains the main engine for the experiment. Process flow is illustrated in the flowchart of Fig. 3.4. At the start of the experiment, it enters a transitory configuration state, where it reads in configuration and start states, and the pre-designed experimental schedule. It then enters an update state, which operates as a state machine that switches state between the following alternatives according to events during the trial:

Redrop state:

This state is evoked at the beginning of each trial, or if the ball drops below a threshold (enabled with the “Redrop Ball” option in 3.3). During the redrop sequence, the ball is clamped at a constant position⁵ while a counter appears and decrements to 0 s (all rendered in `Window` component below). Simultaneously, the encoder is reset and all data buffers are flushed. When the countdown duration expires, the ball drops and enters the (`Juggle` state).

Juggle state:

This state simulates a ball and user-controlled paddle in a gravitational field. The majority of each trial is spent in this state. Several operations are performed during each 1 kHz callback.

⁵Default 0.45 m above the bottom of the monitor

Paddle kinematics

First, the encoder is polled, and changes in count are scaled to veridical hand movement (with an encoder-counts-to-meters conversion factor) and used to update paddle position. Paddle velocity is computed with a differential filter (see Appendix B for further details). Smoothness is enforced by two methods. (1) Resampling the encoder during same loop—a difference between two consecutive encoder reads (from separate runs of the update callback) exceeding 100 counts is interpreted as a sign of jitter, and triggers the encoder to be reread immediately. Although this operation is placed within a `while` loop, it has not caused any violations of real-time system performance to date. (2) Applying a discrete-time polynomial filter (described in Appendix B). We note that this filtering operation probably would have been technically unsound on non-hard-real-time renditions of the juggling task, as assumptions of uniform sampling of data would have been blatantly violated.

Displayed paddle position was updated based on a locking condition specified in the main UI (Fig. 3.3). In **Paddle Free** mode, onscreen paddle position was updated per the encoder count. In **Paddle Lock** mode, paddle position was clamped in fixed position. Because paddle movements were tracked with a digital encoder (see Apparatus), locking was accomplished by retaining encoder data affiliated with hand movements in memory, and simply never using them to update the paddle position onscreen. That is to say, paddle velocity was continually updated, while the locking condition only determined how the positional data was routed and processed.

CHAPTER 3. INFRASTRUCTURE DEVELOPMENT

Essentially, the **Paddle Lock** mode actualized the high bounce assumption discussed in **Chapter 2**.

Ball kinematics

All rendering was done by the Window component (see below). Ball position feedback was presented in 2 modes:

In **Full Ball Vision** mode (Ball flash OFF in Fig. 3.3) the ball was displayed at all instants. A stationary red cross was placed at the peak ball position starting at the apex phase of a cycle and persisted onscreen until the subsequent apex.

In **Partial Ball Vision** mode (Ball flash ON), the ball location was only displayed during an interval of $17k$ ms before and after the apex, where k is an (integer) variable representing some number of frames chosen by the programmer. Accurate rendering of ball trajectory required a forward estimation of the time of ball apex (trivial from ball flight equations), in order to predict when to start rendering the ball. In cases when apex time was perturbed, ball locations were stored in a buffer and showed at the appropriate time.⁶ Additionally, starting at the ball peak, a stationary red cross was placed at the peak ball position for $17k$ ms, so that it disappeared with the ball.

The short duration of ball flash feedback was determined to be a minimal source of juggling difficulty during pilot tests, and is also justified scientifically from previous studies that suggest that visual feedback on the order of milliseconds about the peak is

⁶As discussed in later chapters, all timing perturbations were delayed with respect to veridical physics.

CHAPTER 3. INFRASTRUCTURE DEVELOPMENT

sufficient for juggling [134]. From a design standpoint, restricting the visibility of the ball trajectory to a specific phase facilitated the presentation of spatial perturbations in a plausible way.

Ball position is updated using Euler-Newton integration, while collisions are modeled by a coefficient-of-restitution law (see Chapter 2 and Appendix B). Ball dribbling, which is an example of Zeno behavior (also noted in Chapter 2) is best avoided during perturbation studies where scheduling is important and perturbations must be presented in an ordered manner. Our solution was to incorporate a ball redropping option prior to the onset of dribbling, which could be toggled as outlined in Fig. 3.3. In **Redrops OFF** mode, the ball was allowed to dribble on the paddle (admitting “sticking solutions” and Zeno behavior). In **Redrops ON** mode, a small maximal bounce height (approximately 3 cm or 10% of target height above virtual paddle position) would trigger the trial to be restarted (and cause the software to re-enter **Redrop** state).

During collisions, audio and haptic feedback were presented simultaneously with a stock delay of 33 ms. The specific feedback that would play was toggled by selecting a mode number in the UI (see Fig. 3.3).

Window component

This process rendered graphics using the open-source standard OpenGL libraries (Version 2.3). It only executes drawing functions when it receives new data from

CHAPTER 3. INFRASTRUCTURE DEVELOPMENT

the Main component. The rate at which these objects are rendered is limited by hardware, namely the frame rate of the monitor, and by graphical drivers at disposal (which limited refresh to 60 Hz).

The node receives information about the ball and paddle position, as well as a state variable indicating one of multiple modes: JUGGLE or REDROP. During typical JUGGLE mode, the paddle, the goal (simple rectangle primitives), the ball (a fan primitive), and a cross (two perpendicularly intersecting rectangles) are rendered. If the ball height exceeds the dimensions of the screen, a red arrow pointing upward is drawn.

When Ball Flash mode is OFF, Window receives instructions to render on every loop. During ball flash mode, window node is instructed to receive every 17 loops (corresponding to a 58 Hz rendering rate), starting $3 \cdot 17$ loops before the ball peak position, and ending $3 \cdot 17$ loops afterward. This is intended to make the ball flash animation symmetric about the peak ball position.

During REDROP mode, the node renders a 3-second countdown sequence displayed roughly at the center of the screen, slightly below the target.

Logging component

The logger receives all data and stores it in a buffer. Further details of how this was programmed to avoid violations of real-time constraints are in Appendix B.

Expandability to monitor biopotentials

In the Main component, a flow port was added to record analog signals from the DAQ card. This flow port was routed to the logging node for recording. Monitoring was done using a ROS introspection tool, `rosqt`.

3.4 Validation

Benchmarking and validation was necessary to check timing precision and correct application of perturbations. Three aspects needed to be checked: (1) Real-time accuracy of task physics; (2) accuracy of perturbations; (3) accuracy of monitor display times. An additional validation of (4) adherence to real-time performance (i.e. OS Stress Testing) for the patched operating system was done as a prerequisite, and is discussed more in Appendix B.

Physics

Physical states were programmed to be updated at a 1 kHz rate. Timing accuracy of the physics engine is measured in terms of latencies, or the amount by which consecutive callbacks were late or slow relative to an expected 1-ms period. These latencies are shown in a histogram of more than 11 h of data collection in Figure 3.5. As shown, latencies were almost universally under 10 microseconds.

Perturbations

Visual perturbations were applied simply by adding an offset to the rendered ball position, and thus were trivial to produce. However, to verify accuracy of the timing perturbations, the voltages output by the I/O card were recorded continuously in time, and the timings of their rising edges (onsets) were recorded in memory for comparison to the designed perturbations. Figure 3.6A shows the timing deviations of audio-haptic feedback (mean \pm 3 s.d.) superimposed on the programmed theoretical perturbations for a representative experiment, confirming the desired accuracy and precision. The box plot in Figure 3.6B shows the overall distributions of errors between actual and theoretical timing perturbations across $n = 16$ experiments (note this is *not* the same as jitter, which is drawn in Fig. 3.5). The histogram shows that errors are approximately normally distributed around 0 (perfect accuracy), with precision within 1 ms. This precision—which appeared to be a fundamental limit of the 1 kHz callback rate of the ROS-OROCOS setup⁷—was made relatively minor by making perturbation magnitudes large, resulting in higher signal-to-noise ratios.

Graphical rendering

Because of the drivers available in Xenomai, it was not possible to take advantage of full refresh capabilities of the monitor; thus monitor refresh was limited to 60 Hz

⁷The callback period of the Main node could not be sped up above 1 ms. However, it could be slowed.

(approximately 17 ms refresh period). To verify frame rate, a scanner was developed (Fig. 3.7A), consisting of an array of photodiodes that can read an alternating pattern of gray bars against a black field that can be drawn on the screen by pressing the spacebar. Figure 3.7B shows a typical example of a bar code reading, which is interpreted as a series of rising and falling binary pulses. While there is considerable frame-by-frame variability, the overall average is 17 ms, consistent with a one-frame-every-17 loops rendering signal that was sent from the Main task node.

3.5 Summary

This chapter (and the accompanying Appendix B) outline the development and operation of a hard-real-time juggling system to implement a perturbed juggling task with high flexibility and accuracy. The system allows participants to paddle juggle under realistic perturbations, changing environmental dynamics, and multiple types of sensory cues (here, visual, audio, and haptic). Chapter 4 outlines the basic experimental paradigm applied to this system.

CHAPTER 3. INFRASTRUCTURE DEVELOPMENT

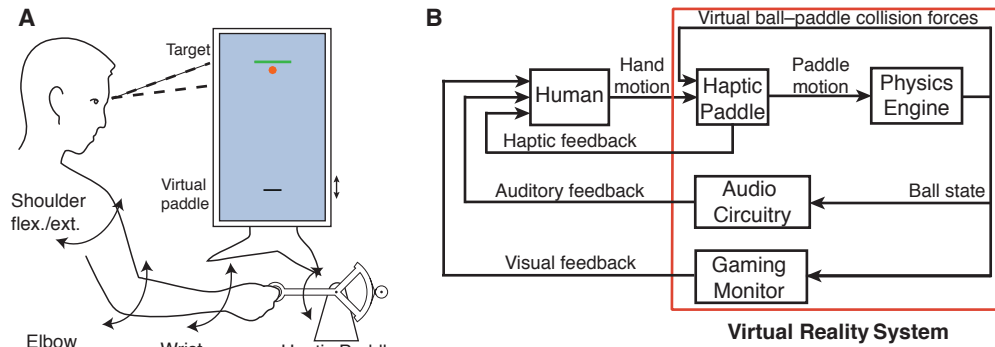


Figure 3.1: Overview of experimental setup. (A) Conceptual drawing of experiments. Subject holds haptic paddle and moves handle up and down (1 dimension vertically), generally by combination of wrist, elbow, shoulder rotations. (B) Information flow between task and juggler.

CHAPTER 3. INFRASTRUCTURE DEVELOPMENT

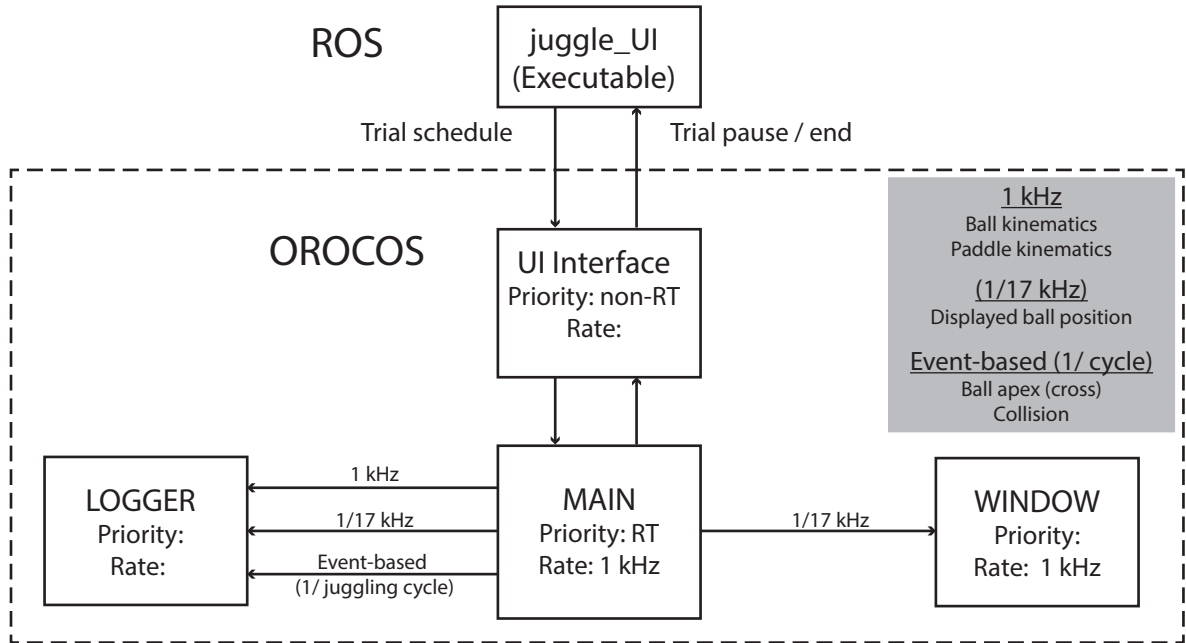


Figure 3.2: Overview of paddle juggling software architecture, showing interfacing between ROS (Robot Operating System) and OROCOS (Open Robot Control Software). Each block is a separate subprogram (“node” or “component”). Message threads connecting each subprogram, and their directionality of data flow, are shown as arrows. Callback and data transfer rates are presented in Hertz (Hz)

CHAPTER 3. INFRASTRUCTURE DEVELOPMENT

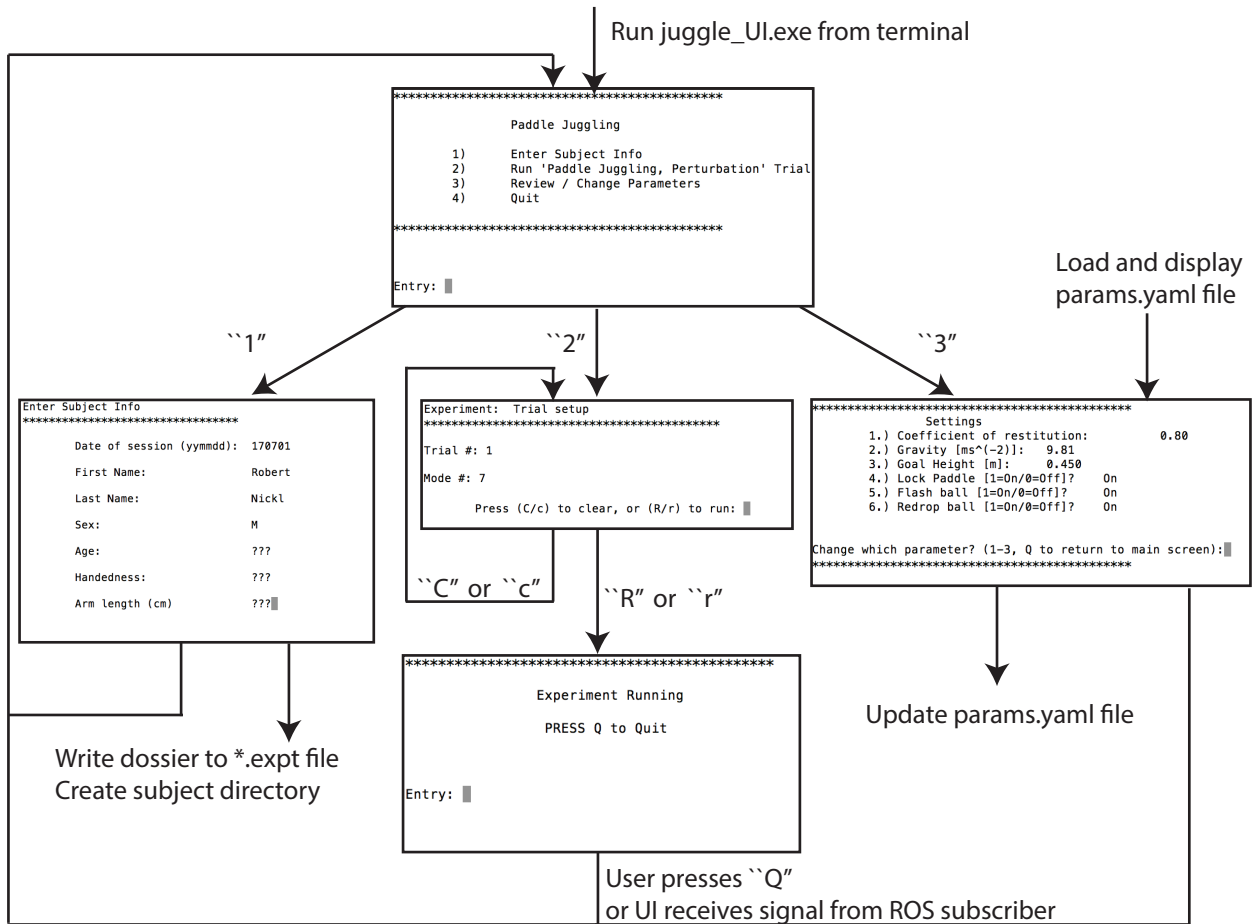


Figure 3.3: User interface (text-based) for experiments

CHAPTER 3. INFRASTRUCTURE DEVELOPMENT

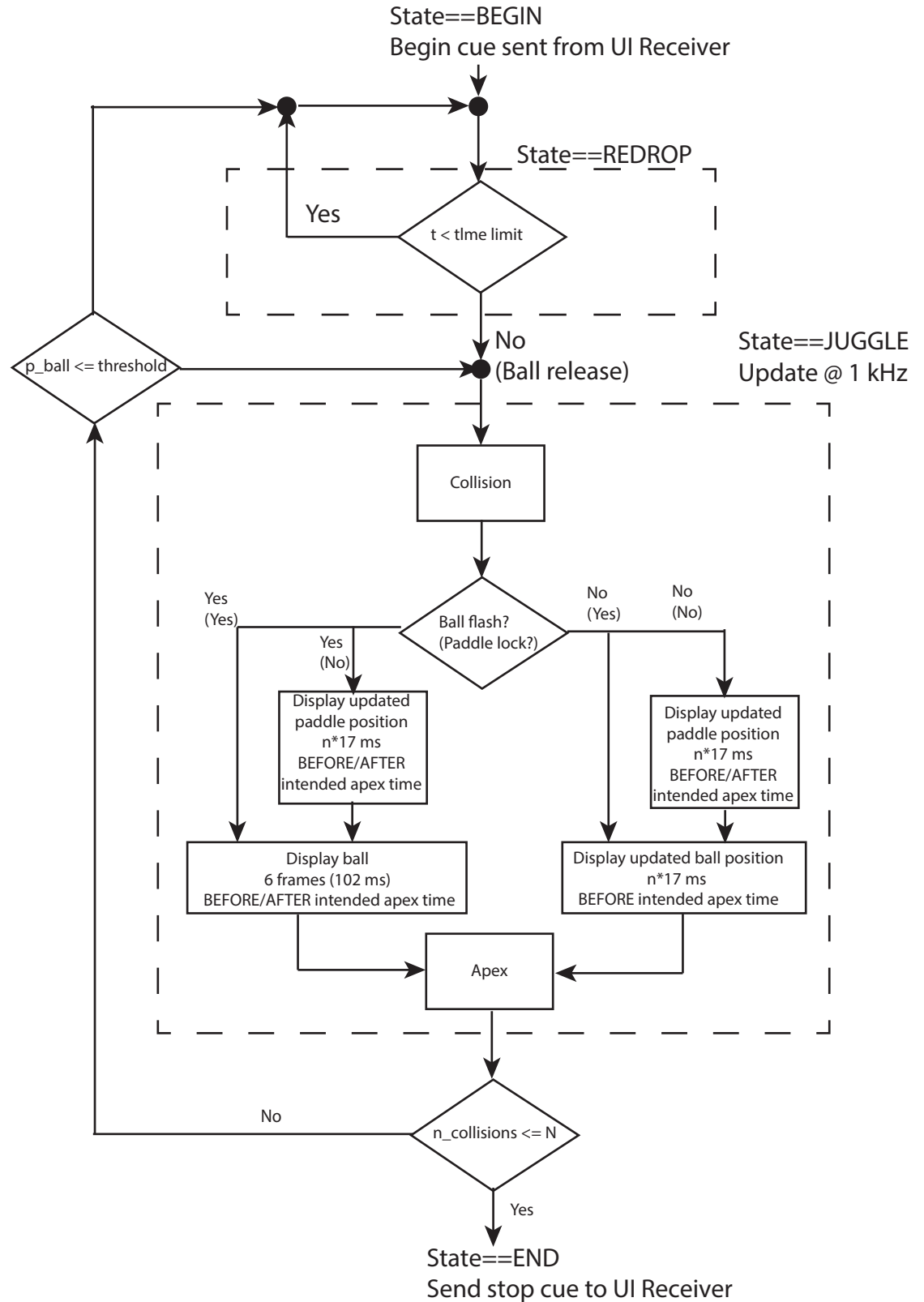


Figure 3.4: Logic flow of each experimental trial (embodied in MAIN node from Fig. 3.2).

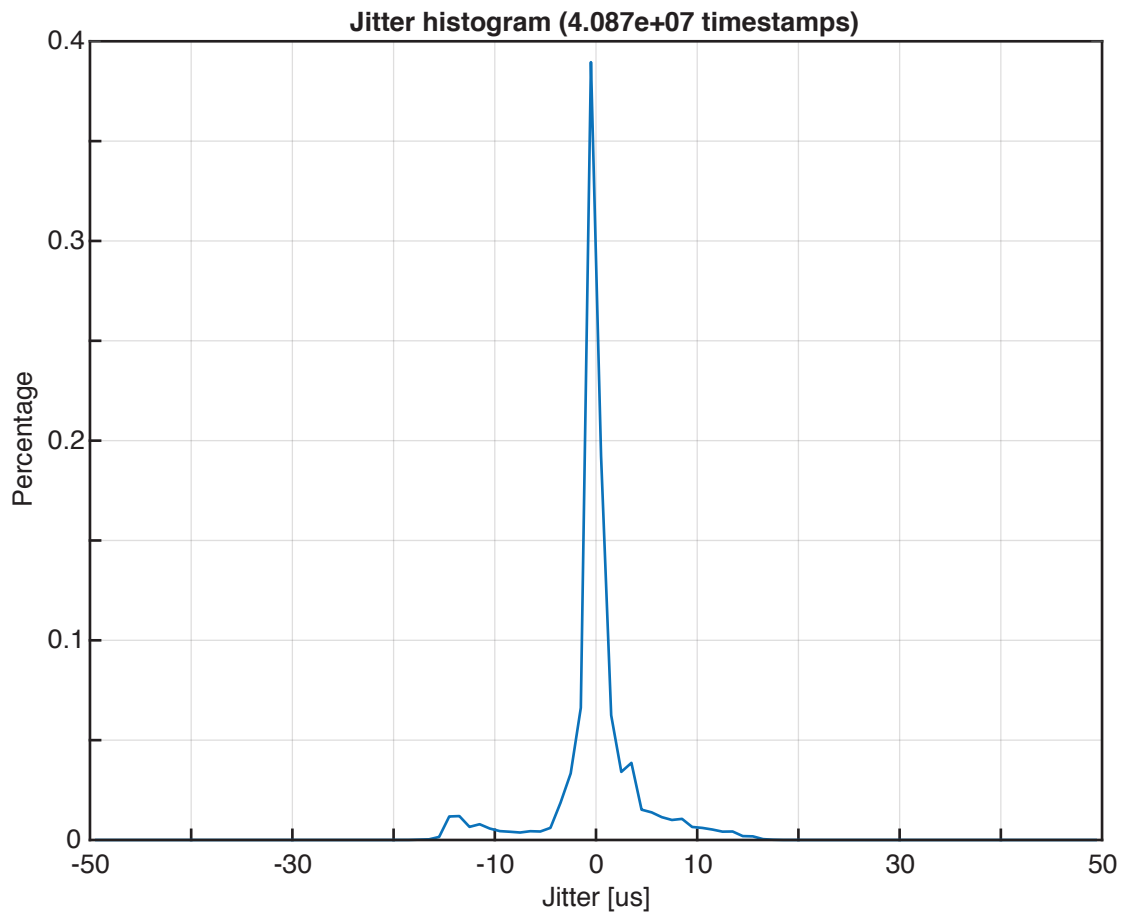


Figure 3.5: Histogram of timing jitters measured during experiments.

CHAPTER 3. INFRASTRUCTURE DEVELOPMENT

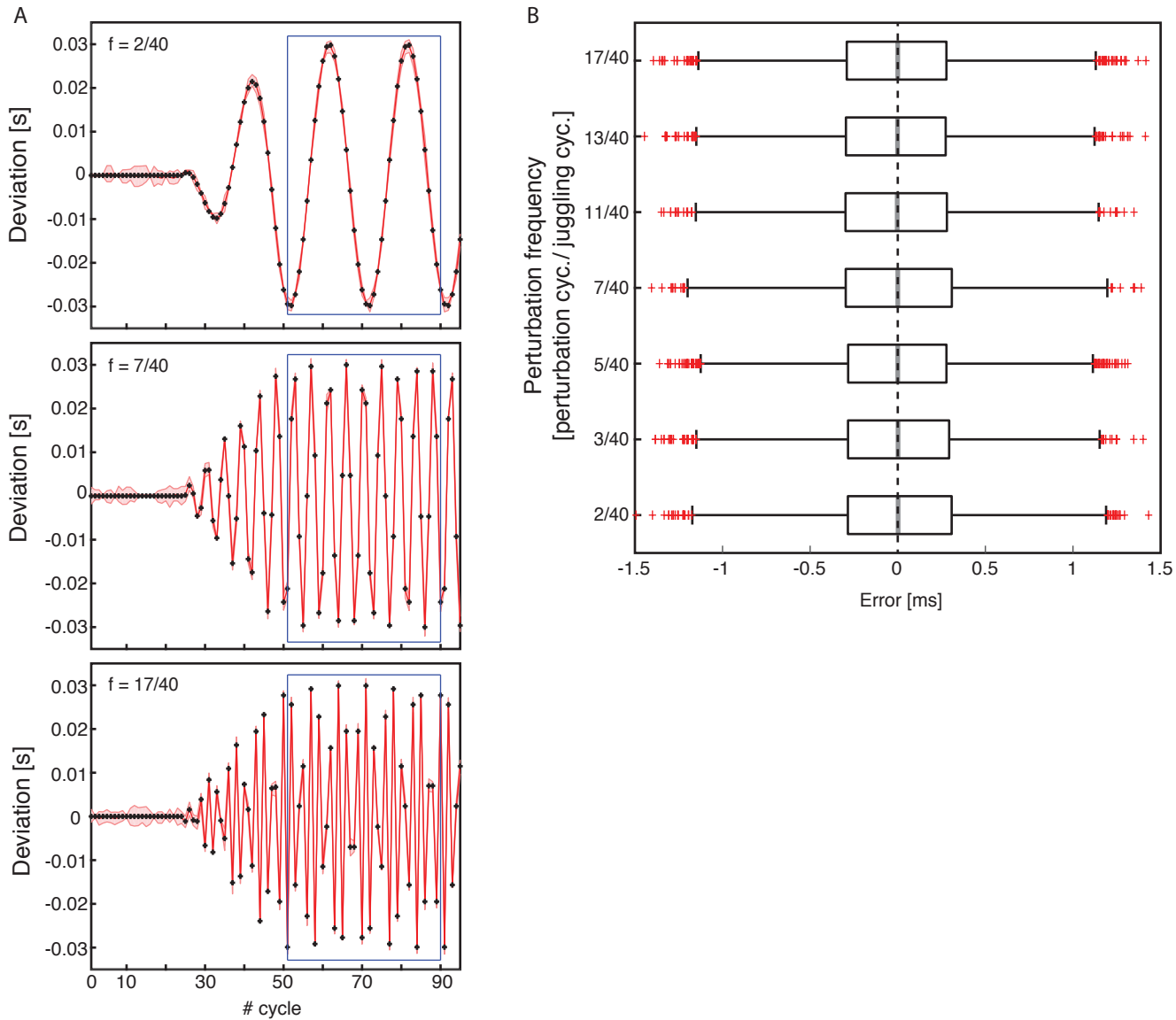


Figure 3.6: Timing perturbation validation. (A) Representative perturbation conditions for one participant (S8). (B) Box plot of timing perturbation accuracies.

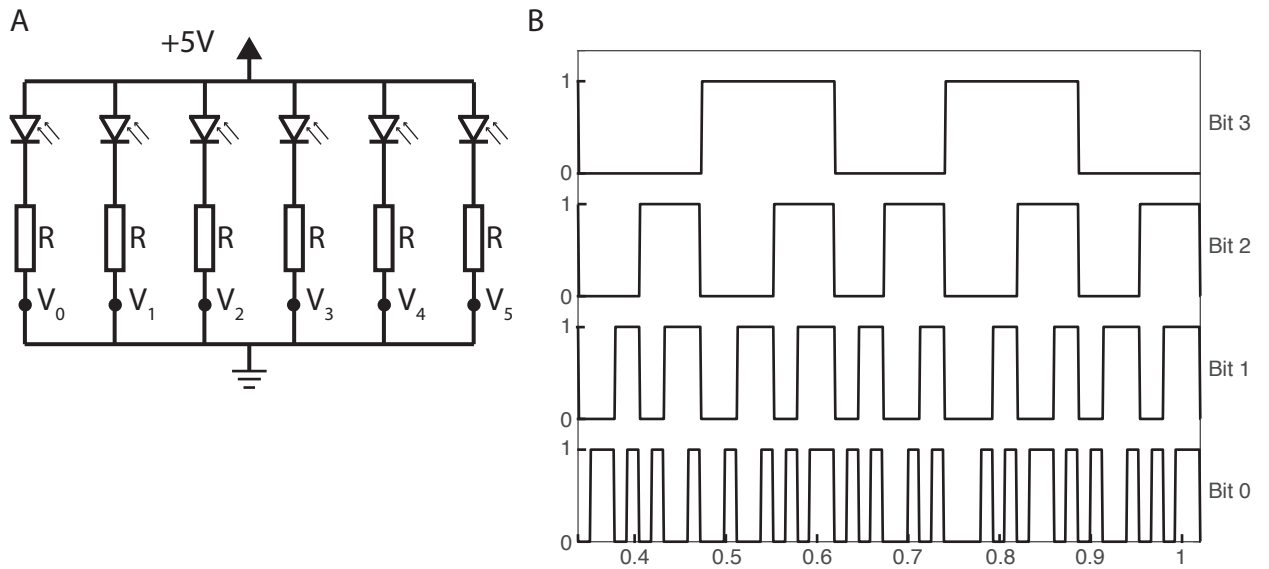


Figure 3.7: Overview of frame rate testing: (A) Bar code scanner, with circuitry facing out. When facing monitor, topology is reflected about vertical midline (axis intersecting source and ground symbols). The circuit is a current divider, with a photodiode and resistor in each branch. Bar patterns are read as on/off bits measured at the nodes V_n . (B) Example bit pattern.

Chapter 4

Experimental Approach

Chapter 3 (with companion Appendix B) presents a hard-real-time platform allowing perturbations of both spatial and—crucially—timing of event-related feedback in juggling for investigation of closed loop regulation of juggling. The following chapter outlines the paradigm of perturbation-based system identification and the basic template for experiments to address the questions raised at the end of Chapter 2. Details of individual experiments, and their results, are reserved for Part III.

4.1 Perturbation-based Identification

Our approach toward investigating the central question of how descending sensory input regulates rhythmic behavior is to perturb sensory feedback at different phases of a juggling cycle (described in more detail in Chapters 5 and 6). We apply two types

CHAPTER 4. OVERVIEW OF EXPERIMENTAL APPROACHES

of perturbation functions, which are classified in terms of how the amplitude and sign of the perturbation vary as a function of time. Because we are interested in cycle-by-cycle control of behavior, this time index is cycle number, and hence perturbations and subsequent analysis are in discrete time.

Experiment mode

The paddle juggling task is shown in Figure 4.1A. The screen displays a ball of radius 1 cm and two bars separated by 35 cm. The upper bar serves as a target, while the lower bar is a virtual reality avatar of the paddle. Participants sit at eye level to the target and control the virtual paddle by vertically moving the handle of a haptic paddle placed right of the monitor [8].

Experiments discussed in this thesis consisted of series of trials, each beginning with the suspension of a virtual ball onscreen at the target height, with a counter displayed slightly below (**Redrop** state, as discussed in Chapter 3, Section 3.3). After a 3 s countdown, the experiment entered the **Juggling** state, where ball physics were simulated with 1D ballistic flight equations and a coefficient-of-restitution-based collision map.

While juggling, participants were instructed to bounce the ball vertically toward the goal as accurately and consistently as possible by moving the handle of the haptic paddle vertically. The experimenter coached participants to juggle with elbow angle at approximately 90 degrees. Each time the ball reached its peak for a given cycle, a

red cross was temporarily drawn at that position (see Fig. 4.1A for typical example).

High juggling (locked-paddle) control

All experiments were run in **Paddle Locked** mode: that is, virtual paddle position was kept stationary while virtual paddle velocity was computed directly from the participants' hand velocities (Fig. 4.1B). As discussed in Chapter 2, this enforces the high-bounce juggling assumption made in several analytical and experimental studies. Additionally, locking the virtual paddle position provided the analytical benefit of making ball kinematics and event times (apex and collision) exactly determinable from the states of the preceding collision.

Locking the paddle did not seem to materially change the task or make it less accessible than prior studies. Participants moved their hands rhythmically in quasi-sinusoidal trajectories as in other paddle juggling apparatuses (Figure 4.1B) [21], and could learn to perform the task successfully after a single training session.

Experiments were run in **Ball Redrop** mode, which made Zeno solutions unreachable. Other than the fact that we were not interested in Zeno behavior, avoiding it was very important for a technical reason. Namely, our system and perturbations were designed under the assumption that juggling cycles have periods on the millisecond scale, and because Zeno behavior clearly violates this assumption, any trials exhibiting it would have produced meaningless data.

The nature and purposes of the redrop criterion were not disclosed to participants.

CHAPTER 4. OVERVIEW OF EXPERIMENTAL APPROACHES

Rather, they were simply informed that hitting the ball to the goal height was perfect performance, while letting it bounce too close to the paddle height would cause the trial to be restarted.

Feedback presentation

Spatial task feedback took the form of visual information about ball position. The experiment was operated in Ball Flash ON mode (discussed in Chapter 3), where the ball trajectory was displayed for 13 frames total (approx. 221 ms),¹ centered about ball peak phase.

Timing information was conveyed through the timing of the simultaneous audio and haptic cues at collisions, and of the onset of the apex flash. To prevent timing perturbations from affecting the participants' actions anti-causally—namely at the collision phases—all event timings were presented with a 33 ms delay bias (subtracted out of Fig. 3.6). Participants likely adapted to this fixed temporal delay, as no one reported that they noticed it.

4.2 General Experimental Structure

Experiments consisted of three sessions carried out on separate days (each spaced apart by 1 or 2 days). The exact format of the latter two sessions varied by experiment

¹ $k = 6$ using the notation of Chapter 3

and will be covered in Part III.

4.2.1 Training protocol (Session 1)

Session 1 of both experiments was a general learning session in which the overall goal was to acclimate participants to the juggling apparatus and to train them to juggle continuously for 100 consecutive cycles under normal test conditions (Figure 5.1B, C). As the purpose of this study was not to assess learning, but measure influence of sensory information during stable behavior in the vicinity of a limit cycle, participants were encouraged to swing the paddle upward during ball collisions.

Each experiment began with an initial demonstration by the experimenter (RN), in which he juggled the ball for two trials (approx. 2 min. total). Examples of accurate juggling, misses and recoveries, and redrops were shown to the participant. In addition, during the second demonstration trial, the experimenter mentioned the importance of swinging the paddle upward during collisions, and told participants to watch his hand as he bounced the ball.²

In order to pass a trial, subjects needed to juggle the ball continuously for the scheduled duration (in *.expt file), which was between 80 and 100 consecutive cycles. For the first 6 trials of Session 1 in all experiments, the ball was shown continually onscreen (**Ball flash OFF**). Participants trained to perform the task as described above, under reduced gravity ($g = -6.54 \text{ m/s}^2$, $\alpha = 0.8$) for trials 1-3; and full gravity

²This demonstration appeared to be vital, as previous pilot testing showed that the haptic paddle was not intuitive for some volunteers to use.

CHAPTER 4. OVERVIEW OF EXPERIMENTAL APPROACHES

for trials 4-6 ($g = -9.81 \text{ m/s}^2$). Participants were informed when gravity was increased and when the ball flash mode would be activated.

From trial 7 onward, subjects juggled under full gravity and intermittent ball feedback centered at the apex (**Ball flash ON**). After Trial 12, perturbations (either sinusoidal or step) were introduced on random trials to provide exposure before the Test sessions began. Subjects were at no time informed of the existence of perturbations.

Beginning with Session 2 of each experiment (described further in Part III), subjects were exposed to perturbations for the entire session following a 6-trial warm-up period without perturbations.

4.2.2 Perturbation design considerations

We apply two types of perturbations: sinusoidal (Ch 5 and 6) and step (Ch 6). We allude to some general design principles for perturbations, reserving more details for Part III.

Amplitude

There is a tradeoff between making a perturbation (1) strong enough to reliably elicit a response and (2) subtle enough to not engage a conscious strategy or throw subjects from their limit cycles. Ultimately, 3 cm was a suitable spatial perturbation magnitude, as determined from empirical observations. Smaller amplitudes were gen-

CHAPTER 4. OVERVIEW OF EXPERIMENTAL APPROACHES

erally insufficient for eliciting consistent responses, likely because paddle juggling is itself a noisy task with high task-related variability. On the other hand, perturbations larger than 3 cm were too distracting and unnatural for jugglers. For timing perturbations, an amplitude of 30 ms was judged to be strong enough to elicit consistent human responses while remaining subliminal.

Perturbation studies conducted by other researchers (e.g. [15, 17]) used sums-of-sines perturbations with several components (generally more than 7). This was generally not feasible for the paddle juggling task. Pilot tests found that the amplitude limit of 3 cm was the maximum that could be tolerated, and if the same perturbation energy were divided among a number of constituent frequencies, the effective stimulus power at each frequency would have been reduced below the empirical threshold for eliciting a response.

Onset timing

We generally found that subjects were thrown from the limit cycle if a continuous perturbation function was turned on too abruptly. Perturbations could be introduced more subtly by ramping them up from zero. A ramp-up duration of 25 cycles for sinusoidal perturbations was ultimately chosen.

Frequency

Stimulus frequencies should be within what may be termed the “sensorimotor bandwidth”: they should encompass frequencies that capture both high-gain and low-gain behavior, and ideally describe the transition band between. Across organisms, closed-loop transfer functions of sensorimotor behavior tend to be low-pass; however, because cutoff frequencies are not known a priori, perturbation frequencies must often be initially guessed or chosen out of practical concerns.

Ultimately, the bandwidth of perturbations was determined by the duration of time a participant was able to bounce the ball to the goal consecutively without tiring or losing rhythmicity. It was found that, with practice, subjects generally had little difficulty attaining 100-consecutive cycle perturbations. Window length of 40 seconds was chosen because this allowed null, ramp-up, and perturbations to safely occur within 1 minute trials. The use of 1-minute trials allowed all experiment sessions to be completed within 90 minutes.

4.3 Summary

In this chapter, we reviewed the basic philosophy and design principles for the experimental paradigm used in this thesis to explore cycle-by-cycle regulation of rhythmic movements about a limit cycle. In Part III, we reiterate the hypotheses of interest, and discuss two perturbation experiments to investigate them.

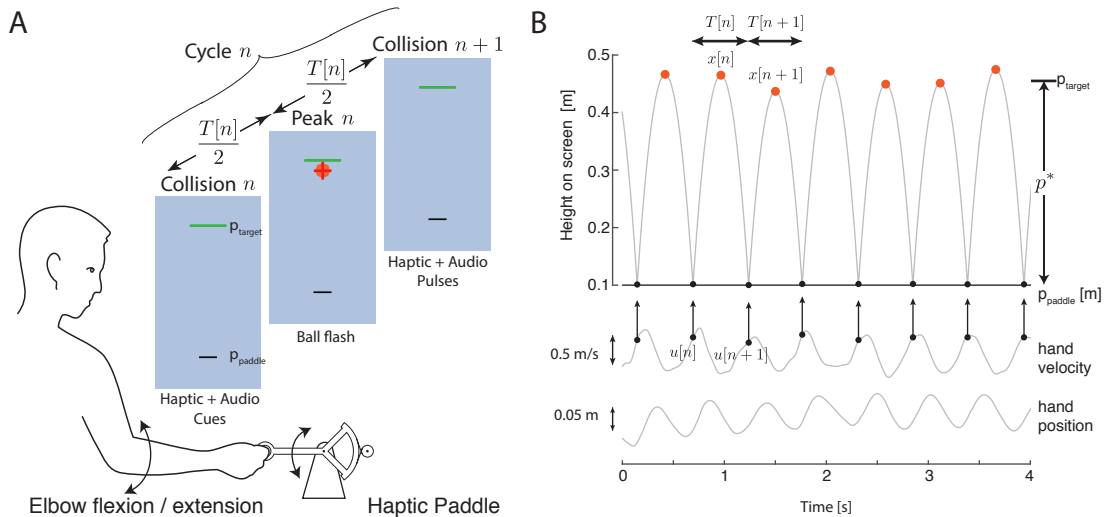


Figure 4.1: Paddle juggling task. The bias is subtracted from both signals, so that they are centered around 0. (A) Overview of paddle juggling task. Participants bounced a virtual ball on a monitor by moving a handle (haptic paddle) up and down, and received sensory cues at different phases of each ball bouncing cycle. (B) Example task kinematics (ball and paddle heights) and hand kinematics (velocity and position) from a typical experiment. For all experiments, virtual paddle position was clamped, while virtual paddle velocity was computed from veridical hand movements.

Part III: Experiments

In Part II, we outlined the development of experimental infrastructure and the experimental template for investigating questions of how rhythmic behavior is regulated in a closed-loop manner using visual, auditory, and haptic information.

During experiments, we asked human volunteers to perform a virtual reality paddle juggling task in which two types of sensory information were subtly perturbed: (1) spatial feedback, in the form of visual display of ball heights at collisions, and (2) timing feedback, in the forms of simultaneous audio and haptic cues at collisions. These perturbations manifested respectively as increases and decreases in displayed ball position, or as advances and delays of when feedback of ball collision and apex events were presented. In contrast to previous perturbation studies, we exclusively perturb sensory feedback instead of task dynamics and measure motor output at given frequencies in the sensory bandwidth (see Chapter 4).

Two hypotheses form the basis of experiments to be discussed in this section.

- **Hypothesis 1:** Spatial and timing feedback are fused into a common estimate of ball movement. To test this, we analyze the relative effects of visual and event-

PART III: EXPERIMENTS

timing feedback perturbations on the control of ball position. This approach is justified by a physics-based closed-loop model in which visual and timing feedback inform ball position, the latter through the coupling of space and time in one-dimensional ballistics.

- **Hypothesis 2:** If Hypothesis 1 is true, we would expect control using visual and timing feedback to have similar dynamics, reflecting processing through similar pathways (e.g. visuospatial). Conversely, if Hypothesis 1 is falsified, we would expect that visual and timing feedback would have different dynamics, reflecting separate cortical pathways and separate descending influences.

These hypotheses will be treated in Chapters 5 and 6, respectively.

Dissemination

Chapters 5 and 6 are adapted from the paper “Human rhythmic arm movements involve complementary spatial- and timing-based control”, under review as of the publication of this thesis.

Chapter 5

Separability of Spatial and Timing Control

5.1 Introduction

Paddle juggling is a particularly well suited task for addressing cycle-by-cycle regulation of rhythmic behavior because of its simplicity and the similarity of its hybrid dynamics to more complex tasks such as spatial juggling and locomotion.

To the extent that prior studies have considered sensory estimation, paddle juggling has been considered a predominantly visual task [104, 132]. Yet, multiple lines of evidence suggest feedback that is not explicitly spatial may have an important role. Stable paddle juggling can be accomplished with only haptic feedback [6]. In addition, haptic event cues at ball–paddle collision instants lead to a categorical improvement

over vision only in how long a person can sustain a given level of rhythmic accuracy [10]. A logical hypothesis that may apply to the juggling task is that non-spatial feedback provides a timing cue that is integrated into an estimate of ball position [10]. Alternatively, non-spatial feedback may be used by the nervous system to regulate pacing of movements.

In this experiment, we use a frequency-domain system identification approach to assess the relationships between motor behavior and sensory stimuli. If timing cues reinforce spatial control of rhythmic arm movements, perturbations of either modality would result in statistically equivalent adjustments of ball height (as outlined in our control model below).

5.2 Model and Hypothesis

Paddle juggling performance is schematized in Figure 5.1A, in terms of general information flow between task dynamics G_{plant} , and the human brain and musculo-skeletal system G_{ctrl} . Our goal is to understand how the human brain uses spatial and timing feedback, as revealed in the structure of G_{ctrl} .

As a result of locking the paddle (per the high bounce juggling assumption), the ball trajectory is completely specified for a given cycle by ball peak position $x[n]$ and the paddle velocity $u[n]$.

Hypothetical model of neural estimation and control

Consistent with previous treatments of paddle juggling, we assume that the explicit goal of the human brain is to reduce error between ball height and target position (Fig. 4.1A).

Derivations of the following hypotheses are shown in Appendix C. As shown in Appendix A, by defining a target position, we implicitly prescribe a target limit cycle, specified by nominal states. In the vicinity of these nominal states, paddle juggling can be modeled by the linearized system:

$$x[n + 1] = \alpha(b[n] - b^*) + (1 + \alpha)t_{\text{flight}}^*(\dot{p}[n] - \dot{p}^*) \quad (5.1)$$

Ball flight time (namely, time to collision) and ball peak position are physically coupled: if a ball is perceived to land later than expected, this implies the ball position was higher than originally believed. Near the limit cycle (i.e. in the vicinity of nominal states), this space–time relationship is:

$$\Delta t[n] = \sqrt{\frac{1}{2gb^*}} x[n] = C_s^t x[n] \quad (5.2)$$

C_s^t represents the approximate physical mapping from spatial information to timing information. Due to this coupling in ballistic physics, one may reasonably con-

jecture that the role of audio or haptic feedback that informs about collision time is to infer ball position; hence that juggling behavior is dominated by spatial control [104, 132].

Observer model

If ball position were the primary behavioral output of relevance to the brain, we would expect timing feedback maps to spatial error via an inverse model, and that the brain would fuse this information with visual feedback— through methods such as Kalman filtering [130]—to estimate ball position [20, 143]. A possible sequence of steps is as follows:

1. While the ball is ascending, the juggler has a prior estimate of the upcoming peak position:

$$\hat{x}[n|n-1]$$

2. When the ball position is flashed on screen, the spatial observation is used to update the ball position estimate via the observer gain L^s :

$$\begin{aligned}\hat{x}[n|n] &= \hat{x}[n|n-1] + L^s[n](y_s[n] - \hat{x}[n|n-1]) \\ &= \hat{x}[n|n-1] + L^s[n](\Delta x[n] - \Delta \hat{x}[n|n-1] + \eta_s[n])\end{aligned}$$

CHAPTER 5. SPATIAL AND TIMING CONTROL ARE SEPARABLE

3. After the ball flashes it descends (invisibly to the participant) and, using this most current estimate, the juggler determines a velocity at which to swing the paddle according to a control policy:

$$u[n] = K\hat{x}[n|n]$$

4. After swinging the paddle, the juggler receives simultaneous audio and haptic feedback (an assumption enforced in reality due to the stock delay in audio-haptic feedback, Chapter 4). Since this feedback is not a function of ball velocity, we assume it provides (only) a timing cue (and not a spatial cue). Because this feedback arrives after the selection of action $u[n]$ (an assumption enforced by the design of our experiment), it informs a delayed update to ball state estimation via an observer gain, L^t :

$$\begin{aligned}\hat{x}[n|y_t[n+1], n] &= \hat{x}[n|n] + L^t[n+1](y_t[n] - \hat{t}_{\text{desc}}[n]) \\ &= \hat{x}[n|n] + L^t[n+1]C_t^s(x[n] - \hat{x}[n|n] + \eta_t[n])\end{aligned}$$

5. The next cycle's ball peak position is predicted by incorporating timing feedback into a forward model of the juggling physics.

$$\hat{x}[n+1|n] = A\hat{x}[n|y_t[n+1], n] + Bu[n]$$

CHAPTER 5. SPATIAL AND TIMING CONTROL ARE SEPARABLE

In the above framework, the estimator gains L^s and L^t , respectively describing how spatial feedback and timing feedback are used to update the juggler's estimate of ball position, are assumed constant. This formulation extends without loss of generality to adaptive estimators that have reached steady state, such as Kalman filters, which have a Bayesian interpretation [130]. This assumption is reasonable because jugglers are trained extensively through 1 - 1.5 hours of practice in Session 1, such that they achieve a consistent level of accuracy and behavior that has signatures of a steady state of performance. In addition, the first several juggling cycles are omitted from analysis to eliminate transients.

During stable ball juggling, if the human brain and musculoskeletal system behaved linearly around the nominal goal, there would be a direct relationship between frequency content of a given sensory input and of motor output via a frequency-dependent scaling, encapsulated in the transfer function, $H[z]$. In the context of ball juggling, this relationship can be expressed in the following frequency-domain equation, where spatial or timing perturbations at a given frequency (captured in the variable z) are represented by $N_s[z]$ or $N_t[z]$:

$$X[z] = H_{CL}^s[z]N_s[z] + H_{CL}^t[z]N_t[z] \quad (5.3)$$

Assuming unbiased spatial and timing estimators L^s and L^t (e.g. Kalman filters) that have reached a steady state over a juggling session, it can be shown that the

transfer functions have the following forms:

$$H_{\text{CL}}^s[z] = \frac{z^{-1}BKL^s}{I - z^{-1}(A + BKL^s) - z^{-2}\left[BK\left(\hat{A} - \hat{B}KL^s\right) + BK\left(L^s\hat{A} + \hat{B}K\right)\right]}$$

$$H_{\text{CL}}^t[z] = \frac{BK\left[I - L^s\right]\hat{A}L^t}{I - z^{-1}(A + BKL^s) - z^{-2}\left[BK\left(\hat{A} - \hat{B}KL^s\right) + BK\left(L^s\hat{A} + \hat{B}K\right)\right]}$$

According to this model—which assumes that both spatial and timing feedback are incorporated into a spatial estimate of ball position—we expect the correlations between *either* type of perturbation and ball position to be statistically equivalent (see Appendix C). This prediction can be tested by applying sinusoidal perturbations to spatial feedback and the timing of event feedback (simultaneous audio and haptic pulses at collisions, and ball flash onsets at apices). Because sinusoidal perturbations allow us to concentrate stimulus energy at various frequencies, we can further test whether this equivalence, if any, holds throughout the sensorimotor bandwidth.

5.3 Experiment

We recruited $n = 10$ participants (ages 18-27, mean = 22.7 years; 3 females), who were right-handed [144] and naïve to paddle juggling. Experiments were carried out in accordance with protocols approved by the Johns Hopkins Institutional Review Board (IRB). Prior to all experiment sessions, participants provided written informed

CHAPTER 5. SPATIAL AND TIMING CONTROL ARE SEPARABLE

consent per IRB guidelines.

Each experiment comprised 3 sessions. Session 1 was a training session as described in Chapter 4. During Sessions 2 and 3, peak phase feedback was provided as ball flashes about peaks, and collision phase feedback as simultaneous 10-ms haptic and audio cues at collisions. We perturbed spatial feedback by adding a height offset to ball feedback ($\eta_s[n]$ in Figures 5.1A, C), so that during each affected cycle, the representation of the ball was higher or lower than the veridical position. We perturbed timing by adding a delay to the display of collision and visual events, on top of a 33 ms delay bias ($\eta_t[n]$ in Figures 5.1A, D). Perturbation amplitudes were restricted to below this delay bias magnitude, to assure that even for temporal advances, the haptic feedback event would occur after ball–paddle collision and not interfere with the hand movements at impact [10]. Because all event feedback from the beginning included this 33-ms delay, we assume subjects perceptually adapted to it so that it did not affect their motor responses.

Perturbations varied sinusoidally over juggling cycle number (Fig. 5.1A) following a period of 25 juggling cycles without perturbation, and 25 juggling cycles of ramping to full amplitude. Full perturbation strength was sustained for over 40 cycles so that discrete-time Fourier transforms could be computed without leakage [145]. Perturbations varied by cycle number n and were applied to spatial ($\eta_s[n]$) or event timing

$(\eta_t[n])$ feedback as follows:

$$\begin{aligned}\eta_s^{sine}[n] &= 0.03 \sin\left(\frac{2\pi n}{N_p} + \phi_p\right)[m] \\ \eta_t^{sine}[n] &= 0.03 \sin\left(\frac{2\pi n}{N_p} + \phi_p\right) + 0.033[s]\end{aligned}\tag{5.4}$$

Here $p = 1, 2, \dots, n_{\text{freq}}$ is the perturbation index number; n_{freq} is the total number of frequencies tested; $\phi_p = \frac{2\pi k}{40}$ is the phase offset for each sinusoid, where k was pseudorandomly selected from $1, 2, \dots, 40$; and $N_p = \frac{2}{40}, \frac{7}{40}, \frac{13}{40}, \frac{17}{40}$ is the period of the perturbation in perturbation cycles per juggling cycle. For intuition on the timescale of these perturbation periods, assume that the juggling period is about 0.5 s, in which case the perturbations repeat every 10 s, 2.86 s, 1.54 s, and 1.18 s, respectively.

5.4 Data Analysis

Time-domain data extraction

For each participant, we analyzed two response variables: the veridical ball position (displayed minus perturbation), and the velocity trajectory of the virtual paddle (equal to the velocity of the hand). Paddle velocities were analyzed cycle-by-cycle by sectioning them into intervals bounded in time by consecutive ball–paddle collisions. Because the period of each cycle varied, we linearly interpolated paddle velocity between two consecutive collision times, $[t_{\text{coll } i}, t_{\text{coll } i+1}]$ and converted to a common

phase axis $[0, 360]$.

To account for the possibility that the response to event timing perturbations may not manifest in ball apex positions or velocity magnitudes, we considered an additional variable related to timing—the shift of the paddle relative to the actual collision time for a given cycle, in seconds. This variable was computed as the timing of the first crossing of the 95% maximum velocity point, coinciding with upward paddle movement during collision events [104, 126]. This avoids the noisy estimates that are typical when identifying the time of extrema events [146].

Consistent with our modeling framework in terms of deviations from nominal juggling behavior, all behavioral variables were analyzed with respect to their mean value. For sinusoidally perturbed trials, this mean was computed within the 40-cycle window between cycles 51 and 90, after full perturbation strength was applied; and for step perturbed trial.

Estimating transfer (frequency-response) functions

To estimate transfer functions, we used a frequency domain-based system identification approach of adding sinusoidally varying perturbations to sensory feedback of the juggling task (Eqn. 5.4) and measuring motor output. From an information processing perspective, this corresponds to measuring how the nervous system responds as the sensory inputs are manipulated at specific frequencies within the sensorimotor bandwidth.

CHAPTER 5. SPATIAL AND TIMING CONTROL ARE SEPARABLE

For each sinusoidally perturbed trial, we first performed a pre-processing step of windowing off each time-domain perturbation and response signal between cycles 51 and 90 (using rectangular windows), and subtracting the corresponding means across this interval: this converted all perturbations and motor responses into deviations about the nominal for the trial.

We then calculated discrete Fourier transforms (DFTs) of these windowed signals in MATLAB (The MathWorks, Natick, MA) using the Fast Fourier Transform. Transfer function estimates (sometimes called frequency-response functions, or FRFs) were computed using standard methods: for each stimulus frequency, the DFT of the output behavior was divided by the DFT of the perturbation at that frequency, resulting in a N_p -point estimate of the FRF corresponding to the number of unique stimuli. Mean FRF values were computed by averaging raw (complex-valued) DFT values and then computing magnitude and phase (translated to a $[-300, 60]$ degree domain). Dispersions of magnitude and phase responses were determined by computing DFTs of individual measurements at each stimulus frequency and performing either of the following operations: (1) computing a range from the minima and maxima of the magnitude and phase responses, or (2) calculating standard error, based on bootstrap resampling among individual magnitude and phase responses. The type of dispersion measurement used is identified case-by-case in each figure.

Estimating spectral coherence

Defining $N[z]$ to be the DFTs of either perturbation and $X[z]$ to be that of either output behavior, coherence [147] is calculated as:

$$C_{\eta, x}[z] = \frac{|G_{\eta, x}[z]|^2}{G_{\eta, \eta}[z]G_{x, x}[z]}$$

$|G_{\eta, x}|$ is magnitude of the cross-spectral density between the perturbation $\eta[n]$ and motor output $x[n]$, and $G_{\eta, \eta}$ and $G_{x, x}$ are respectively the power spectral densities of the perturbation and output. In the absence of noise, variables that are related by a (linear) transfer function have a coherence of 1; thus coherence is a measure of a system's linearity [15, 17]. If our model in Eqn. 5.3 correctly captures the system dynamics, we would expect that by separately perturbing spatial ($N^s[z]$) or timing ($N^t[z]$) feedback, we would see comparably high coherence to either type of perturbation. Therefore, measuring and comparing coherence enables us to test our hypothesis that spatial and timing information are incorporated indistinguishably into ball position control. A systematic and significant differential effect on coherence based on input modality would be evidence of a different control structure where distinct but complementary states are driven by spatial and timing feedback respectively (Fig. 5.1).

5.5 Results

The purpose of Experiment 1 was to test the hypothesis that spatial and timing perturbations have statistically equivalent effects on the spatial variable of ball position. For each subject, we analyzed two response variables: the actual unperturbed ball bouncing trajectory (unseen by subjects), and actual hand velocity to control the virtual paddle.

While some participants incidentally commented that their ease of hitting the height target appeared to vary throughout the experiments, there was no pattern to when they made these comments, or which perturbation conditions tended to elicit them. Participants expressed no awareness of the onset and nature of perturbations.

Spatial and timing regulation exhibit linearity

Figure 5.2 demonstrates the response of a typical juggler to slow and fast sinusoidal perturbations of both spatial feedback (Fig. 5.2A) and event timing (Fig. 5.2B). Under slow spatial perturbations (2 perturbation cycles / 40 juggling cycles, left panel of Fig. 5.2A), participants hit the displayed ball to the goal line on average (blue line), but oscillated noticeably above and below the target per cycle. Hence, the observed ball error failed to converge to zero.

Timing perturbations (Fig. 5.2C, D) were implemented as fluctuating delays of feedback with respect to veridical physics. We examined the timing of paddle movements, as reflected as phase shifts with respect to peak velocity. Similar but weaker

CHAPTER 5. SPATIAL AND TIMING CONTROL ARE SEPARABLE

magnitudes of timing behavior are observed at higher perturbation frequencies (7 perturbation cycles per 40 juggling cycles, left panel, Fig. 5.2D).

In light of the strong correspondences between spatial perturbations and actual ball position, and between temporal perturbations and paddle timing shifts, we examined these signals in the frequency domain as a test of linearity. Spectral power of ball position was almost exclusively concentrated at spatial perturbation frequencies (Fig. 5.3A), while spectral power of paddle timing shifts were almost exclusively concentrated at timing perturbation frequencies (Fig. 5.3B). These correspondences signify that there are strong correlations between ball position and spatial feedback on one hand, and paddle timing and event timing perturbations on the other.

Spatial and timing control are dissociable

Previous research suggests that rhythmic task control, for tasks such as juggling, is purely spatial, and that ball position is the primary control variable of interest [125, 132]; were this true—and the role of timing feedback could be sufficiently described via a mapping to spatial ball position—paddle juggling could be sufficiently described as a multiple-input, single-output system where perturbations to both spatial and timing feedback are equivalently correlated to ball position. We tested this hypothesis by computing the spectral coherences of each stimulus–response pair at all frequencies. For each test frequency, the mean coherence of spatial perturbation with ball position was greater than with paddle timing shift (Fig. 5.3C). Conversely,

CHAPTER 5. SPATIAL AND TIMING CONTROL ARE SEPARABLE

for each test frequency of timing perturbations, coherences with paddle timing shifts were greater than with ball positions (Fig. 5.3D).

Analysis of variance (ANOVA) reveals that for spectral coherence, there was a significant interaction between type of perturbation and behavioral response ($F = 81.04$, $p < 0.005$), suggesting that spatial or timing perturbations have dissociable effects on behavior. Within each perturbation modality, there was a main effect of behavioral response ($F = 25.26$, $p < 0.001$ for spatial perturbations, $F = 57.32$, $p < 0.001$ for timing perturbations), but not for perturbation frequencies, indicating that differences in correlation were primarily driven by stimulus type. Post-hoc comparisons of spatial perturbation trials (Tukey's HSD test) showed that coherence with ball height was higher on average than with paddle timing for all frequencies, reaching statistical significance for frequency 13 stimulus cycles / 40 juggling cycles ($p < 0.001$). Conversely, the same analysis for timing perturbation trials showed that coherence with paddle time shift was significantly higher than with ball height for all frequencies ($p < 0.001$ for frequencies 2/40 and 7/40; $p < 0.05$ for frequencies 13/40 and 17/40). Altogether, these analyses shed light on the nature of the differential effect of perturbation type on behavior: spatial perturbations induce coherent responses in a spatial behavior (namely ball bounce height), and timing perturbations induce coherent responses in a separate timing-related behavior (paddle shifts).

When we examined the *actual* ball position (as opposed to displayed), jugglers showed a propensity to hit the oscillations anti-phase to the perturbations (red line),

CHAPTER 5. SPATIAL AND TIMING CONTROL ARE SEPARABLE

as if to cancel them out (5.2B). As perturbation frequencies increase (7 perturbation cycles per 40 juggling cycles in right panel, 5.2B), response weakens (magnitude decreases). We observed that jugglers not only shift the timing of peak paddle velocity at the frequency of perturbation (Figure 5.2B), but do so *in-phase* with perturbations.

Response magnitudes in dB measure the relative sensitivity (in a colloquial sense) of output behavior to input stimuli of various frequencies. The magnitude responses of both Bode plots show that motor output sensitivity becomes progressively weaker with increasing stimulus frequency, coinciding with the observation that behavioral response in the time domain diminished with perturbation frequency (Fig. 5.3). Response magnitudes (Fig. 5.3C,D; gain plots) monotonically decrease as frequency increases; that is, they are low-pass. By inspection, the rate of decrease of the spatial response is slower than for the timing response, suggesting the bandwidth of the spatial closed-loop behavior is smaller than that of the timing closed-loop controller.

The phase shifts (lower panels), however, are markedly different. The phase response of the spatial frequency-domain plots shows a phase lag indicative of perturbation rejection, consistent with the anti-phase behavior shown in Figure 5.2A. For timing perturbations however, paddle time shifts are in-phase with timing perturbations, indicating entrainment.

5.6 Discussion

Rhythmic tasks such as paddle juggling are widely assumed to be predominantly visuospatial in nature, and all previous analyses, to our knowledge, consider the controlled states of interest to be spatial and ultimately map to ball position. Although it is generally observed that haptic or audio feedback cues are sufficient for stable performance [6], or conducive to task control [10] or learning [148], their influence on movement—particularly rhythmic—is poorly understood.

Both spatial and timing feedback perturbations impact human behavior. We hypothesized that spatial and timing feedback are fused into a common estimate of ball movement; our results falsify this concept. Rather, two distinguishable responses are observed: (1) out-of-phase corrections (compensation) of spatial perturbations and (2) in-phase movement paddle adjustments (entrainments) to timing perturbations. These patterns generalized across individuals, despite the fact that they were not informed of the existence of perturbations and experienced them only implicitly through feedback.

Previous studies, under an assumption of sinusoidal paddle trajectories, have considered phase of paddle movement (but not timing) as a behavioral state during juggling [125], while others have observed a general correlation between overall paddle and ball periods [7]. However, our study reveals that paddle timing may be a separately controlled variable driven by the timing of feedback events, with a control objective reflecting synchrony (judging by the in-phase response of Bode plots in

CHAPTER 5. SPATIAL AND TIMING CONTROL ARE SEPARABLE

Fig. 5.3).

This finding is consistent with observations in the temporal discrimination literature that suggest that, in the presence of temporally conflicting visual and auditory information, human perception of timing is biased in the direction of audition. We investigate the dynamics of these seemingly different processes in a follow-up experiment discussed in Chapter 6.

CHAPTER 5. SPATIAL AND TIMING CONTROL ARE SEPARABLE

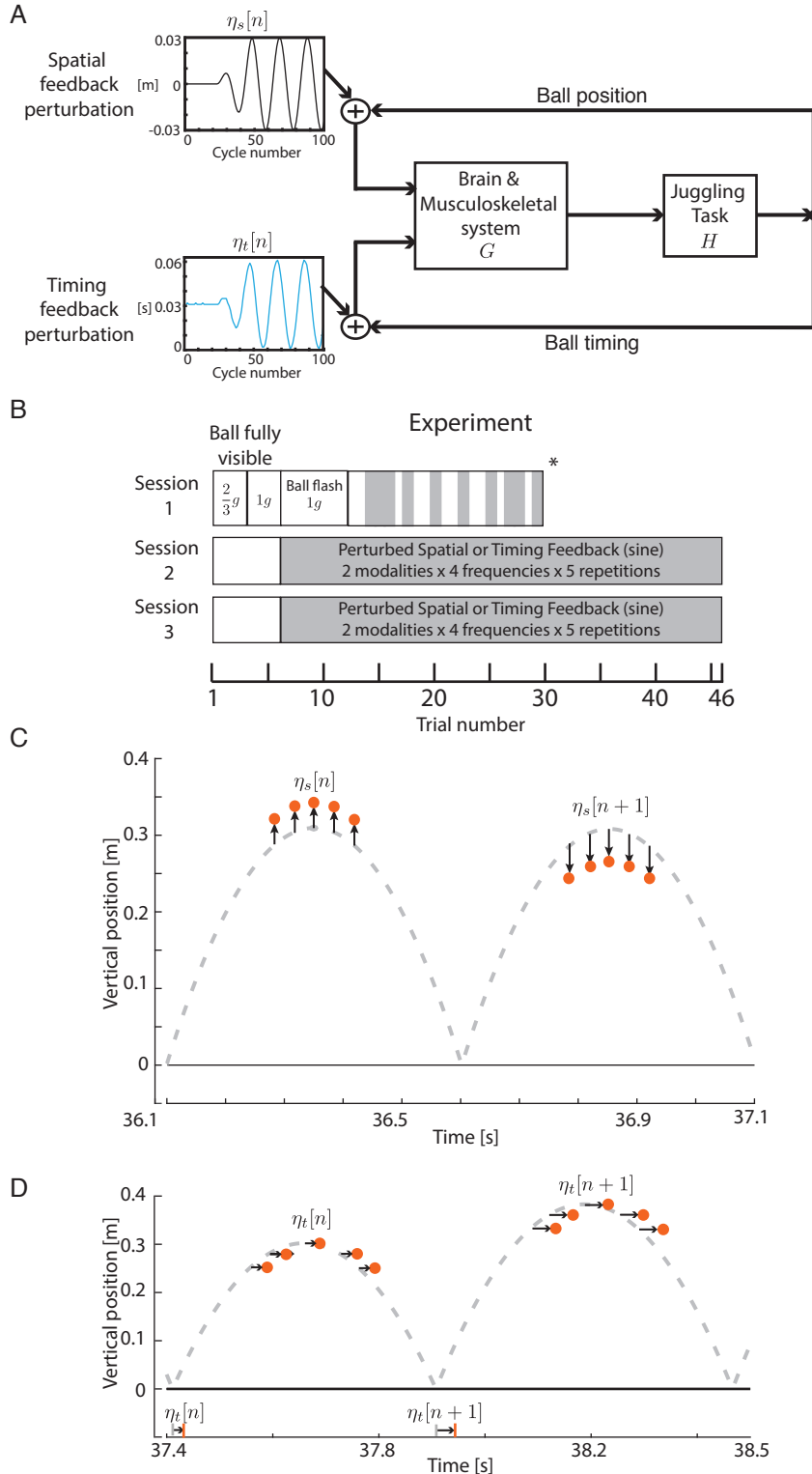


Figure 5.1: Overview of Experiment 1. (A) Perturbation schema (spatial, and event timings). Block diagram represents general information flow between juggler (G) and task (H) dynamics. (B) Experimental structure. Session 1 was a training session (see Chapter 4). Sessions 2 and 3 included sinusoidal perturbations with equal numbers of spatial and timing perturbations per session. (C,D) Example perturbations of spatial (C) or timing (D) feedback.

CHAPTER 5. SPATIAL AND TIMING CONTROL ARE SEPARABLE

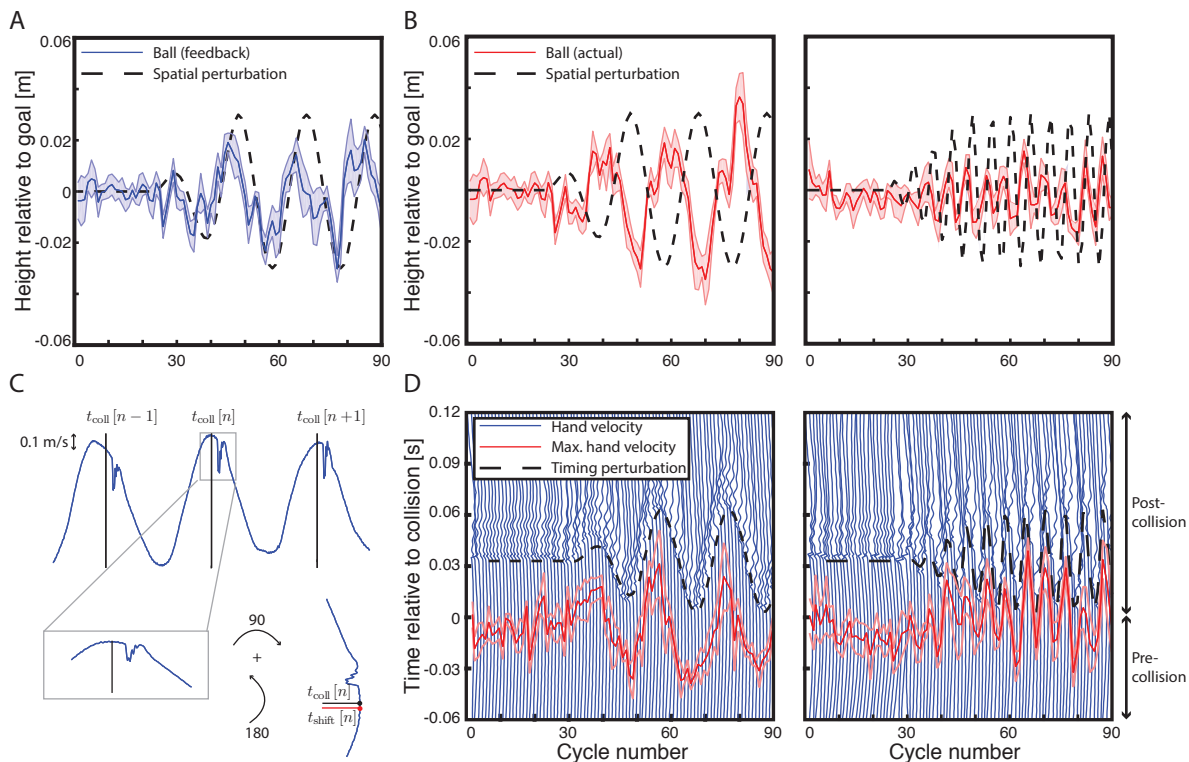


Figure 5.2: Time-domain responses to spatial and temporal perturbations. Data in panels A, B, and D is averaged across 5 trials for 1 juggler (mean ± 1 s.e.). Perturbations in all panels are shown in dashed black lines. All frequencies are in perturbation cycles per juggling cycle. (A) Visual feedback of ball peak height relative to goal (sinusoidal perturbation, 2/40). (B) Actual ball height for perturbation stimuli of frequencies 2/40 (left) and 7/40 (right). (C) Paddle (hand) velocities for timing response. For plotting, velocity curve is partitioned around peak velocities for each cycle, rotated, and lined by increasing cycle number along the x axis to form a contour plot (D). (D) Velocity contour is ridged where haptic and audio (i.e. timing) feedback is applied. Red curves show location of maximum hand velocity relative to collision time for perturbation frequencies 2/40 (left) and 7/40 (right).

CHAPTER 5. SPATIAL AND TIMING CONTROL ARE SEPARABLE

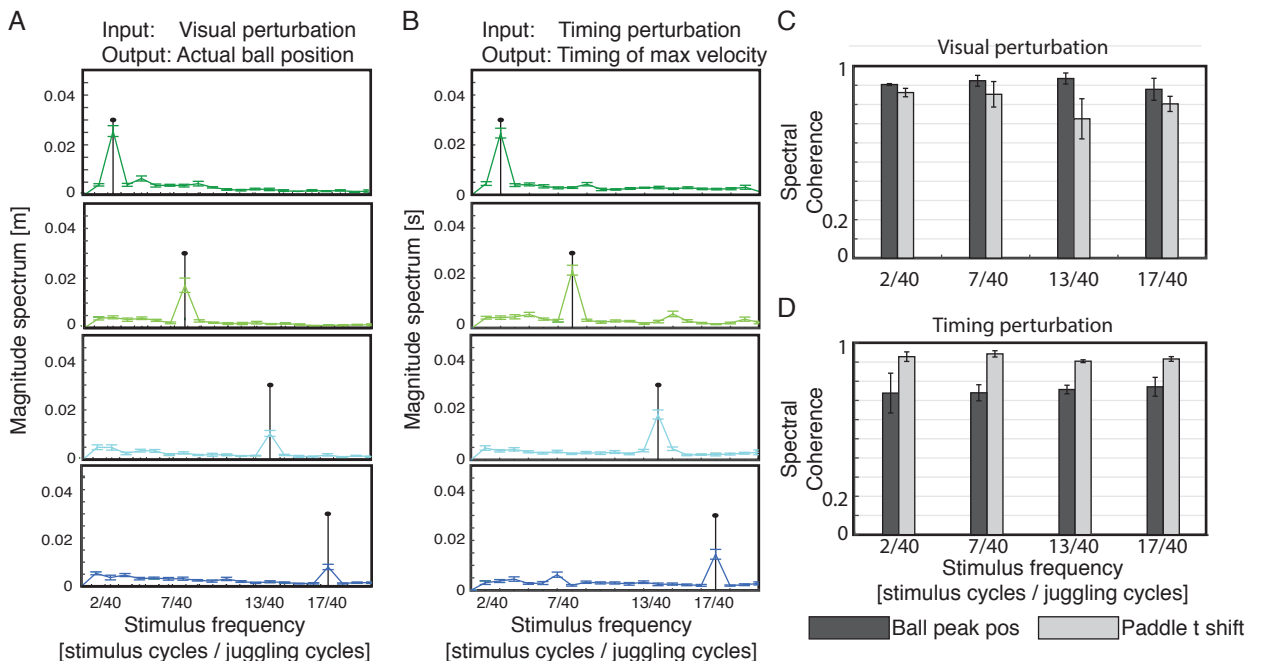


Figure 5.3: Experiment 1: Frequency-domain analysis of perturbation responses. (A, B) Magnitude spectra of spatial and timing responses to spatial or timing perturbations (black stems). Responses are averaged over all participants ($n = 10$; bars are ± 1 s.e. estimated by statistical bootstrap). (A) Magnitude spectra of visual perturbation and actual ball position. (C, D) Spectral coherence between spatial (C) and timing (D) stimuli and both ball position and paddle timing responses.

Chapter 6

Dynamics of Spatial and Timing

Control

6.1 Introduction

In Chapter 5, we presented evidence that spatial and timing perturbations invoke separable correction mechanisms. However, as the identification method relied on windowed Fourier analysis, it has poor timing resolution and therefore limited utility for parsing cycle-by-cycle dynamics. This shortcoming is addressed in the follow-up experiment described in this chapter, which utilizes both sinusoidal and step perturbations.

Step perturbations enable the use of model-selection and model-fitting methods to assess the time-domain dynamics and ultimately develop parametric models of the

spatial and timing-based closed-loop methods employed by the nervous system. We test the following hypotheses. (1) Spatial and timing control have distinct dynamics, a premise that would be validated if we were to apply model selection processes to the data of spatially and temporally perturbed feedback and reveal different optimal models. (2) Distinct dynamics, if found, are analogous to the control of other tasks involving spatial and timing regulation, and these tasks might involve different brain networks.

6.2 Experiment

Experiments were carried out in accordance with protocols approved by the Johns Hopkins IRB. Prior to all experiment sessions, participants provided written informed consent per IRB guidelines.

A total of $n = 16$ right-handed participants [144] were recruited (5 in common with Experiment 1; ages 18-33, mean = 24.4 years; 8 females). The gross structure of Experiment 2 (Fig. 6.1) paralleled that of Experiment 1 with the following within-session differences: (1) perturbations were exclusively either spatial or temporal (with order counterbalanced across sessions); (2) the 40 perturbation trials were evenly divided into 20 sinusoidal perturbations and 20 step perturbations intermixed in random order. Sinusoidal perturbations were as in Eqn. 5.4 in Chapter 5. Step perturbations were ± 0.04 m for spatial (corresponding to sudden positive or nega-

tive jump in displayed ball position), and ± 0.03 s for temporal (corresponding to an advanced or delayed display of feedback), as in Eqn. 6.1:

$$\eta_s^{step}[n] = \begin{cases} 0 & n \leq N_d \\ \pm 0.04 & n > N_d \end{cases} \quad [m] \quad (6.1)$$

$$\eta_t^{step}[n] = \begin{cases} 0.033 & n \leq N_d \\ 0.033 \pm 0.03 & n > N_d \end{cases} \quad [s]$$

Here N_d is a delay (in the total number of juggling cycles) uniformly distributed between 15 and 20 relative to the beginning of the trial.

6.3 Methods

The overall method is to analyze step-perturbed and sinusoidally perturbed behavior in a two-pronged approach.

Given evidence that closed-loop behavior could be described by a linear (discrete-time) system (Chapter 5), we assumed that closed-loop behavior was encompassed by the set of rational-polynomial models [149]. Assuming this general class of models, we performed an initial *model selection* procedure to determine the model order (in terms of number of poles and zeros) that achieved the best balance of model accuracy and reliability (“consistency” in the colloquial sense). Once this model was selected,

a *model fitting* procedure was performed for individual jugglers, in which specific parameters within this model form were determined. We presently elaborate on each stage of this analysis.

Signal analysis / preprocessing

As in Experiment 1 (Chapter 5), we analyzed two response variables for each participant: the veridical ball position (displayed minus perturbation), and the time shift of the paddle for a given cycle, as determined from hand velocity.

Analyzed trials featured either sinusoidal or step perturbations. Sinusoidally-perturbed trials were analyzed using a windowing method described in Chapter 4. Step-perturbed trials were likewise analyzed with respect to their mean value, here defined within a 7-cycle frame prior to the perturbation. Given the results of Chapter 5, we considered ball position as the dependent variable of spatial regulation, and paddle time shift as the dependent variable of timing regulation.

Candidate models

All model fitting was performed in the time domain using step responses. Controller candidate models were chosen among frequency response functions of rational

CHAPTER 6. DYNAMICS OF SPATIAL AND TIMING CONTROL

polynomial form [149]:¹

$$G_{\text{Ctrl}}^{M,N}[z] = \frac{U[z]}{Y[z]} = K \frac{\prod_{m=1}^M (z - a_m)}{\prod_{n=1}^N (z - b_n)}, \quad N \geq M \quad (6.2)$$

Here $z = \exp\{-j\omega\}$ is a complex-valued function of the stimulus frequency ω (radians / s), and there are $N + M + 1$ real-valued scalar parameters, K , a_m , and b_m . The causality constraint $N \geq M$ guarantees that outputs are never dependent on future inputs.

Each of these candidate controllers was placed inside a closed-loop system based on our block diagram of paddle juggling in the previous chapter (repeated in Fig. 6.1A). From this diagram, a closed-loop transfer function, relating perturbation input to behavioral output, can be calculated thus:

$$G_{\text{CL}} = \frac{G_{\text{plant}}G_{\text{ctrl}}}{1 + G_{\text{fdbk}}G_{\text{plant}}G_{\text{ctrl}}} \quad (6.3)$$

Here G_{ctrl} is defined in Eqn. 6.2, and G_{fdbk} corresponds to the feedback gain associated with a given sensory modality. It is of unity gain with a sign reflecting whether the closed-loop behavior suggested negative feedback control (error correcting) or positive feedback control (entrainment). Specifically $G_{\text{fdbk}} = -1$ for spatial control

¹Technically, such a factorization assumes that all poles and zeros are real-valued, which eliminates closed-loop systems exhibiting behavior that is oscillatory in cycle number, particularly as MATLAB's search space for optimization functions is the real domain. However, this was deemed not to be a critical limitation because (1) a more general transfer function expression consisting of unfactored polynomials did not lead to better fits; and (2) this factorization allows for boundaries to be placed on parameter search spaces in Matlab, which are easier to enforce than nonlinear constraints.

and $G_{\text{fdbk}} = 1$ for timing control.

G_{plant} , the plant transfer function, assumes one of two forms depending on the stimulus-response pair considered: spatial perturbation—[actual] ball position ($N_s[z], X[z]$); or timing perturbation—paddle (hand) timing shift ($N_t[z], T_{\text{shift}}[z]$). For the spatial case, the plant is described by the the (linearized) juggling dynamics relating paddle velocity to ball apex height in Eqn. (5.1), assuming that participants are skilled enough to hit the ball to a consistent height and achieve near-limit-cycle behavior. This can be expressed in the frequency domain as follows (derived in Appendix C):

$$G_{\text{plant}} = \frac{b^* (1 + \alpha)z}{g (z - \alpha)} \quad (6.4)$$

For the temporal case, we adopt a parsimonious plant model of $G_{\text{plant}} = 1$, since we are taking timing of the motor command directly as the motor output and ball-paddle collision always occurs at the same height.

Statistical analyses and model fitting

All statistical analyses and model selection procedures were performed on subject-averaged data in MATLAB. Because the sensorimotor behavior being modeled was strongly suspected to be linear (see Chapter 5), two options were considered—frequency-domain fitting of FRFs, or time-domain fitting of step responses. A model fit to either

CHAPTER 6. DYNAMICS OF SPATIAL AND TIMING CONTROL

domain was expected to be equivalent to a fit in the other domain.² Thus, one indicator of the underlying truth of a model fit was its ability to cross-validate from one domain to the other.

Fits were initially performed on bootstrap-sampled FRF averages in MATLAB by means of the `fmincon` function, using a least-squares cost function.³ While the frequency-domain-based fitting approach was successful in other studies [16, 150], when applied to the human data gathered in this experiment, it was unable to yield fits that cross-validated to the time domain. There was also core difficulty in fitting to low-gain, high-band frequency data. Weighted cost functions could not overcome the poorness of these fits and their cross-domain validation results. The problem seemed to be rooted in the lack of proper constraints: when cost functions were plotted, they were relatively flat, lacking clear minima. This was reflected in the fact that bootstrap-resampled solutions formed hyperbolic solution surfaces, suggesting the data was underconstrained, with many solutions showing signs of biological infeasibility (e.g. weightings that greatly exceeded 100 percent).

To improve cross validation to the time domain, while still fitting to the frequency domain, we next tried to impose nonlinear inequality constraints to enforce closed-loop stability,⁴ Final-Value-Theorem, and Initial-Value-Theorem constraints. However these additional constraints did not materially improve fits: resulting solutions

²Depending on the region of convergence of the Z transform

³Of form $J = \Sigma(\hat{H}[z] - H[z])^2$

⁴eigenvalues of closed loop transfer function ≤ 1

CHAPTER 6. DYNAMICS OF SPATIAL AND TIMING CONTROL

did a poor job of predicting the step response between its initial and final points, and MATLAB appeared to only softly enforce constraints that were not explicit bounds on parameter search spaces.

Ultimately, we chose an alternate approach of model fitting to step responses in the time domain, since a least-squares fit in this domain would naturally obey all of the above constraints. We minimized the squared Euclidean norm of the error between the measured [closed-loop] step response $x[n]$ and \hat{x} estimated from simulating the step response of $H_{CL}[z]$.

$$J = \sum_{N_d-7}^{N_d+30} (\hat{x}[n] - x[n])^2$$

$$\hat{x}[n] = \eta_s^{step}[n] * \hat{h}_{cl}[n]$$

Here, the convolution operation was implemented using `lsim` in Matlab (replacing $\hat{h}[n]$ with $G_{CL}[z]$ determined from selecting a hypothetical model of Eqn. 6.2 and plugging into Eqn. 6.3).

We close with remarks about the failure of direct FRF fitting for this data. A possible explanation is that other studies where this fitting was more successful [16, 17, 150] involved more densely sampled frequency spectra through the use of sum-of-sines stimuli that allowed multiple frequencies in the FRF to be probed within a single trial. However, as discussed in Chapter 4, we suspect that variability, or “noisiness”, is much greater for the paddle juggling task than for these other tasks (whole body movements of animals), such that sum-of-sines stimuli would not have elicited detectable behavioral responses for this task.

Model selection

Model selection was based on a method outlined in [16], which balances model accuracy and inter-person reliability (“consistency” in the colloquial sense), summarized here. For each model and each given step perturbation, a training data set was generated by averaging the step responses across all data, minus one participant (set aside as a test data point). The parameters of the model were optimized in a least-squares error sense, and a leave-one-out cross validation error was computed as the squared error of this optimal fit against the average of the excluded participant’s data (test set). This process was repeated for each participant, to generate distributions of cross-validation errors and optimal parameter fits. Model accuracy was determined as the average cross-validation error across participants, while reliability was determined as the maximum singular value across the ensemble of optimal parameter sets.

Assessment of model quality was an iterative process where a model of the form in Eqn. 6.2 was chosen and placed in a transfer function of form in Eqn. 6.3; a step response was simulated under an initial set of model parameters (K, a_m, b_n) ; goodness of fit was computed between the simulated step response and the averaged behavioral step response from step perturbation trials (in terms of least-square error); and model parameters (K, a_m, b_n) to minimize least-square error were determined via nonlinear optimization (fmincon in MATLAB). This process was repeated for all models of complexity up to 5 free parameters (a gain K and $(M, N) = (1, 3)$). The optimal model was determined to be the one that maximized accuracy and reliability; that is,

minimized both the cross-validation error and the singular value.

6.4 Results

Spatial control is proportional–integral

Coherence analysis (Fig. 5.3) suggests that spatial- and timing-based control affect ball position and paddle timing selectively. Time-domain behavior (Fig. 5.2) further implies that jugglers hit the ball to counter spatial perturbations, but adjust their hand movements to follow timing perturbations. We sought to determine the feedback control structure of spatial and timing control parametrically, and with it, how the brain integrates spatial and timing feedback into movement on a cycle-by-cycle basis.

Fig. 6.2 shows that generally, models with fewer parameters tend to have less accuracy but greater inter-juggler reliability, as they tend to capture fewer nuances of data in favor of a parsimonious model. Models with higher numbers of parameters are generally more accurate, but at the cost of overfitting data, resulting in low inter-subject reliability. For spatial control (Fig. 6.2A), the best model that achieved a combination of low cross-validation error and high intersubject parameter reliability was a model of form $(M, N) = (1, 1)$. Algebraically, this corresponds to the following

discrete-time control law:

$$u[n] = b_s u[n-1] + K y_s[n] + K a_s y_s[n-1] \quad (\text{Spatial})$$

Here $u[n]$ is paddle velocity, $y_s[n]$ is ball feedback error relative to the goal; and b_s, a_s are scalar coefficients representing the influence of the previous cycle's paddle velocity and error. This corresponds to a proportional–integral (PI) Model with a leaky memory term. We also fitted to a “pure” PI model (pole = 1, of form $u[n] = b_s u[n-1] + K y_s[n] + K a_s y_s[n-1]$) and found this to be more reliable, but inferior in accuracy, likely due to underfitting data.

Timing control is proportional

Using similar methods to those above, we assessed the fit of several models to timing perturbation response (Fig. 6.2B). The optimal controller was of the form (N, M) = (0, 1), which algebraically corresponds to the following discrete-time control law:

$$t_{\text{shift}}[n] = K t_{\text{shift}}[n-1] + b_t \eta_t[n-1] \quad (\text{Timing})$$

where $t_{\text{shift}}[n]$ is paddle timing shift as defined in Fig. 5.2. This law suggests that paddle timing is chiefly a function of the previous cycle's paddle timing and the

current timing perturbation, and is hence a proportional law.

Control models predict step responses

Having determined forms of spatial and timing control laws, we proceeded to (1) estimate model parameters for individual subjects and (2) test their generalizability across time-domain and frequency-domain data.

Figure 6.3 shows average human response to spatial and timing perturbations, in both time and frequency domains. The perturbation (red), average subject response (black), and the response from the juggler models (blue) selected in Fig. 6.2 are shown. Time-domain behavior is presented as the step response to feedback that is abruptly jumped up or down by a constant value in the spatial case, or jumped forward or backward in time in the temporal case. Consistent with responses to sinusoidal perturbations (Fig. 5.2), participants attempt to cancel the perturbation in the spatial case (Fig. 6.3A, $n = 16$), while their paddle time shift is in the direction of the temporal perturbation (Fig. 6.3B, $n = 6$). The step response to spatial perturbations is in the form of a decreasing exponential ($r^2 = 0.9756$), which is a signature of a proportional-integral controller. As expected, at late time steps there is a monotonic decrease (Spearman's $\rho = -0.4320$, $p < 0.05$). Specifically, this is well approximated by a linear decrease function ($F = 5.9$, $p = 0.025$). The step response to timing perturbations exhibits signatures of a step function ($r^2 = 0.9139$), which saturates at a value lower than the perturbation magnitude. Consequently at late time steps

error appears to level off and there is no significant correlation with cycle number (Spearman’s rank test, $p = 0.22$).

Spatial- and timing-based closed-loop control are distinct, approximately linear processes

We repeated the spectral-coherence-based ANOVA from Experiment 1 on the data from Experiment 2, to verify whether spatial and timing control were still statistically dissociable. This ANOVA confirmed an interaction between stimulus modality and behavioral response ($F = 4.05$, $p = 0.047$ for spatial; $F = 7.8$, $p < 0.01$ for timing).

Combining step and sinusoidal perturbations in Experiment 2 enabled us to assess not only correction dynamics across cycle number, but frequency response of the spatial and timing controllers. These data provided a further test of the assumption that closed-loop control of spatial information (the ball) and timing information (the paddle timing) are linear. Namely, the best-fit model of each controller in the time domain should theoretically correspond to the best-fit in the frequency domain.

To assess similarity between both time-domain and frequency-domain models, we computed the frequency-domain representation of the spatial- and timing-based controllers and compared it to the frequency domain control behavior directly gathered from sinusoidal perturbation trials (Figures 6.3C and D). For conceptual clarity, these frequency domain plots map from the current cycle’s perturbation $\eta^{sine}[n]$ to

the subsequent cycle's response $x[n + 1]$ or $t_{\text{shift}}[n + 1]$.

As in Experiment 1 in Chapter 5, we computed Bode plots from the sinusoidal perturbations. Interestingly, the controllers, whose parameters were fitted in the time domain, closely align with the frequency domain responses, and fall within the ranges measured in sinusoidal-perturbation experiments. This provides further evidence that the spatial and timing-based closed-loop control are both approximately linear.

Control models specify responses of individuals

Results presented thus far represent group averaged data. To develop a distribution of the parameters, we performed statistical bootstrapping by resampling (with replacement) each subject. This process was repeated 200 times to achieve the scatter plots in Figure 6.4. The centroid of these distributions corresponds to the best-fit controller model.

For the spatial controller, our bootstrap mean estimates were $(K, b, a) = (-1.14, 0.81, 0.920)$, corresponding to a control law of:

$$u[n + 1] = 0.92u[n] - 1.14y_s[n] - 0.9234y_s[n - 1]$$

For the timing controller, our bootstrap estimates were $(K, a) = (0.7769, 0.7567)$,

corresponding to a control law of:

$$t_{\text{shift}}[n + 1] = 0.7567t_{\text{shift}}[n] + 0.7769y_t[n]$$

$|a| < 1$ is signature of a “leaky” memory process.

We asked whether controller fits were simply an emergent property across subjects, or whether they accounted for behavior observed across individual subjects. Individual best-fits for subjects (red crosses in Fig. 6.4) tend to lie along the axes of the ellipsoid of bootstrap fits, as expected. Figure 6.5 shows results for four representative subjects (A, B: spatial perturbations; C, D: timing perturbations), indicating that spatial-based and timing-based control are accurate models of subject behavior in the time domain. As shown (left column), they also align with frequency domain estimates, suggesting both control processes are linear among individual subjects.

6.5 Discussion

In this experiment, we interrogated the spatial- and timing-based controllers by introducing abrupt jumps (step perturbations) into visual and timing feedback, and cross validating with frequency-response functions. Our approach contrasts with previous studies which have focused predominantly on correlations between factors [3, 132] or behavior at long-term trial-averaged scales rather than short-term cycle-by-cycle resolutions [126].

CHAPTER 6. DYNAMICS OF SPATIAL AND TIMING CONTROL

The control laws we estimated are in the form of 1st order difference equations, consistent with previous studies suggesting that error correction in tasks as diverse as discrete reaching [151] and rhythmic ball bouncing [3,10,126] occurs on fast timescales (typically fewer than 3 repetitions). Specifically, the spatial correction pattern we observe in Figure 6.3 is a decaying exponential, equivalent to a class of error correction widely demonstrated in visuospatial control without explicit timing components [152]. Our model selection process determines how 1-step history of error and motor output leads to this correction pattern by way of a proportional–integral controller.

By manipulating event time feedback, we determined that timing-based control resembles a proportional control process wherein action on a given cycle depends on the previous action and the most recent feedback. Congruently, we found that responses to timing perturbations are a different class, in which behavioral corrections saturate (Fig. 6.3), indicating a ceiling in synchronization performance.

These models not only describe average subject behavior, but also capture idiosyncrasies of individual participants (Fig. 6.5). By cross-validating these models with frequency-domain system functions measured from sinusoidal perturbations, we verified our assumption that both spatial and temporal-based control of skilled (i.e. accurate) juggling are effectively linear processes.

The exponential spatial correction pattern we observe appears similar to a class of error correction widely demonstrated in visuospatial control without explicit timing components [152]. As we show, this spatial correction is achieved by a (history-

CHAPTER 6. DYNAMICS OF SPATIAL AND TIMING CONTROL

dependent) proportional–integral controller. However timing synchronization resembles a (memoryless) proportional control process, akin to models of synchronization behavior of tapping to a metronome without visual cues [153]. Such analogies may hint at cortical methods underlying the control processes discovered in our closed-loop methods, a possibility discussed in the concluding chapter of this thesis.

CHAPTER 6. DYNAMICS OF SPATIAL AND TIMING CONTROL

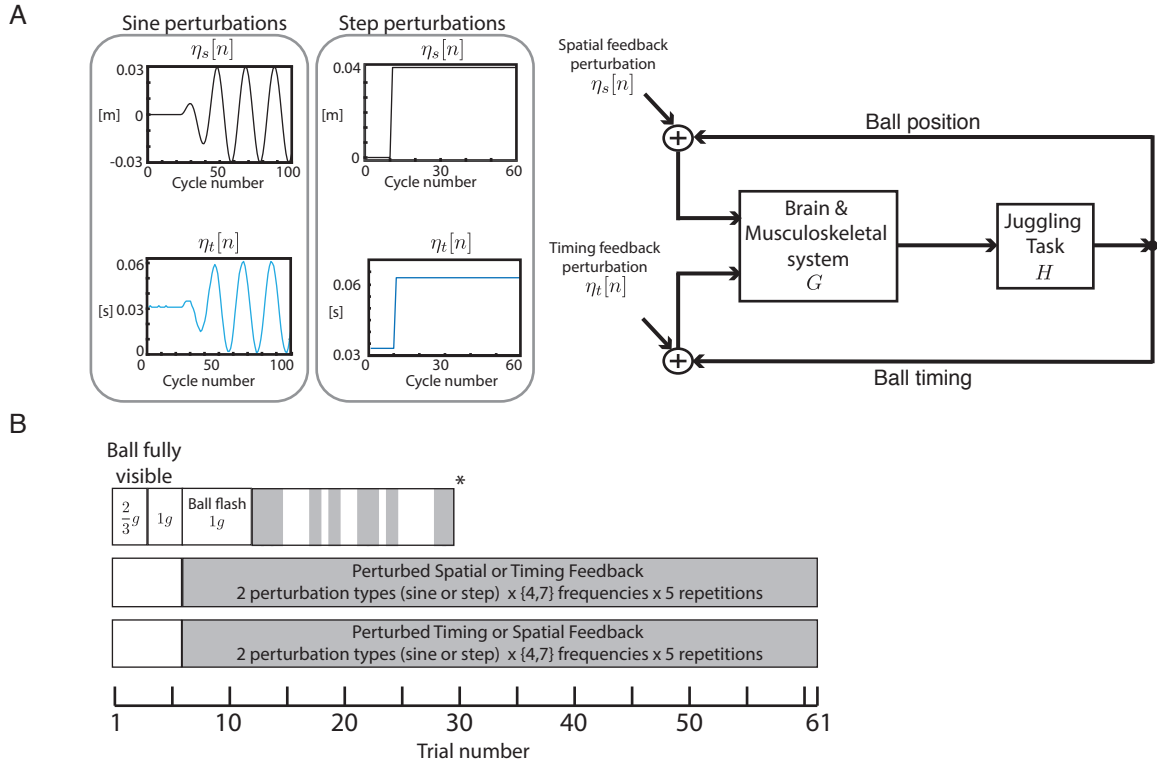


Figure 6.1: Overview of Experiment 2. (A) Ball position (spatial feedback) or event times (timing feedback) of the paddle juggling task are perturbed with offsets varying either sinusoidally or as a step function over cycle number. Block diagram represents general information flow between juggler (G) and task (H) dynamics. (B) Experimental structure. Session 1 is as discussed in Chapter 4 (*: trials varied in number based on juggler skill, but continued until end of session). Sessions 2 and 3 consisted of equal mixes of sinusoidal and step perturbations of spatial feedback in one session, or timing feedback in the other (order counterbalanced across subjects).

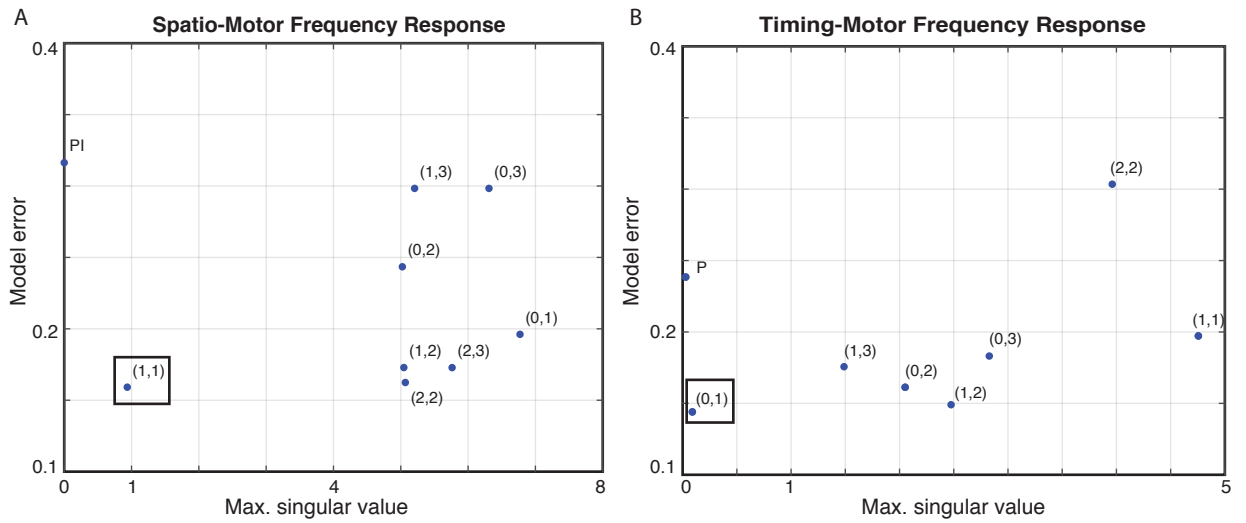


Figure 6.2: (A, B) Model selection plots for spatially based (A) and timing based (B) controllers. Plots show tradeoff between model accuracy (y-axis) and inter-person model reliability (x-axis) for various controllers, labeled in terms of number of control model parameters (M zeros, N poles of controller transfer function). Boxed data points show the models optimally balancing accuracy (y-axis) and reliability (x-axis).

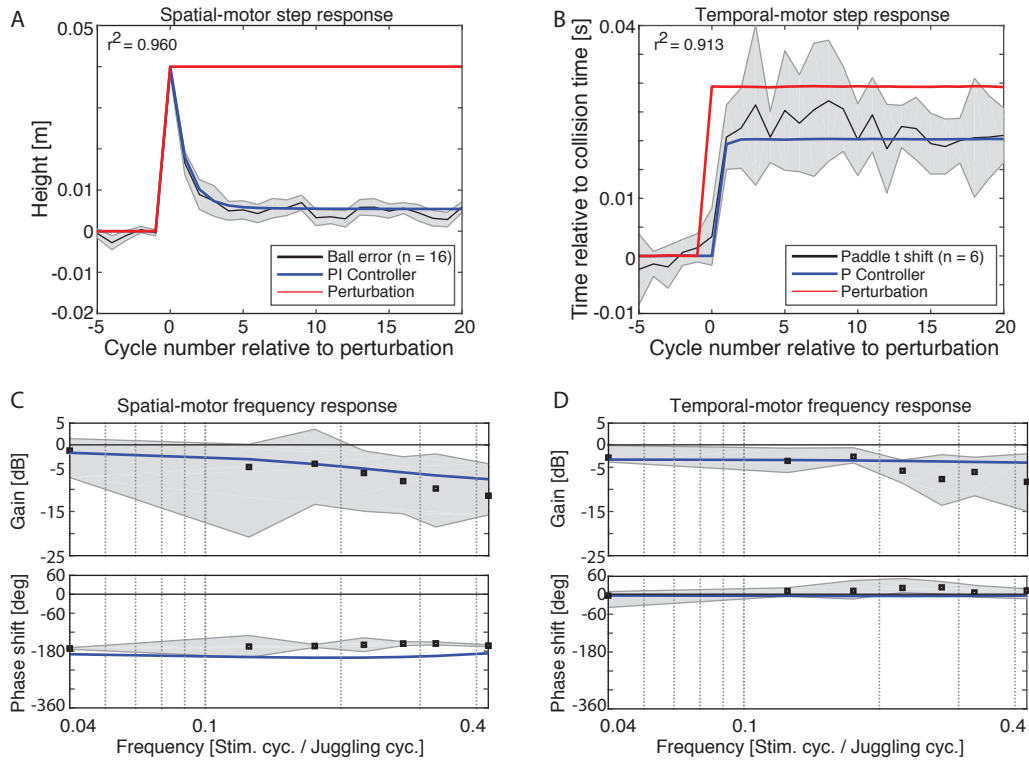


Figure 6.3: Time- and frequency-domain behavior of spatial- and timing-based controllers. (A, B) Step responses of spatial controller (A, $n = 16$) and timing controller (B, $n = 6$). Perturbations are shown in red. Black curves are averages across jugglers ± 1 s.e. Equivalent controllers (blue) are least-squares fits based on models selected in Fig. 6.2. (C, D) Frequency-response plots of spatial and timing controllers, determined from sinusoidal perturbations. Black curves are averaged across jugglers (C, D; $n = 16$). Shaded areas represent total ranges of magnitude and phase responses. Best-fit models are shown in blue lines.

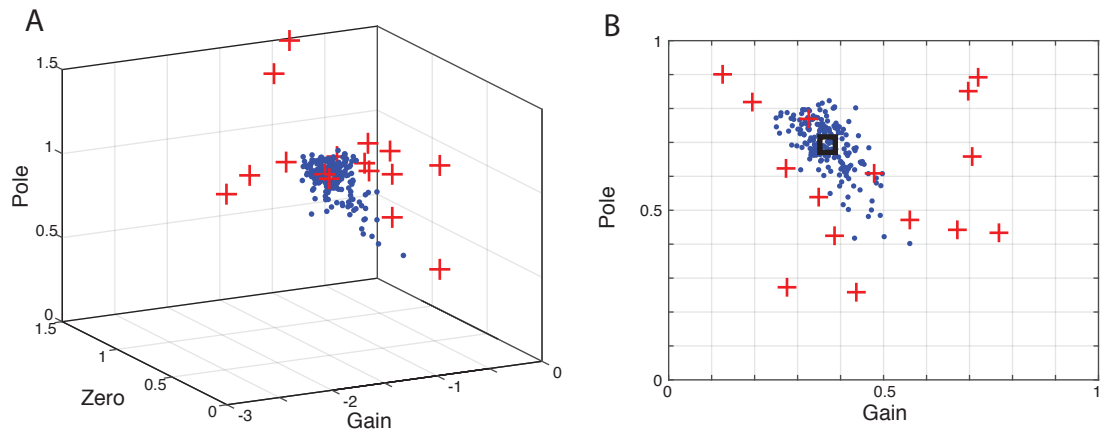


Figure 6.4: Distributions of parameter fits for spatial (A) and timing (B) controller models. Blue dots are bootstrap estimates of inter-juggler averages (200 resamples). Red crosses show individual juggler best fits.

CHAPTER 6. DYNAMICS OF SPATIAL AND TIMING CONTROL

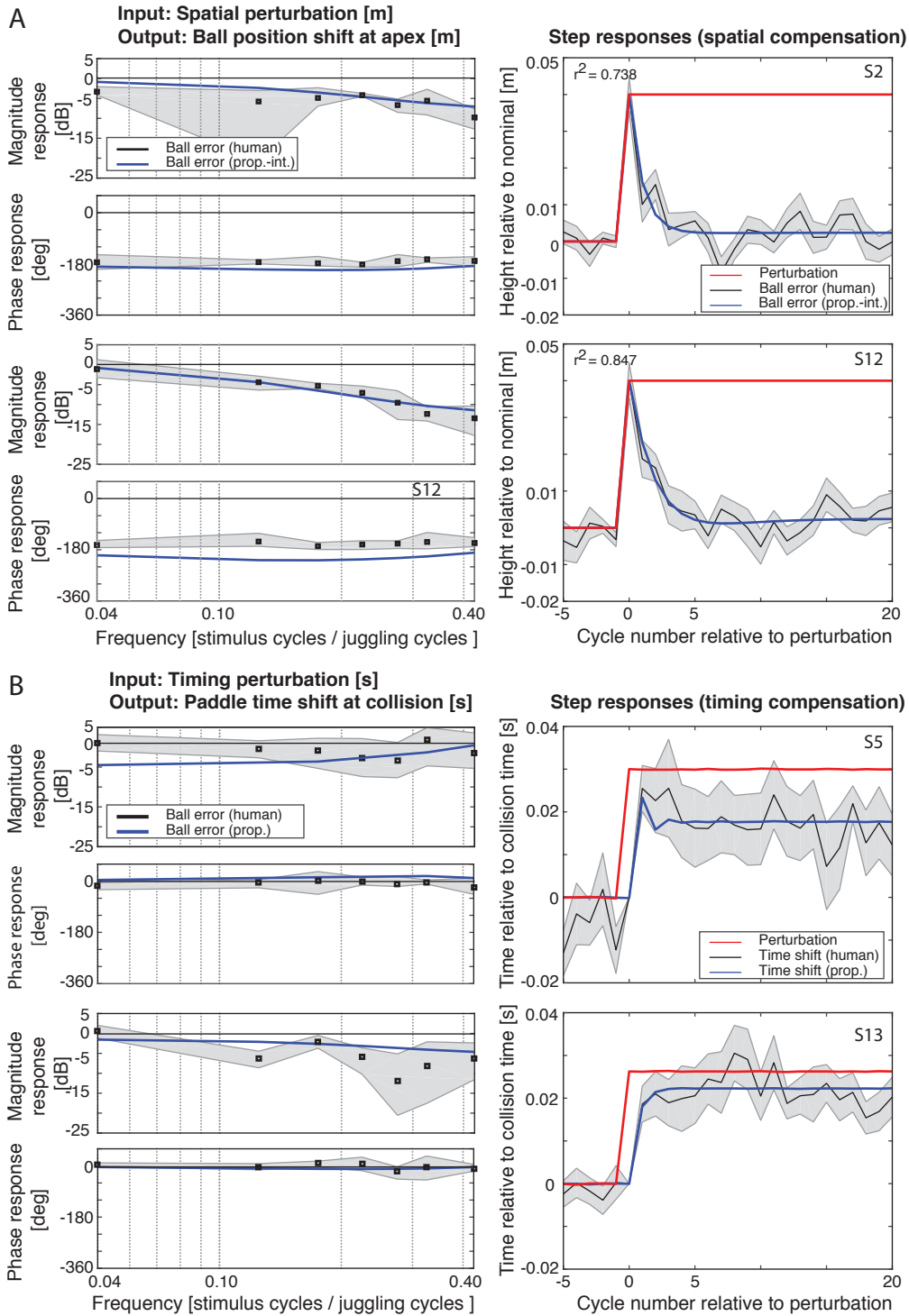


Figure 6.5: Cross-validation of parametric models in frequency and time domains for four representative jugglers. Each row represents one individual. (A) Closed-loop models of spatial control. (B) Closed-loop model of timing compensation. All frequency-domain plots (left column) show data in black (mean; range in shaded area), and best-fit models as blue lines. All time-domain plots show data in black (mean \pm 1 s.e.), best-fit model in blue, and perturbation in red.

Part IV: Conclusions and Appendices

Chapter 7

Conclusions and Future Directions

Rhythmicity is essential to survival throughout the biological world. Rhythmic movements in particular are critical to behaviors such as repetitive tool use, communication, music making, and locomotion. We began in Part I with an overview of rhythmic movements, focusing on studies that have revealed their relative automaticity, and tying them into the broader issue of coordination. Evidence suggests that this automaticity is rooted in spinal primitives that may be capable of oscillating autonomously, but are also modified by feedback and descending corticospinal influences. Although many studies have characterized the biological “hardware” available for rhythmic movement execution, a description of the feedback control processes underlying their regulation is lacking.

The goal of this thesis has been to characterize the closed-loop control processes employed during a model rhythmic task of paddle juggling, which we argue is a

CHAPTER 7. CONCLUSIONS / FUTURE DIRECTIONS

simple yet powerful paradigm for understanding how the human brain controls spatial and timing variables to rhythmically act in dynamic environments that may feature intermittent feedback [2, 3, 6, 7, 10, 94, 104, 125, 126, 132, 137, 154].

To parse the roles of spatial and timing feedback in regulating rhythmic movements in this task context, we developed a novel experimental system (Part II) and conducted two experiments in which we selectively perturbed spatial and timing cues with necessarily high precision (Part III). The outcomes of these experiments imply two distinguishable control processes: spatial accuracy regulation, and temporal synchronization to the feedback of the task (in this case, to ball–paddle collisions).

As expected from the discussion in Chapter 1, it is likely that the juggling arm movement patterns involved subcortical circuitry. Anecdotally, the attempts of some participants to initiate conversations in the middle of trials did not cause noticeable effects on performance (ball accuracy or arm movement). Yet, this presumably spinal circuitry was clearly also influenced by active control at all times, as our jugglers apparently did not rely on passive (open-loop) control, as shown in Figures 7.1 and 7.2. This active control is likely mediated by cortical networks, as discussed in the following section.

7.1 Interplay of Spatial and Timing Control

Our first experiment indicates that humans use spatial and timing feedback in separate regulation processes specific to those modalities. This result contradicted our original hypothesis (Chapter 5). The processes are dynamically different: spatial control has a proportional-integral (1-step-history dependent) nature, and has temporal dynamics that closely match error correction processes seen in discrete tasks such as visual error correction in reaching [152]. Timing control is described by a proportional controller that is believed to typify the behavior of tapping in synchrony with auditory cues [153].

The arm movements of juggling are characterized by alternating flexor-extensor activity of the wrist, elbow, and likely the shoulder, typical of rhythmic movement. This raises the possibility that the closed loop control we model is due to cortical influence on CPG-like circuitry in the spinal cord or arm, in a fashion not unlike the common-core model (Chapter 1). The areas of the brain directly involved in spatial and timing control cannot be ascertained from the black-box studies in this thesis; however, previous studies suggest that they may leverage different specialized pathways [155–157] and involve different computations. The spatial control process likely uses visual error correction mechanisms similar to those observed in discrete tasks like reaching, and may rely on adaptive control based on comparing feedback

CHAPTER 7. CONCLUSIONS / FUTURE DIRECTIONS

with an internal model of ball flight that is based in the cerebellum [20, 152]. The temporal control process potentially involves motor timekeeping networks, which are essentially present in all areas of the brain. It appears to be analogous to metronome synchronization in an SCT task, which is possibly the outcome of a temporal decision making process implemented by accumulator neurons that ultimately converge on SMA, an area involved in assembly of movement sequences (Chapter 1).

Given that these correction processes overlap neuroanatomically, it is possible that they can exert mutual influences. We investigate this idea through an exploratory data analysis on low-frequency perturbation data, shown in Figure 7.3. Beginning with the right hand column, which shows responses to temporal perturbation, we see that jugglers shift the timing of their hand movements in the direction of perturbations in an almost linear fashion, as we established in Part III (panel C: Spearman's $\rho = 0.5280$, $p = 3.08 \times 10^{-47}$). However, there is no concomitant effect on spatial accuracy (panel D); that is, temporal perturbations exclusively impact motor timing.

Conversely, spatial perturbations influence both spatial accuracy and timing, and indeed appear to preempt timing synchronization control. To see this, consider a spatial perturbation where the ball is displayed higher than its actual position. If a juggler perceives the ball as artificially high, then the ensuing (unperturbed) collision timing feedback would arrive earlier than expected, resulting in a negative effective timing perturbation. If the timing controller we identified under timing perturbations were manifested, we would expect to see a shift in paddle timing in the direction of

CHAPTER 7. CONCLUSIONS / FUTURE DIRECTIONS

perturbations. Yet, as shown in Panel A, jugglers do *not* entrain to the timing of the cue (Spearman’s $\rho = -0.2235$, $p = 1.0888 \times 10^{-08}$). Rather, they shift the paddle in a manner to correct ball height (Panel C). Timing subserves synchrony when event timing is perturbed, and it subserves error correction when spatial feedback is perturbed. Whether or not this is a statistically significant principle is an open question; however we note that these correlations are most pronounced at the slowest frequency (2/40).

Therefore, the timing of hand movements appears to be flexible depending on which sensory modalities have the most salient error (as determined the modality where perturbations are injected), or which feedback (kinesthetic or visual) is more relevant at the time it is perceived [158]. This observation, that the brain places more emphasis on synchronization than error correction in certain cases, is consistent with some findings in perceptual psychology. For example, in tasks where the goal is to track temporal patterns, auditory signals are implicitly upweighted, as they have been shown to cause interference with tracking of visual rhythms [157]. Likewise, in decision-theoretic experiments on audiovisual simultaneity (i.e. the “ventriloquist effect”, the point of perceived simultaneity (or the range of time differences in which simultaneity is observed) is shifted in the direction of auditory perturbations [159]).

The above discussion is not to suggest that sensory modalities become unimportant in different contexts. Rather, the separability of spatial and timing control may be a sign of control redundancy where one type of control can be masked by the other,

and yet the presence of both makes rhythmic motor control more robust [160].

7.2 Significance and Future Work

Tasks such as walking, running, dancing, or playing a musical instrument require continuous interactions with environments and task constraints that vary dynamically. Rhythmic movements, by their nature, suggest reliance on a continuous sense of timekeeping based in the cerebellum [81, 161] or corticospinal system [70, 77]. This is particularly the case for intermittently controlled movements that have implicit constraints relating to the timings of action initiation and execution, of which juggling is a prime example. The findings of this thesis both raise awareness of a duality of control processes that is active during (at least some types of) rhythmic movements, and offer a departure point for future research into the understanding of the neural mechanisms and the development of rehabilitation methods.

7.2.1 Physiology

While our experiments reveal a great deal about closed-loop control roles and algorithms, they do so at an abstract black-box level. To understand these processes at a more mechanistic level, further experiments are needed to understand physiology at muscular and cortical levels.

Arm oscillatory primitives

Many researchers theorize that rhythmic arm movements like those employed in paddle juggling are the product of synergetic organization of shoulder, elbow, and wrist oscillatory circuits that manifest as reciprocal inhibition firing patterns between agonist-antagonist pairs at each joint. The ROS / OROCOS experimental system developed in Part II is capable of interfacing with an electromyography (EMG) amplifier system to record and visualize muscle activity (see Figure 7.4). Initial experiments have been conducted to test how different combinations of feedback (or “mode” numbers in the language of Chapter 3) may affect muscular coordination by influencing EMG firing patterns over time and juggling cycle.

Cortical signatures

As discussed in Chapter 1, the coordination the brain employs to direct rhythmic arm movements may involve an ongoing decision process based on an internal representation of task temporal dynamics that is based on accumulator circuitry. In virtual ball interception tasks, which also involve temporal decision making, evidence of Bayesian integration has been found in behavioral signatures [162] and in firing patterns of individual neurons in the cerebellum [163].

As discussed in Chapter 1, areas such as the cerebellum, frontal cortex [86], and premotor cortex [88] have been shown to contain neurons that are tuned to timing or behave as integrators, and thus may reflect temporal decision making (Chapter

1). Electroencephalography (EEG)—specifically the analysis of cortical readiness potentials (RP) (or *Bereitschaftspotentialen*) is believed to reflect neural accumulator activity in a noninvasive manner [164]. The incorporation of such measurements into the juggling studies in this thesis may lead to greater insight into the cortex’s role in timekeeping during rhythmic arm movement.

7.2.2 Rehabilitation

Juggling shares a hybrid dynamical nature with other essential rhythmic tasks, including walking. Conceptual ties between juggling and walking are indeed pervasive throughout the literature, and potentially date back to discussions between Claude Shannon and Mark Raibert, a trailblazer of walking robotics [95]. As in juggling, oscillatory CPG-like networks have been used as a framework for understanding walking [68]. A modification of the juggling model in Chapter 2 from a task with an impulsive collision map, to one admitting ball-in-hand dwell phases (sketched in Section 2.2, “Juggling Dynamics and Definitions”), would approximate a dynamical model of walking proposed by Geyer et al. [165].

Although more everyday rhythmic movements such as walking are less cortical (unless learning is in the early stages) and may rely on central pattern generators, juggling may give us a template for understanding the functional role and value of timing cues. Many areas of the brain involved in coordination contain “chronometer-like” neurons that operate as accumulators (integrate-and-fire). Yet there is growing

CHAPTER 7. CONCLUSIONS / FUTURE DIRECTIONS

evidence that internal timekeeping may be fragile in the absence of feedback. In the premotor cortex, single-unit recordings in macaque show that, although neurons are tuned variously to timing interval length, in many cases, they give biased estimates of time [166]. The consequences of imperfect timing on actions (biological or robotic) have implications that are only now beginning to be considered from a control theoretical standpoint [12].

The use of enhanced timing cues with salience or additional information content is a potentially interesting area for rehabilitation research. During my studies, I have supervised tapping research in my lab that has investigated how humans synchronize to auditory cues of various tempos and rhythmic content (beats).¹

Ultimately, the applicability of juggling findings to locomotor tasks will need to be tested directly in experiments. However, some parallels are noteworthy. As observed earlier in this chapter, although stable ball height is theoretically achievable through passive control, human jugglers nevertheless actively control the paddle at essentially all times—even in the absence of perturbations (Figures 7.1 and 7.2). This is in keeping with a body of evidence that open-loop passive control is relatively insignificant in juggling [7, 10, 126, 132]. Similarly, even though passive walking has been shown feasible through bipedal robots [119], evidence in humans suggests that postural stability and cadence are actively regulated cycle by cycle [167, 168].

On the other hand, walking may involve energetic considerations that are relatively

¹Samson et al. (2015); Ortega et al. (in preparation); Deshmukh et al. (in progress)

inconsequential in paddle juggling, and this in turn may affect the generalizability of our results for rhythmic arm movement to locomotion. Namely, humans prefer to be energy economical when learning walking patterns [169], whereas the role of energetic optimality in juggling is believed to be minor [125]. This discrepancy may manifest in the behavior of the spatial or synchronization controller of rhythmic movement. For instance, our findings suggest that humans adjust the timing of their arm movements in the direction of feedback perturbations, which we interpret as a sign that the brain may act to resolve a discrepancy between its own noisy reckoning of time and what is perceived to be a deterministic clock implied by task dynamics. In walking, humans show evidence of a synchronization behavior of a different nature: namely, when the ankle is mechanically perturbed (perhaps analogous to our haptic feedback perturbation), humans adjust their gait timing in order to exploit the perturbation for propulsion. This response was impervious to auditory feedback [170]. Thus, while other types of rhythmic behavior may exhibit both error-reducing and synchronicity-enforcing control processes, the relative influence and objectives may be different based on context.

7.3 General conclusion

In this study, we study the particular case of skilled juggling behavior at what we suspected were the two most task-relevant phases of movement: the ball collision

CHAPTER 7. CONCLUSIONS / FUTURE DIRECTIONS

and the ball peak. We note that because juggling is a time-periodic (LTP) task, full testing and identification of skilled and unskilled ball bouncing would require perturbing all combinations of vision and timing feedback at all phases of juggling. Analytical methods are in their infancy [168,171] but may as a next step shed light on complementary roles of spatial and timing feedback throughout entire cycles of rhythmic movement.

CHAPTER 7. CONCLUSIONS / FUTURE DIRECTIONS

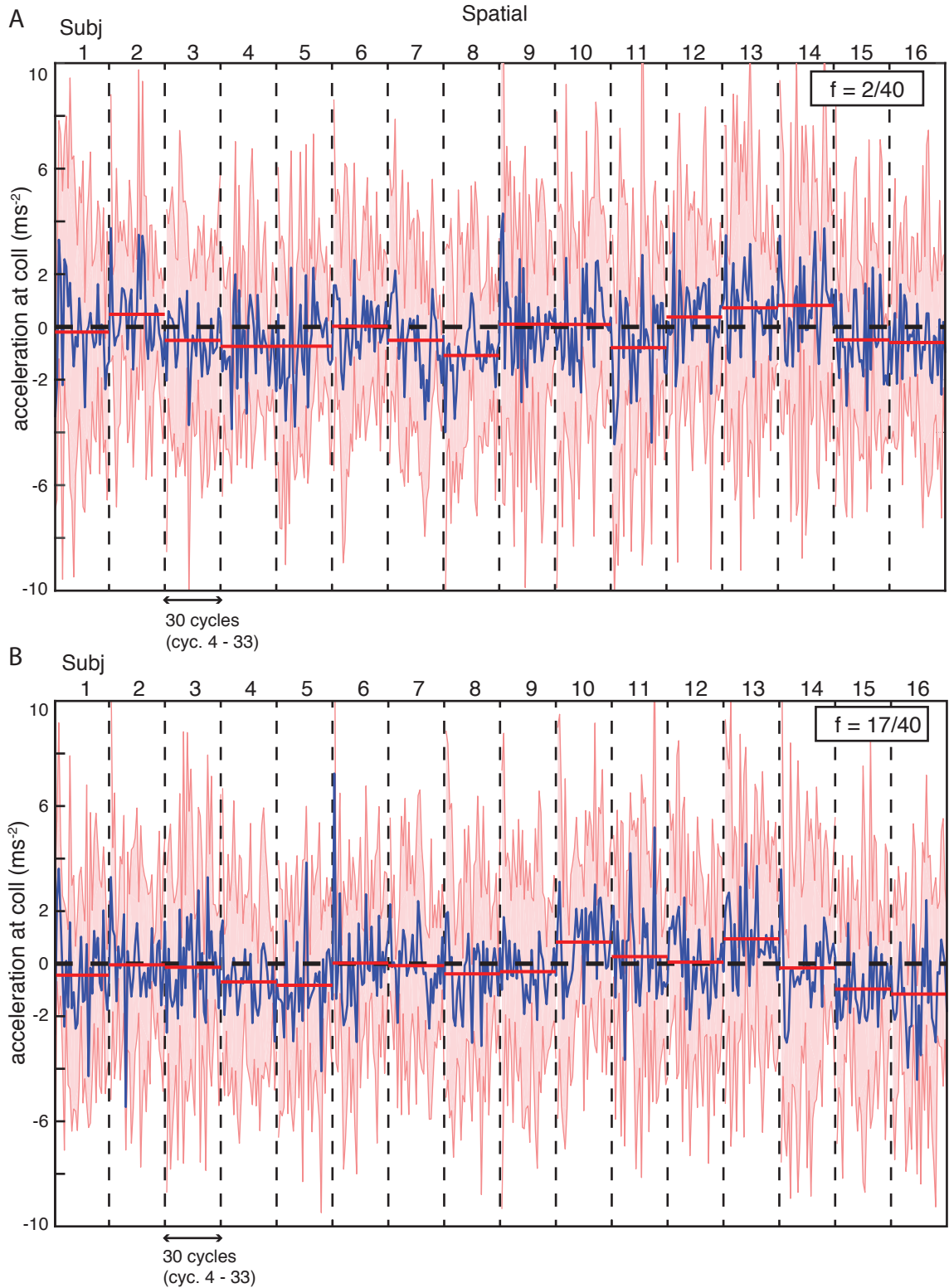


Figure 7.1: Average paddle accelerations at collision times across 5 trials for each subject (using Experiment 2, $n = 16$). Data is taken between pre-perturbation and early ramping periods. Shown are 95% confidence intervals (shaded red), and mean acceleration for entire subject (solid red), with reference to the passive stability threshold of 0 ms^{-2} , negative values being necessary for passive control (A) Lowest-frequency and (B) highest-frequency perturbations.

CHAPTER 7. CONCLUSIONS / FUTURE DIRECTIONS

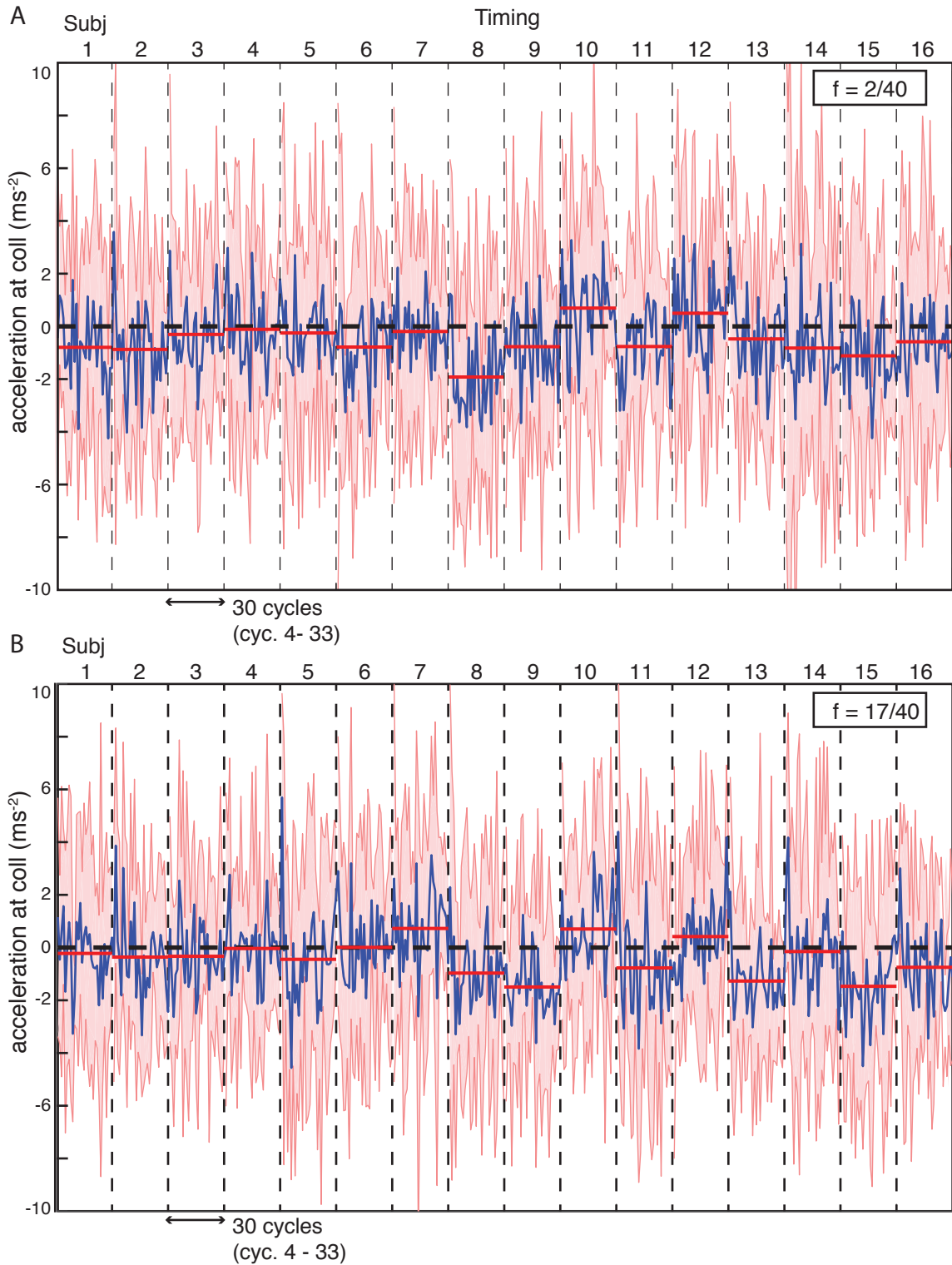


Figure 7.2: Average paddle accelerations at collision times across 5 trials for each juggling participant (data from Experiment 2, $n = 16$). Data is as described in Fig. 7.1, but for timing perturbation trials under the lowest- (A) and highest-frequency (B) perturbations.

CHAPTER 7. CONCLUSIONS / FUTURE DIRECTIONS

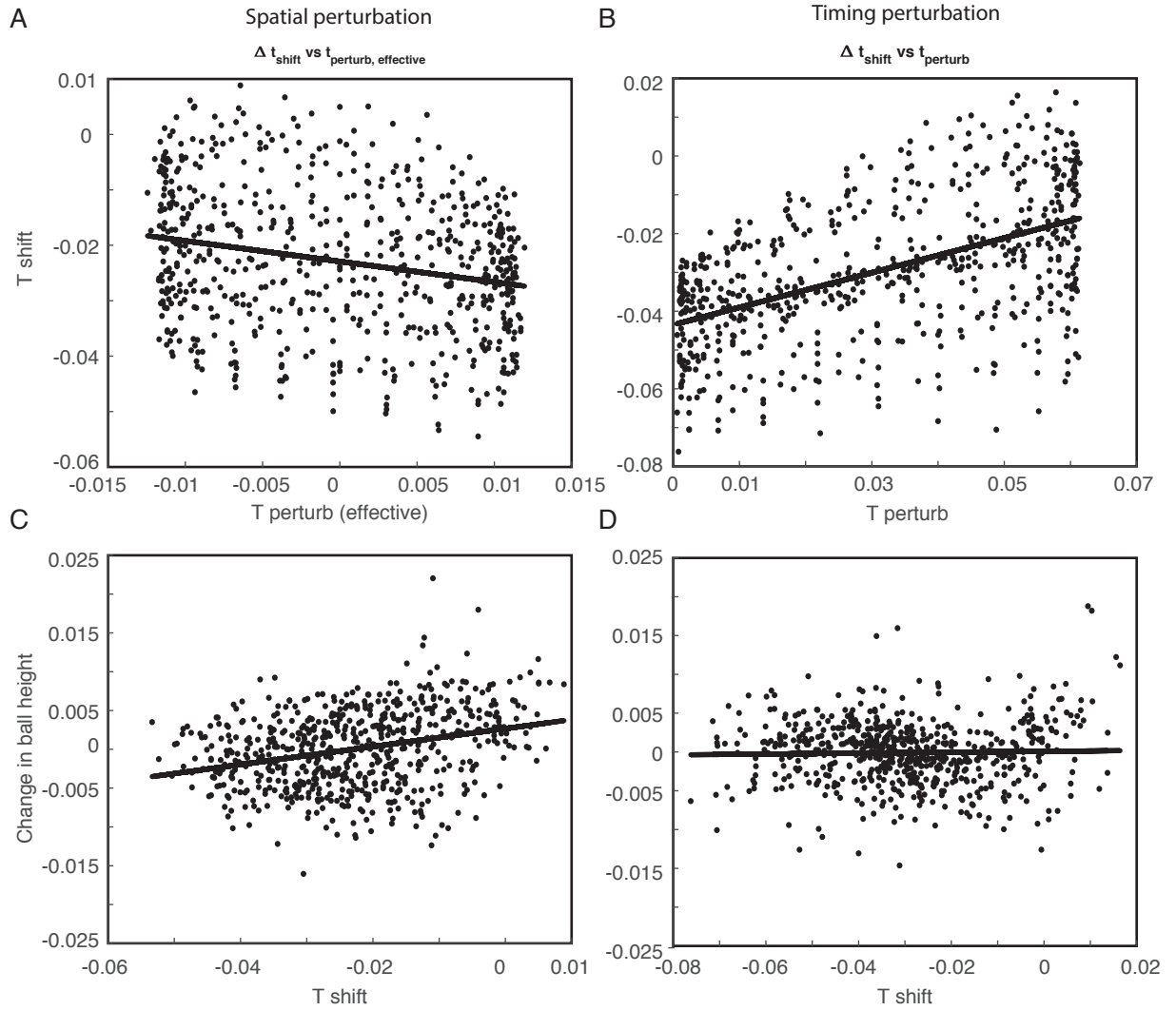


Figure 7.3: Relationships between timing perturbations and temporal (paddle shift) and spatial (change in ball height) behavior under both perturbation modalities studied. (A, C) Spatial perturbations. Because the ball is displayed artificially higher or lower than actuality, the following collision timing cue would be perceived earlier or later than expectation (“T perturb (effective)”). Juggler time shifts are anti-correlated to this effective perturbation (A). Time shifts, however, correlate with spatial corrections (C). (B, D) Timing perturbations. Here, collision (and apex) event cues are directly manipulated to be later or earlier than actuality. Paddle timing shifts positively correlate with perturbations as expected from Experiments 1-2 (B), but not with ball position (D).

CHAPTER 7. CONCLUSIONS / FUTURE DIRECTIONS

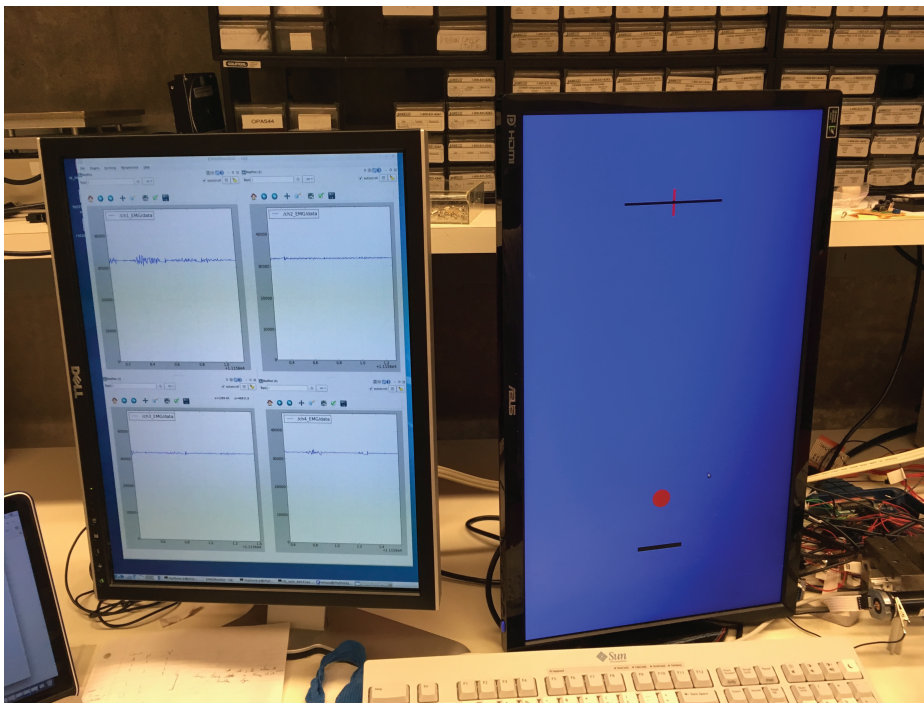


Figure 7.4: Extension of hard-real-time juggling system to allow recording of EMG signals. During experiments (right monitor), EMG signals are recorded and displayed online on a separate monitor in a software environment (`rosqt`) that can be inspected privately in (soft) real-time by the experimenter.

Appendix A: Vertical 1-juggling

Dynamics—Basic Results

Collision map and coefficient of restitution

We provide intuition about the meaning and form of the coefficient-of-restitution law that is the basis of the juggling collision map (Chapter 2). This map describes the ball velocity at two instants infinitesimally before $[\cdot]^-$ and after $[\cdot]^+$ a collision.

We make the standard assumption that the mass of the paddle far exceeds that of the ball ($m_p \gg m_b$), so that the momentum of the paddle, and thus its velocity, is relatively unchanged by the collision.

Let us consider the total energy of the system encompassing the ball and paddle only. Assuming the collision of these two objects is inelastic (but not perfectly so), so that the proportion of total kinetic energy remaining after the collision is γ , the

APPENDIX A: VERTICAL 1-JUGGLING—BASIC RESULTS

total energies before and after the collision are:

$$\gamma(KE + PE)^- = (KE + PE)^+$$

Recentering the reference frame at the height of collision and substituting the kinetic energies of the ball and paddle yields:

$$\begin{aligned} \gamma(KE)^- &= (KE)^+ \\ \gamma\left(\frac{1}{2}m_b(\dot{b}^-)^2 + \frac{1}{2}m_p(u^-)^2\right) &= \left(\frac{1}{2}m_b(\dot{b}^+)^2 + \frac{1}{2}m_p(u^+)^2\right) \\ \left(\frac{1}{2}m_b(\alpha\dot{b}^-)^2 + \frac{1}{2}m_p(\alpha u^-)^2\right) &= \left(\frac{1}{2}m_b(\dot{b}^+)^2 + \frac{1}{2}m_p(u^+)^2\right) \end{aligned}$$

Here we introduced the variable α , such that $\gamma = \alpha^2$. We will call α the *coefficient of restitution*. Further, we note the equivalencies: $\alpha\dot{b}^- = \dot{b}^+$ and $\alpha u^- = u^+$. Isolating terms in the above expression and factoring:

$$m_b\left(\alpha\dot{b}^- - \dot{b}^+\right)\left(\alpha\dot{b}^- + \dot{b}^+\right) = m_p\left(u^+ - \alpha u^-\right)\left(u^+ + \alpha u^-\right) \quad (\text{A.1})$$

The total momentum of the system is:

$$\begin{aligned} m_p(u^+) + m_b(\dot{b}^+) &= m_p(\alpha u^-) + m_b(\alpha\dot{b}^-) \\ \rightarrow m_p(u^+ - \alpha u^-) &= m_b(\alpha\dot{b}^- - \dot{b}^+) \end{aligned}$$

APPENDIX A: VERTICAL 1-JUGGLING—BASIC RESULTS

Combining with Eqn. A.1:

$$\alpha \dot{b}^- + \dot{b}^+ = u^+ + \alpha u^-$$

Allowing $u = u^+ \approx u^-$ by assumption of the paddle's large inertia, yields the collision map of Eqn. 2.2. Intuitively α is a measure of the amount of energy dissipation in the system due to the collision. In context of the high-ball juggling assumption, each launch of the ball is at a velocity α -times the previous collision velocity.

Proof of rhythmicity in paddle juggling

In this section, we formally justify our claim that paddle juggling is a rhythmic behavior. Mathematically, this is proved by showing the existence of a limit cycle. The standard approach for 2- and 3-dimensional nonlinear system uses the Poincaré-Bendixson Theorem to show sufficient conditions for the existence of a limit cycle. However, there is no equivalent theorem for hybrid systems with jump discontinuities such as paddle juggling [172]. Alternatively, a necessary and sufficient condition for rhythmicity is the existence of a Poincaré return map [173].

Given that the vertical-1-paddle-juggle system is planar under the high ball assumption (Fig. 2.2), a Poincaré section S is a 1-dimensional surface (line) through which the ball trajectory passes. Let: $S = (b, \dot{b} | \dot{b} = 0)$, corresponding to the apex phase (noted in Fig. 2.2). S has a return map (of period 1) if it contains a fixed point

APPENDIX A: VERTICAL 1-JUGGLING—BASIC RESULTS

x^* , since $x^* = P^1(x^*)$.

Let b^* be any explicitly defined target height relative to paddle position. We maintain our definition from Chapter 2 of $g < 0$. The ball flight time is:

$$\sqrt{-\frac{2}{g}(b^*)} = t_{\text{asc}}^* = t_{\text{desc}}^* = \frac{1}{2}t_{\text{flight}}^* \quad (\text{A.2})$$

The descent phase ($x^* \rightarrow [b^-]^*$) has the following mapping:

$$[\dot{b}^-]^* = gt_{\text{desc}}^*$$

By definition, our apex return map requires that no ball energy be dissipated during the collision ($\dot{b}^* = [b^+]^* = -[b^-]^*$), which implies from the collision map:

$$u^* = \dot{b}^* \frac{(1 - \alpha)}{(1 + \alpha)}$$

The ascent phase ($[b^-]^* \rightarrow x^*$) has the mapping:

$$b^* = [\dot{b}^+]^* t_{\text{asc}}^* + \frac{1}{2}g(t_{\text{asc}}^*)^2$$

Altogether, the unique set of (nominal) states specifying the fixed point—namely,

APPENDIX A: VERTICAL 1-JUGGLING—BASIC RESULTS

ball position (b^*), ball velocity (\dot{b}^*), and paddle velocity (\dot{p}^*)—are:

$$\begin{aligned}
 b^* &= [\dot{b}^+]^* t_{\text{asc}}^* + \frac{1}{2} g (t_{\text{asc}}^*)^2 \\
 t_{\text{asc}}^* &= \sqrt{-\frac{2}{g} (b^*)} \\
 \dot{b}^* &= [\dot{b}^+]^* = -[\dot{b}^-]^* = -g \sqrt{-\frac{2}{g} (b^*)} = \sqrt{-2gb^*} \\
 \dot{p}^* &= u^* = \dot{b}^* \frac{(1-\alpha)}{(1+\alpha)}
 \end{aligned}$$

Appendix B: Software

Infrastructure

This Appendix contains supplementary details on the setup and implementation of the hard-real-time hardware/software platform discussed in Chapter 3.

Software Requirements

For our infrastructure, the Linux distribution needed to be selected based on the latest version of the real-time Xenomai kernel that was compatible with *both* ROS and OROCOS. At the time of construction, the newest such Linux kernel was version 3.5.7.² This corresponded to version 2.6.2.1 of Xenomai,³ ROS distribution Hydro,⁴ and version 2.8.2 of the OROCOS toolchain.⁵

²Linux distribution was Lubuntu 12.04 LTS, no longer actively supported

³Available for download at: <https://xenomai.org/downloads/xenomai/stable/>

⁴Available at <http://wiki.ros.org/hydro/Installation/Ubuntu>

⁵Downloaded as the separate ROS package `rtt-ros integration` (version 2.8.2), available at: <http://www.orocos.org/wiki/orocos/toolchain/getting-started>

Linux kernel configuration

Procedures for building and installing Linux kernels, and downloading and applying the Xenomai patch, can be found elsewhere and will not be detailed here. The “tuning” of the real time properties of the kernel occurs during the configuration process, which is streamlined in the Linux Menuconfig interface. A few configurations are critical to hard-real-time performance and bear mentioning here. Under submenu `Real time sub-system`, the following are necessary:

- `ENABLE Xenomai`
- `ENABLE ANALOGY drivers`

The following additional options were sufficient to achieve hard-real-time performance with latencies under 40 microseconds on an Intel i5, Dual-kernel / 4 thread computer, as determined by benchmark testing (see Stress Testing section below).

- `Disable CPU Frequency scaling`
- `Disable advanced power settings`
- `Disable frequency scaling`
- `Disable advanced power management (APM)`

However, these options cannot be guaranteed to suffice for all computer hardware. Generally, achieving desired latencies requires an iterative process of trying

APPENDIX B: SOFTWARE INFRASTRUCTURE

different configuration options, rebuilding, reinstalling, and re-rerunning stress tests until desired latency requirements are met.

One drawback to the Xenomai kernel is that it is incompatible with many proprietary device drivers. For example, our inability to install proprietary drivers for our graphics card (NVIDIA) forced us to use Xenomai’s default hard-real-time graphics drivers,⁶ which were not capable of changing the monitor refresh rate from 60 Hz (a limitation noted in our bar code tests described in Chapter 3 under “Graphical rendering”).

OS stress testing

To verify correct Xenomai configuration, stress testing was performed, wherein all computer threads were first loaded to maximum capacity, and a test program issued interrupts in order to measure latencies. Xenomai comes with a suite of stress testing programs, including `xeno-test`, which report maximum latency over a set period of testing. Approaches to stressing the computer include (1) opening several shells and tasking them with writing continuously to the Linux null device⁷ and (2) opening several data intensive programs such as browser sessions. After all threads were taxed to 100% capacity,⁸ `xeno-test` was run. Xenomai was decided to be properly configured if no violations in average or maximum interrupt latency were

⁶nouveau

⁷`sudo dd if=/dev/zero of=/dev/null`

⁸By running `htop` from the terminal

APPENDIX B: SOFTWARE INFRASTRUCTURE

observed.

Over the course of development, several computers were prepared with the patched Linux Kernel, ranging from a dual core 2-thread computer (replaced due to hardware failure) to a 6-core 12-thread Lenovo workstation.

At earlier stages, Xenomai performance was compared with another Linux real-time kernel, RT-PREEMPT. Ultimately RT-PREEMPT was rejected in favor of Xenomai because its latencies (determined under the same approach, but using `latency-test` instead of `xeno-test`) exceeded those for Xenomai, with jitters exceeding 10 ms being common (as predicted in [140]), which was significant compared to the experimental timing perturbation amplitudes used in Chapters 5 and 6.

Software operating system

As noted in Chapter 3, ROS was chosen as the experimental platform based on the control, data handling, and evaluation tools available and its wide support in the robotics community [141]. As ROS was not then capable of hard-real-time control, we interfaced with the Open Robot Control System (OROCOS) real-time toolchain via the ROS extension package `rtt_ros_integration` [142].

ROS / OROCOS package structure

As of the writing of this thesis, the experiment is contained in the ROS package `haptic_paddle` on the computer `rhythmic-jr`. Per ROS package conventions,

APPENDIX B: SOFTWARE INFRASTRUCTURE

`haptic_paddle` is defined by the markup script `package.xml`,⁹ and contains a set of programs coded in C++ language (“nodes”¹⁰) that are capable of running autonomously, but can mutually influence each other by exchanging data via message threads.¹¹ These “nodes” can be manipulated directly by the user in the Linux terminal,¹² which is cumbersome during an experiment. The User Interface mentioned in Chapter 3 was developed to alleviate this burden.

Software organization

The metastructure of the juggling system is 2 ROS Nodes: (1) one contains an interface for receiving messages from a non-real-time user interface (`UI_receiver`) and a second one (2) is a “deployer” node, which launches an OROCOS Deployer session consisting of 4 components which control the experiment directly. The system is launched with the launch file, and stands by for input from the UI.

As noted above, the software is currently implemented in ROS Hydro version. However, it should be more-or-less directly transferrable to more recent ROS distributions that use the same build structure.¹³

⁹also known as a manifest file

¹⁰“Components” in OROCOS. Architecturally, each “node” or “component” is a state machine, which is of type `class`

¹¹called “advertisers / subscribers” in ROS, or “flowports” in OROCOS

¹²`roscore` in ROS; `Deployer` in OROCOS

¹³`catkin`, which is still applicable as of the newest ROS distribution, Lunar

Launching of sessions

Experiments (in the package `haptic_paddle`) are executed in two steps that must be run in order: (1) Launching of ROS nodes,¹⁴ (2) Execution of the user interface `juggle_UI`,¹⁵ which, as noted in Chapter 3, must handshake with the node `UI_receiver`. Steps (1) and (2) must be done in separate shell windows.

Node scheduling

A schematic of nodes and their connectivities was presented earlier in Figure 3.2. We note that, upon launching of a trial, `Main` runs autonomously at a callback rate of 1 kHz, `Logger` autonomously at a 2 Hz rate (to avoid violations of real-time in `Main`), and the remainder run as needed when a graphical scene must be rendered (`Window` component) or the current trial is stopped by timeout or intervention by the experimenter.

Physics engine

The physics of the paddle and ball were implemented using Euler integration in the respective classes `Padsysrtt` and `Ballsysrtt`, invoked in the node `Main_1kHz`.

In `Padsysrtt`, paddle position was updated by reading counts from the encoder mounted to the paddle motor.¹⁶ Paddle position was first updated by re-reading

¹⁴`$roslaunch rtt_unix_ui.launch`

¹⁵in package directory in `roscpp`, or in `catkin_ws/devel/lib/haptic_paddle` directory in ROS Hydro

¹⁶Device functions were coded as class `daqapi` by Robert Nickl and Manu Madhav

APPENDIX B: SOFTWARE INFRASTRUCTURE

the encoder, and paddle velocity was then estimated from the difference between consecutive positions. An additional smoothing step was performed by applying a 9th order (discrete-time) polynomial filter,¹⁷ a step that was enabled because the callback rate was approximately constant in hard-real-time, enabling (approximately) uniform sampling.

As noted in Chapter 3, encoder counts were scaled,¹⁸ so that the displacement of the virtual paddle approximately equaled actual vertical hand displacement¹⁹ around the horizontal position. During experiments, jugglers were trained to move the paddle about this position, with their arms approximately horizontal (elbow angle ≈ 90 degrees).

In **Ballsyrтт**, the ball was updated by Euler integrating 1D ballistic flight equations, first for ball velocity and then for ball position. When ball–paddle collisions occurred between callbacks, ball launch velocities \dot{b}^+ were computed by inferring the collision time, and updating ball kinematics based on piecewise analysis before and after that instant.

Logging

While the Main node executed during a trial, logging data instantaneously to a file caused violations of hard real time. To avoid this, it was sufficient to run the logger

¹⁷In class `LSQ_filt` written by Robert Nickl, derived from the open-source **Eigen** libraries

¹⁸This factor was $N_{cts} = 0.000015$ meters-per-encoder count, for the CUI-103 encoder (2048 counts per revolution)

¹⁹linear, not angular displacement

APPENDIX B: SOFTWARE INFRASTRUCTURE

at a slower rate of 0.5 Hz. Each time the loop runs, the Node checks through the data flowports, sequentially reads them and empties them into buffers large enough to accommodate a trial of over 5 minutes. When a trial ends, each buffer is written to a file, and flow ports are flushed. No data points were observed to be lost throughout the Experiment 1 and 2 data.

Design of trial programs

Experiments consist of a set of trials, generated in by Matlab scripts.²⁰ Given the rhythmic nature of the task, the trial can be conceptualized as a series of cycles. Each trial is defined by a file that contains, in each line, the perturbation magnitudes for (1) ball position, (2) audio feedback timing, and (3) haptic feedback timing. In addition, the experimental system was set up to allow perturbations in (4) paddle height (for the paddle locked / high bounce setting), (5) gravity, (6) coefficient of restitution, and (7) the scaling relationship between hand movement and virtual paddle movement (for the paddle unlocked setting)

As noted in Chapter 3, these trial files needed to be generated before execution of `juggle_UI`.

²⁰Located in `OctaveScripts` folder of `haptic_paddle` package

Appendix C: Derivation of Closed-Loop Juggling Model

Linearization of paddle juggling dynamics

In the following, we cast the nonlinear paddle juggling dynamics (under the standard high bounce assumption) into the form

$$x[n + 1] = Ax[n] + Bu[n]$$

In the derivation to follow, $n \in N$ is the cycle number; and $x, x_1, u, A, B \in R$. Cycle n begins *immediately after* the ball-paddle collision. Recall the collision map (Chapter 2 and Appendix A):

$$\dot{b}^+[n + 1] = (1 + \alpha)\dot{p}[n] - \alpha\dot{b}^-[n] \tag{C.1}$$

APPENDIX C: CLOSED-LOOP CONTROL MODEL

The high bounce assumption implies $p[n]$ is constant throughout a given cycle.

Defining $b[n]$, $\dot{b}[n]$, $t_{\text{asc}}[n]$, and $g < 0$ as in Chapter 2, the liftoff velocity $\dot{b}[n] = \dot{b}^+[n]$ and apex height $b[n]$ of the ball relate thus:

$$\begin{aligned} b[n] &= \frac{1}{2}gt_{\text{asc}}[n]^2 + \dot{b}[n]t_{\text{asc}}[n] \\ &= \frac{1}{2}\frac{\dot{b}[n]^2}{g} - \frac{\dot{b}[n]^2}{g} = -\frac{1}{2}\frac{\dot{b}[n]^2}{g} \\ &\rightarrow \dot{b}[n]^2 = -2gb[n] \end{aligned}$$

The collision map (C.1) in terms of apex position $x[n]$ is therefore:

$$\begin{aligned} \sqrt{-2gb[n+1]} &= (1+\alpha)\dot{p}[n] + \alpha\sqrt{-2gb[n]} \\ \rightarrow b[n+1] &= -\frac{1}{2g}\left[(1+\alpha)\dot{p}[n] + \alpha\sqrt{-2gb[n]}\right]^2 = f(\dot{p}[n], b[n]) \end{aligned}$$

We linearize the collision-map dynamics about the nominal (limit cycle) state (Appendix A) as follows:

$$\begin{aligned} b[n+1] - b^* &= \frac{\delta}{\delta b[n]}f(\dot{p}[n], b[n])\Big|_{(b^*, u^*)} \left(b[n] - b^*\right) \\ &\quad + \frac{\delta}{\delta \dot{p}[n]}f(\dot{p}[n], b[n])\Big|_{(b^*, \dot{p}^*)} \left(\dot{p}[n] - \dot{p}^*\right) \\ &= -\frac{1}{g}\left[(1+\alpha)\dot{p}^* + \alpha\sqrt{-2gb^*}\right]\left[\frac{\alpha}{2\sqrt{-2gb^*}}\right] [-2g]\left(b[n] - b^*\right) \\ &\quad - \frac{1}{g}\left[(1+\alpha)\dot{p}^* + \alpha\sqrt{-2gb^*}\right]\left[1+\alpha\right]\left(\dot{p}[n] - \dot{p}^*\right) \end{aligned}$$

APPENDIX C: CLOSED-LOOP CONTROL MODEL

Denoting $x[n] = \Delta b[n] = b[n] - b^*$ and $u[n] = \Delta \dot{p}[n] = \dot{p}[n] - \dot{p}^*$ as the deviations of ball position and paddle velocity from their nominal states on cycle n (where nominal paddle position p^* is held to be the center of our frame of reference), we simplify the previous equation:

$$x[n+1] = \alpha \left[\frac{(1+\alpha)}{\sqrt{-2gb^*}} \dot{p}^* + \alpha \right] x[n] - \frac{1+\alpha}{g} \left[(1+\alpha) \dot{p}^* + \alpha \sqrt{-2gb^*} \right] u[n]$$

Substituting the nominal states (see Appendix A):

$$\begin{aligned} x[n+1] &= \alpha \left[(1-\alpha) + \alpha \right] x[n] \\ &\quad + \frac{1+\alpha}{g} \left[(1-\alpha) + \alpha \right] \sqrt{-2gb^*} u[n] \\ &= \alpha x[n] + (1+\alpha) \sqrt{\frac{-2b^*}{g}} u[n] \\ &= \alpha x[n] + (1+\alpha) t_{\text{asc}}^* u[n] \\ &= Ax[n] + Bu[n] \end{aligned} \tag{C.2}$$

Paddle juggling (plant) transfer function

In all Bode plots presented in this thesis, output signals were delayed by 1 cycle to make explicit the anti-phase correction of the spatial controller and in-phase correction of the timing controller. Defining $x_1[n]$ as the time-advanced version of x , i.e. $x_1[n] = x[n+1]$, the transfer functions relating input to output states for the

APPENDIX C: CLOSED-LOOP CONTROL MODEL

juggling plant are derived from Eqn. C.1 as follows:

$$\begin{aligned} x_1[n] - Ax_1[n-1] &= (1 + \alpha)t^*u[n] \\ \xrightarrow{Z} (1 - z^{-1}\alpha)X_1[z] &= (1 + \alpha)t^*U[z] \\ \frac{X_1[z]}{U[z]} &= \frac{(1 + \alpha)t^*}{1 - z^{-1}\alpha} = \frac{z(1 + \alpha)t^*}{z - \alpha} \end{aligned}$$

Around the nominal defined by $h = 0.35[\text{m}]$:

$$\frac{X_1[z]}{U[z]} = \frac{z(1 + \alpha)t^*}{z - \alpha} = \frac{(1.8)(0.2671)z}{z - \alpha} = \frac{0.4808z}{z - \alpha} = H_{\text{plant}}[z]$$

Note on transfer function fitting

H_{plant} was operationally defined to be a mapping from $y_s[n]$ ([perturbed] feedback at cycle n) to the subsequent peak position.

Because we directly fit the spatial controller to the FRF data relating perturbation at cycle n to actual ball position at cycle $n+1$, a 1-cycle advance was added to the feedback path of the closed-loop control model:

$$\hat{H}_{\text{CL, spatial}} = \frac{H_{\text{plant}}H_{\text{ctrl, s}}}{1 + z^{-1}H_{\text{fdbk}}H_{\text{plant}}H_{\text{ctrl, s}}}$$

As discussed in Chapter 6, the free parameters to be optimized are the gain

coefficient, zero, and pole of $H_{\text{ctrl},s}$.

Observer model

Basic definitions

We introduce two linear observers: L^t , which relates the “descent time” observation to the estimate of the previous apex position (i.e. is crossmodal); and L^s , which relates the “apex position” observation to the estimate of the apex position on the current cycle n (i.e. is spatial).

Recall that cycle n begins with the n^{th} ball launch. The causative paddle strike velocity is defined to have occurred on the previous cycle $n - 1$. Audio and haptic feedback are assumed to mark the occurrence of timing cues (the ball onset flash of cycle n is identically temporally perturbed for consistency but we assume it does not provide new timing information). Because audio and haptic feedback occur after the collision, we associate them and the associated timing measurement with cycle n and assume it is used to revise the ball position estimate of the previous cycle, and this estimate is projected forward during the ascending phase of cycle n via an internal model of ball ascent.

$C_s^s = 1$ is the observation matrix transforming spatial to spatial information, and C_t^s is the observation matrix from timing error to spatial error that is defined by the following linearization of the space-time coupling of 1D ballistic dynamics, where h

APPENDIX C: CLOSED-LOOP CONTROL MODEL

is the target (nominal) ball height, and $b[n], t[n], g < 0$ are defined as above:

$$\begin{aligned}
 b[n] &= \frac{1}{2}gt^2[n] \\
 t[n] &= \sqrt{\frac{2b[n]}{g}} \\
 \Delta t[n] &= \frac{1}{2}\sqrt{\frac{g}{2b^*}}\frac{2}{g}\Delta b[n] = \sqrt{\frac{1}{2b^*g}}x[n] \\
 &\rightarrow C_t^s = \sqrt{-2b^*g} = \sqrt{-2hg}[m/s]
 \end{aligned}$$

System of equations (observer + controller)

The following discussion walks through a hypothetical ball estimation process in which ball estimate is sequentially updated with spatial and timing feedback. We expect that it is valid for how the experiment is implemented, especially given delays in event feedback). The following sequence parallels the overall model discussed in Chapter 5, but provides additional analytical detail. For conformity with standard linear systems notation, we let $x[n], \hat{x}[n]$ be the actual and estimated states respectively (in this case ball peak position), and Δ represent their deviations from the nominal x^* .

1. Just prior to apex n , assume juggler has an estimate of ball position that is informed by both timing and collision feedback: $\hat{x}[n|n-1]$.

APPENDIX C: CLOSED-LOOP CONTROL MODEL

2. Update apex estimate using visual error:

$$\begin{aligned}
 \Delta \hat{x}[n|n] &= \Delta \hat{x}[n|n-1] + L^s[n]C_s^s(y_s[n] - \Delta \hat{x}[n|n-1]) \\
 &= \Delta \hat{x}[n|n-1] + L^s[n](\Delta x[n] - \Delta \hat{x}[n|n-1] + \eta_s[n]) \\
 &= \Delta \hat{x}[n|n-1] + L^s[n]((x[n] - \hat{x}[n|n-1]) + \eta_s[n]) \\
 &= \Delta \hat{x}[n|n-1] + L^s[n](x[n] - \hat{x}[n|n-1]) + L^s[n]\eta_s[n]
 \end{aligned}$$

3. When timing feedback (audio and haptic) is received, the estimate of previous ball peak is retroactively updated.

$$\begin{aligned}
 \hat{t}_{desc}[n] &= C_s^t \hat{x}[n|n] \\
 y_t[n+1] &= \Delta t_{desc}[n] + \eta_t[n] = C_s^t \Delta x[n] + \eta_t[n] \\
 \Delta \hat{x}[n|y_t[n+1], n] &= \Delta \hat{x}[n|n] + L_t[n+1]C_s^t(x[n] - \hat{x}[n] + C_t^s \eta_t[n]) \\
 \Delta \hat{x}[n|y_t[n+1], n] &= \Delta \hat{x}[n|n] + L_t[n+1]C_s^t(x[n] - \hat{x}[n]) + L_t[n+1]\eta_t[n]
 \end{aligned}$$

4. The ball's upcoming apex position (cycle n) is estimated using the paddle movement and a forward projection of the current "time-updated" estimate of the ball apex through the internal model of the task dynamics.

$$\Delta \hat{x}[n+1|n] = A\Delta \hat{x}[n|y_t[n+1]] + B\Delta u[n]$$

APPENDIX C: CLOSED-LOOP CONTROL MODEL

These steps are repeated in subsequent cycles.

Controller model

Recall $\hat{x}[n|n]$ is the ball estimate after the visual update (i.e. during ball descent).

Under a linear controller:

$$\Delta u[n] = K\Delta\hat{x}[n|n]$$

Ball dynamics with estimator

Begin with the linear form in Eqn. (C.2) **from section in this Appendix**

$$\Delta x[n] = A\Delta x[n-1] + B\Delta u[n-1] = A\Delta x[n-1] + BK\Delta\hat{x}[n-1|n-1]$$

Substituting the spatial phase of estimation:

$$\begin{aligned}\Delta x[n] &= A\Delta x[n-1] \\ &\quad + BK \left[\Delta\hat{x}[n-1|n-2] + L^s[n](x[n-1] - \hat{x}[n-1|n-2]) \right] \\ &\quad + BKL^s[n]\eta_s[n-1]\end{aligned}$$

APPENDIX C: CLOSED-LOOP CONTROL MODEL

Substituting the timing estimate:

$$\begin{aligned}
\Delta x[n] &= A\Delta x[n-1] + BKL^s[n]\Delta x[n-1] \\
&\quad + BK \left[\Delta \hat{x}[n-1|n-2] - L^s[n]\Delta \hat{x}[n-1|n-2] \right] + BKL^s[n]\eta_s[n-1] \\
&= A\Delta x[n-1] + BKL^s[n]\eta_s[n-1] \\
&\quad + BKL^s[n]\Delta x[n-1] + BK \left[I - L^s[n] \right] \underline{\Delta \hat{x}[n-1|n-2]}
\end{aligned}$$

Substituting the forward model:

$$\begin{aligned}
\Delta x[n] &= A\Delta x[n-1] + BKL^s[n]\eta_s[n-1] + BKL^s[n]\Delta x[n-1] \\
&\quad + BK \left[I - L^s[n] \right] \left(\hat{A}\Delta \hat{x}[n-2|y_t[n-1]] + \hat{B}\Delta u[n-1] \right)
\end{aligned}$$

Adding the timing update:

$$\begin{aligned}
\Delta x[n] &= A\Delta x[n-1] + BKL^s[n]\eta_s[n-1] + BKL^s[n]\Delta x[n-1] \\
&\quad + BK \left[I - L^s[n] \right] \left(\hat{A} \left(\Delta \hat{x}[n-2|n-2] + L^t \left(y_t[n-1] - \Delta \hat{t}_{desc} \right) \right) \right. \\
&\quad \left. + \hat{B}\Delta u[n-1] \right)
\end{aligned}$$

Adding the mapping from timing to space, so that our expression is explicitly in

APPENDIX C: CLOSED-LOOP CONTROL MODEL

terms of spatial and timing perturbations

$$\begin{aligned}
\Delta x[n] &= A\Delta x[n-1] + BKL^s[n]\eta_s[n-1] + BKL^s[n]\Delta x[n-1] \\
&\quad + BK \left[I - L^s[n] \right] \left(\hat{A} \left(\Delta \hat{x}[n-2|n-2] \right. \right. \\
&\quad \quad \left. \left. + L^t C_s^t \left(\Delta x[n-2] - \Delta \hat{x}[n-2|n-2] \right) + L^t(\eta_t[n]) \right) \right. \\
&\quad \quad \left. + \hat{B}\Delta u[n-1] \right) \\
&= A\Delta x[n-1] + BKL^s[n]\eta_s[n-1] + BKL^s[n]\Delta x[n-1] \\
&\quad + BK \left[I - L^s[n] \right] \left(\hat{A} \left[I - L^t C_s^t \right] \Delta \hat{x}[n-2|n-2] + \hat{A} L^t C_s^t \Delta x[n-2] \right. \\
&\quad \quad \left. + \hat{B}\Delta u[n-1] \right) + BK \left[I - L^s[n] \right] \hat{A} L^t \eta_t[n] \\
&= (A + BKL^s[n])\Delta x[n-1] + BKL^s[n]\eta_s[n-1] + BK \left[I - L^s[n] \right] \hat{A} L^t \eta_t[n] \\
&\quad + BK \left[I - L^s[n] \right] \left(\hat{A} \left[I - L^t C_s^t \right] \Delta \hat{x}[n-2|n-2] + \hat{A} L^t C_s^t \Delta x[n-2] \right. \\
&\quad \quad \left. + \hat{B}\Delta u[n-1] \right)
\end{aligned}$$

Substituting in for $\Delta u[n]$:

$$\begin{aligned}
\Delta x[n] &= (A + BKL^s[n])\Delta x[n-1] + BKL^s[n]\eta_s[n-1] + BK \left[I - L^s[n] \right] \hat{A} L^t \eta_t[n] \\
&\quad + BK \left[I - L^s[n] \right] \left(\hat{A} \left[I - L^t C_s^t \right] \Delta \hat{x}[n-2|n-2] + \hat{A} L^t C_s^t \Delta x[n-2] \right. \\
&\quad \quad \left. + \hat{B}K\Delta \hat{x}[n-2|n-2] \right)
\end{aligned}$$

APPENDIX C: CLOSED-LOOP CONTROL MODEL

$$\begin{aligned}
&= (A + BKL^s[n])\Delta x[n-1] + BKL^s[n]\eta_s[n-1] + BK\left[I - L^s[n]\right]\hat{A}L^t\eta_t[n] \\
&\quad + BK\left[I - L^s[n]\right]\left(\left[\hat{A}(I - L^tC_s^t) + \hat{B}K\right]\Delta\hat{x}[n-2|n-2] \right. \\
&\quad \quad \left. + \hat{A}L^tC_s^t\Delta x[n-2]\right) \\
&= (A + BKL^s[n])\Delta x[n-1] + BKL^s[n]\eta_s[n-1] + BK\left[I - L^s[n]\right]\hat{A}L^t\eta_t[n] \\
&\quad + BK\left[I - L^s[n]\right]\hat{A}L^tC_s^t\Delta x[n-2] \\
&\quad + BK\left[I - L^s[n]\right]\left(\left[\hat{A}(I - L^tC_s^t) + \hat{B}K\right]\Delta\hat{x}[n-2|n-2]\right) \quad (*)
\end{aligned}$$

Now assume an unbiased filter (such as a Kalman filter) for L^t, L^s , the following hold:

$$\begin{aligned}
E\left[\hat{x}[n|y_s[n]] - x[n]\right] &= 0 \rightarrow E\left[\hat{x}[n|y_s[n]]\right] = x[n] \\
E\left[\hat{x}[n|y_t[n]] - x[n]\right] &= 0 \rightarrow E\left[\hat{x}[n|y_t[n]]\right] = x[n]
\end{aligned}$$

APPENDIX C: CLOSED-LOOP CONTROL MODEL

Resuming from $\{*\}$ and incorporating this assumption:

$$\begin{aligned}
\Delta x[n] &= (A + BKL^s[n])\Delta x[n-1] + BKL^s[n]\eta_s[n-1] + BK\left[I - L^s[n]\right]\hat{A}L^t\eta_t[n] \\
&\quad + BK\left[I - L^s[n]\right]\hat{A}L^tC_s^t\Delta x[n-2] \\
&\quad + BK\left[I - L^s[n]\right]\left(\left[\hat{A}(I - L^tC_s^t) + \hat{B}K\right]\Delta x[n-2]\right) \\
&= (A + BKL^s[n])\Delta x[n-1] + BKL^s[n]\eta_s[n-1] + BK\left[I - L^s[n]\right]\hat{A}L^t\eta_t[n] \\
&\quad + BK\left[I - L^s[n]\right]\left(\hat{A}L^tC_s^t\Delta x[n-2] + \hat{A}\Delta x[n-2] \right. \\
&\quad\quad\quad \left. - \hat{A}L^tC_s^t\Delta x[n-2] + \hat{B}K\Delta x[n-2]\right) \\
&= (A + BKL^s[n])\Delta x[n-1] + BKL^s[n]\eta_s[n-1] + BK\left[I - L^s[n]\right]\hat{A}L^t\eta_t[n] \\
&\quad + BK\left[I - L^s[n]\right]\left(\hat{A}\Delta x[n-2] + \hat{B}K\Delta x[n-2]\right) \\
&= (A + BKL^s[n])\Delta x[n-1] + BKL^s[n]\eta_s[n-1] + BK\left[I - L^s[n]\right]\hat{A}L^t\eta_t[n] \\
&\quad + BK\left[I - L^s[n]\right]\left(\hat{A} + \hat{B}K\right)\Delta x[n-2]
\end{aligned}$$

APPENDIX C: CLOSED-LOOP CONTROL MODEL

$$\begin{aligned}
&= (A + BKL^s[n])\Delta x[n - 1] \\
&\quad + \left[BK\hat{A} - BKL^s[n]\hat{A} + BK\hat{B}K - BKL^s[n]\hat{B}K \right] \Delta x[n - 2] \\
&\quad + BKL^s[n]\eta_s[n - 1] + BK \left[I - L^s[n] \right] \hat{A}L^t\eta_t[n] \\
&= (A + BKL^s[n])\Delta x[n - 1] + \left[BK \left(\hat{A} - \hat{B}KL^s[n] \right) \right. \\
&\quad \left. + BK \left(L^s[n]\hat{A} + \hat{B}K \right) \right] \Delta x[n - 2] \\
&\quad + BKL^s[n]\eta_s[n - 1] + BK \left[I - L^s[n] \right] \hat{A}L^t\eta_t[n]
\end{aligned}$$

Isolating terms:

$$\begin{aligned}
&\Delta x[n] - (A + BKL^s[n])\Delta x[n - 1] \\
&\quad - \left[BK \left(\hat{A} - \hat{B}KL^s[n] \right) + BK \left(L^s[n]\hat{A} + \hat{B}K \right) \right] \Delta x[n - 2] \\
&\quad = BKL^s[n]\eta_s[n - 1] + BK \left[I - L^s[n] \right] \hat{A}L^t\eta_t[n] \tag{**}
\end{aligned}$$

Assuming Kalman gains have stabilized by time perturbation has been applied,

i.e.:

$$\lim_{n \text{ large}} E[L^s[n]] = \text{const} = L^s$$

$$\lim_{n \text{ large}} E[L^t[n]] = \text{const} = L^t$$

APPENDIX C: CLOSED-LOOP CONTROL MODEL

{**} becomes:

$$\begin{aligned}\Delta x[n] - (A + BKL^s)\Delta x[n-1] - \left[BK\left(\hat{A} - \hat{B}KL^s\right) + BK\left(L^s\hat{A} + \hat{B}K\right) \right] \Delta x[n-2] \\ = BKL^s\eta_s[n-1] + BK\left[I - L^s\right]\hat{A}L^t\eta_t[n]\end{aligned}$$

Converting to the discrete-time frequency domain via Z transform:

$$X[z] = Z\{\Delta x[n]\}$$

$$N_s[z] = Z\{\eta_s[n]\}$$

$$N_t[z] = Z\{\eta_t[n]\}$$

$$\begin{aligned}X[z] - z^{-1}(A + BKL^s)X[z] - z^{-2}\left[BK\left(\hat{A} - \hat{B}KL^s\right) + BK\left(L^s\hat{A} + \hat{B}K\right) \right] X[z] \\ = z^{-1}BKL^sN_s[z] + BK\left[I - L^s\right]\hat{A}L^tN_t[z] \\ X[z]\left(I - z^{-1}(A + BKL^s) - z^{-2}\left[BK\left(\hat{A} - \hat{B}KL^s\right) + BK\left(L^s\hat{A} + \hat{B}K\right) \right]\right) \\ = z^{-1}BKL^sN_s[z] + BK\left[I - L^s\right]\hat{A}L^tN_t[z]\end{aligned}$$

And this is of the form:

$$X[z] = H_{\text{CL}}^s N_s[z] + H_{\text{CL}}^t N_t[z]$$

APPENDIX C: CLOSED-LOOP CONTROL MODEL

where:

$$H_{CL}^s = \frac{z^{-1}BKL^s}{I - z^{-1}(A + BKL^s) - z^{-2}\left[BK\left(\hat{A} - \hat{B}KL^s\right) + BK\left(L^s\hat{A} + \hat{B}K\right)\right]}$$

$$H_{CL}^t = \frac{BK\left[I - L^s\right]\hat{A}L^t}{I - z^{-1}(A + BKL^s) - z^{-2}\left[BK\left(\hat{A} - \hat{B}KL^s\right) + BK\left(L^s\hat{A} + \hat{B}K\right)\right]}$$

Coherence hypotheses

If the above model captures the essential dynamics of paddle juggling (i.e. the controlled variable is spatial), we predict the following:

1. Perturb ball position only ($N_t[z] = 0$) \rightarrow

$$X[z] = H_{CL}^s N_s[z]$$

$$\|X[z]\| = \|H_{CL}^s\|^2 \|N_s[z]\| \quad (\text{Defn of PSD})$$

$$C_{\eta_s, x} = \frac{\|X[z]N_s[z]\|}{\|X[z]\| \cdot \|N_s[z]\|} = \frac{\|H_{CL}^s\|^2 \|N_s[z]\|^2}{\|H_{CL}^s\|^2 \|N_s[z]\| \cdot \|N_s[z]\|} = 1$$

2. Perturb collision timing only ($N_s[z] = 0$) \rightarrow

$$X[z] = H_{CL}^t N_t[z]$$

$$\|X[z]\| = \|H_{CL}^t\|^2 \|N_t[z]\| \quad (\text{Defn of PSD})$$

$$C_{\eta_t, x} = \frac{\|X[z]N_t[z]\|}{\|X[z]\| \cdot \|N_t[z]\|} = \frac{\|H_{CL}^t\|^2 \|N_t[z]\|^2}{\|H_{CL}^t\|^2 \|N_t[z]\| \cdot \|N_t[z]\|} = 1$$

APPENDIX C: CLOSED-LOOP CONTROL MODEL

For linear systems, the spectral coherences between either perturbation modality and ball position would be approximately one; but in practice values above 0.8 are strong indicators of linearity [15,17]. Nonetheless, we would expect the coherences to be statistically equivalent.

Bibliography

- [1] P. Reist and R. D’Andrea, “Design of the pendulum juggler,” in *Proc IEEE Int Conf Robot Autom*, 2011, pp. 5154–5159.
- [2] A. Morice, I. Siegler, B. Bardy, and W. Warren, “Learning new perception-action solutions in virtual ball bouncing,” *Exp Brain Res*, vol. 181, no. 2, pp. 249–265, 2007.
- [3] A. de Rugy, K. Wei, H. Mueller, and D. Sternad, “Actively tracking ‘passive’ stability in a ball bouncing task.” *Brain Res*, vol. 982, pp. 64–78, 2003.
- [4] A. Rizzi and D. E. Koditschek, “Preliminary experiments in robot juggling,” in *Proc Int Symp on Experimental Robotics*, 1991.
- [5] M. Buehler, D. E. Koditschek, and P. J. Kindlmann, “A one degree of freedom juggler in a two degree of freedom environment,” in *Proc IEEE Int Workshop on Intelligent Robots*, 1988.
- [6] D. Sternad, M. Duarte, H. Katsumata, and S. Schaal, “Bouncing a ball: tuning

BIBLIOGRAPHY

- into dynamic stability,” *J Exp Psychol-Hum Percept Perform*, vol. 27, no. 5, pp. 1163–1184, 2001.
- [7] I. A. Siegler, B. B.G., and W. H. Warren, “Passive vs. active control of rhythmic ball bouncing: The role of visual information,” *J Exp Psychol*, vol. 36, pp. 729–750, 2010.
- [8] A. Okamura, C. Richard, and M. Cutkosky, “Feeling is believing: using a force-feedback joystick to teach dynamic systems,” *J Eng Educ*, vol. 91, no. 3, pp. 345–349, 2002.
- [9] A. De, “Neuromechanical control of paddle juggling,” Master’s thesis, Johns Hopkins University, 2010.
- [10] M. M. Ankarali, H. T. Şen, A. De, A. M. Okamura, and N. J. Cowan, “Haptic feedback enhances rhythmic motor control by reducing variability, not improving convergence rate,” *J Neurophysiol*, vol. 111, no. 6, pp. 1286–1299, 2014.
- [11] A. Lamperski and N. J. Cowan, “Time-changed linear quadratic regulators,” in *European Control Conference*, 2013.
- [12] —, “Optimal control with noisy time,” *IEEE Trans Autom Control*, vol. 61, no. 2, pp. 319–333, 2016.
- [13] S. Lavalle and M. Egerstedt, “On time: clocks, chronometers, and open-loop control,” in *Proc IEEE Int Conf on Decision Control*, 2007.

BIBLIOGRAPHY

- [14] N. J. Cowan and E. S. Fortune, “The critical role of locomotion mechanics in decoding sensory systems,” *J Neurosci*, vol. 27, no. 5, pp. 1123–1128, 2007. [Online]. Available: <http://dx.doi.org/10.1523/JNEUROSCI.4198-06.2007>
- [15] E. Roth, K. Zhuang, S. A. Stamper, E. S. Fortune, and N. J. Cowan, “Stimulus predictability mediates a switch in locomotor smooth pursuit performance for *Eigenmannia virescens*.” *J Exp Biol*, vol. 214, no. 7, pp. 1170–1180, 2011.
- [16] M. S. Madhav, S. A. Stamper, E. S. Fortune, and N. J. Cowan, “Closed-loop stabilization of the jamming avoidance response reveals its locally unstable and globally nonlinear dynamics,” *J Exp Biol*, vol. 216, no. 22, pp. 4272–4284, 2013. [Online]. Available: <http://dx.doi.org/10.1242/jeb.088922>
- [17] S. Sponberg, J. P. Dyrh, R. W. Hall, and T. L. Daniel, “Luminance-dependent visual processing enables moth flight in low light,” *Science*, vol. 348, no. 6240, pp. 1245–1248, June 2015.
- [18] E. Sutton, A. Demir, S. Stamper, E. Fortune, and N. Cowan, “Dynamic modulation of visual and electrosensory gains for locomotor control,” *J R Soc Interface*, vol. 13, no. 118, pp. 1–10, May 2016.
- [19] R. W. Nickl, “The medial premotor cortex as a bridge from internal timekeeping to action,” *J Neurosci*, vol. 37(37), pp. 8860–8862, 2017.
- [20] R. Shadmehr, M. A. Smith, and J. W. Krakauer, “Error correction, sensory

BIBLIOGRAPHY

- prediction, and adaptation in motor control,” *Annu Rev Neurosci*, vol. 33, pp. 89–108, 2010.
- [21] N. Hogan and D. Sternad, “On rhythmic and discrete movements: reflections, definitions and implications for motor control,” *Exp Brain Res*, vol. 181, pp. 13–30, 2007.
- [22] T. Flash and N. Hogan, “The coordination of arm movements: an experimentally confirmed mathematical model,” *J Neurosci*, vol. 5, no. 7, pp. 1688–1703, 1985.
- [23] B. C. M. Smits-Engelsman, G. P. Van Galen, and J. Duysens, “The breakdown of Fitts’s law in rapid, reciprocal aiming movements,” *Exp Brain Res*, vol. 145, no. 2, pp. 222–230, 2002.
- [24] F. Lacquaniti, “Central representations of human limb movement as revealed by studies of drawing and handwriting,” *Trends Neurosci*, vol. 12, no. 8, pp. 287–291, 1989.
- [25] A. G. Feldman, “Superposition of motor programs. I. Rhythmic forearm movements in man,” *Neuroscience*, vol. 5, no. 1, pp. 81–90, 1980.
- [26] G. Cappellini, Y. P. Ivanenko, R. E. Poppele, and F. Lacquaniti, “Motor patterns in human walking and running,” *J Neurophysiol*, vol. 95, no. 6, pp. 3426–3437, 2006.

BIBLIOGRAPHY

- [27] Y. Guiard, “On Fitts’s and Hooke’s laws: Simple harmonic movement in upper-limb cyclical aiming,” *Acta Psychologica*, vol. 82, no. 1, pp. 139–159, 1993.
- [28] C. E. Shannon, “A mathematical theory of communication,” *Bell Sys Tech J*, vol. 27, pp. 379–423, 623–656, 1948.
- [29] P. M. Fitts, “The information capacity of the human motor system in controlling the amplitude of movement.” *J Exp Psychol*, vol. 47, no. 6, pp. 262–269, 1954.
- [30] P. M. Fitts and J. R. Peterson, “Information capacity of discrete motor responses,” *J Exp Psychol*, vol. 67, no. 2, pp. 103–112, 1964.
- [31] V. B. Brooks, “Some examples of programmed limb movements,” *Brain Res*, vol. 71, no. 2, pp. 299–308, 1974.
- [32] I. Kozlovskaya, A. Atkin, F. Horvath, J. Thomas, and V. Brooks, “Preprogrammed and feedback-guided movements of monkeys,” *Behav Biol*, vol. 12, no. 2, pp. 243–248, 1974.
- [33] S. Schaal and D. Sternad, “Origins and violations of the 2/3 power law in rhythmic three-dimensional arm movements,” *Exp Brain Res*, vol. 136, no. 1, pp. 60–72, 2001.
- [34] M. Roerdink, E. D. Ophoff, C. E. Peper, and P. J. Beek, “Visual and musculoskeletal underpinnings of anchoring in rhythmic visuo-motor tracking,” *Exp Brain Res*, vol. 184, no. 2, pp. 143–156, 2008.

BIBLIOGRAPHY

- [35] N. Bernstein, *The Coordination and Regulation of Movements*. Pergamon Press, Oxford, 1967.
- [36] J. A. S. Kelso, “The dynamic brain in action: coordinative structures, criticality, and coordination dynamics,” in *Criticality in Neural Systems*, D. Plenz and E. Niebur, Eds. Weinheim, Germany: Wiley, 2014.
- [37] A. D. Kuo, “The relative roles of feedforward and feedback in the control of rhythmic movements,” *Motor Control*, vol. 6, no. 2, pp. 129–145, 2002.
- [38] B. A. Kay, J. A. Kelso, E. L. Saltzman, and G. Schöner, “Space–time behavior of single and bimanual rhythmical movements: Data and limit cycle model.” *J Exp Psychol Hum Percept Perform*, vol. 13, no. 2, p. 178, 1987.
- [39] J. A. S. Kelso, K. G. Holt, P. Rubin, and P. N. Kugler, “Patterns of human interlimb coordination emerge from the properties of non-linear, limit cycle oscillatory processes: theory and data,” *J Motor Behav*, vol. 13, no. 4, pp. 226–261, 1981.
- [40] H. Haken, J. S. Kelso, and H. Bunz, “A theoretical model of phase transitions in human hand movements,” *Biol Cybern*, vol. 51, no. 5, pp. 347–356, 1985.
- [41] P. J. Beek, C. E. Peper, and A. Daffertshofer, “Modeling rhythmic interlimb coordination: Beyond the haken–kelso–bunz model,” *Brain Cogn*, vol. 48, no. 1, pp. 149–165, 2002.

BIBLIOGRAPHY

- [42] B. A. Kay, E. L. Saltzman, and J. Kelso, “Steady-state and perturbed rhythmic movements: A dynamical analysis.” *J Exp Psychol Hum Percept Perform*, vol. 17, no. 1, p. 183, 1991.
- [43] N. G. Hatsopoulos and W. H. Warren, “Resonance tuning in rhythmic arm movements,” *J Motor Behav*, vol. 28, no. 1, pp. 3–14, 1996.
- [44] G. Schöner, P. G. Zanone, and J. A. S. Kelso, “Learning as change of coordination dynamics: theory and experiment,” *Journal Mot Beh*, vol. 24, no. 1, pp. 29–48, 1992.
- [45] P. G. Zanone and J. A. Kelso, “Evolution of behavioral attractors with learning: nonequilibrium phase transitions.” *J Exp Psychol Hum Percept Perform*, vol. 18, no. 2, pp. 403–421, 1992.
- [46] P. J. Beek and W. J. Beek, “Tools for constructing dynamical models of rhythmic movement,” *Hum Mov Sci*, vol. 7, no. 2-4, pp. 301–342, 1988.
- [47] D. J. Bennett, J. M. Hollerbach, Y. Xu, and I. W. Hunter, “Time-varying stiffness of human elbow joint during cyclic voluntary movement,” *Exp Brain Res*, vol. 88, no. 2, pp. 433–442, 1992.
- [48] R. Balasubramanian, R. D. Howe, and Y. Matsuoka, “Task performance is prioritized over energy reduction,” *IEEE Trans Biomed Eng*, vol. 56(5), pp. 1310–1317, 2009.

BIBLIOGRAPHY

- [49] P. Holmes, R. J. Full, D. Koditschek, and J. Guckenheimer, “The dynamics of legged locomotion: Models, analyses, and challenges,” *SIAM Review*, vol. 48, no. 2, pp. 207–304, 2006.
- [50] C. S. Sherrington, *The Integrative Action of the Nervous System*. Yale University Press, 1911.
- [51] E. Marder and R. L. Calabrese, “Principles of rhythmic motor pattern generation,” *Physiol Rev*, vol. 76, no. 3, pp. 687–717, 1996.
- [52] Y. I. Arshavsky, “Cellular and network properties in the functioning of the nervous system: from central pattern generators to cognition,” *Brain Res Rev*, vol. 41, no. 2, pp. 229–267, 2003.
- [53] A. de Rugy and D. Sternad, “Interaction between discrete and rhythmic movements: reaction time and phase of discrete movement initiation during oscillatory movements,” *Brain Research*, vol. 994, no. 2, pp. 160–174, 2003.
- [54] J. B. Wagman, “What is responsible for the emergence of order and pattern in psychological systems?” *J Theor Philos Psychol*, vol. 30, no. 1, p. 32, 2010.
- [55] P. Wallen and T. L. Williams, “Fictive locomotion in the lamprey spinal cord in vitro compared with swimming in the intact and spinal animal.” *J Physiol*, vol. 347, pp. 225–239, 1984.

BIBLIOGRAPHY

- [56] S. Grillner, “The motor infrastructure: from ion channels to neuronal networks.” *Nat Rev Neurosci*, vol. 4, pp. 573–586, 2003.
- [57] O. Andersson and S. Grillner, “Peripheral control of the cat’s step cycle. I. Phase dependent effects of ramp-movements of the hip during ‘fictive locomotion’,” *Acta Physiol Scand*, vol. 113, pp. 89–101, 1981.
- [58] B. Calancie, “Interlimb reflexes following cervical spinal cord injury in man,” *Exp Brain Res*, vol. 85, pp. 458–469, 1996.
- [59] J. Yang, M. Stephens, and R. Vishram, “Infant stepping: a method to study the sensory control of human walking,” *J Physiol*, vol. 507, no. 3, pp. 927–937, 1998.
- [60] F. Delcomyn, “Neural basis of rhythmic behavior in animals,” *Science*, vol. 210, no. 4469, pp. 492–498, 1980.
- [61] E. S. Harcombe and R. J. Wyman, “Diagonal locomotion in de-afferentated toads,” *J Exp Biol*, vol. 53, pp. 255–263, 1970.
- [62] P. J. Beek, “Timing and phase locking in cascade juggling,” *Ecol Psychol*, vol. 1, no. 1, pp. 55–96, 1989.
- [63] M. T. Turvey and R. E. Shaw, “Ecological foundations of cognition. I: Symmetry and specificity of animal-environment systems,” *J Conscious Stud*, vol. 6, no. 11-12, pp. 95–110, 1999.

BIBLIOGRAPHY

- [64] B. Conway, H. Hultborn, and O. Kiehn, “Proprioceptive input resets central locomotor rhythm in the spinal cat.” *Exp. Brain Res*, vol. 68, pp. 643–656, 1987.
- [65] S. Rossignol and G. M. Jones, “Audio–spinal influence in man studied by the H-reflex and its possible role on rhythmic movements synchronized to sound,” *Electroencephalogr Clin Neurophysiol*, vol. 41, pp. 83–92, 1976.
- [66] E. Zehr, “Neural control of rhythmic human movement: the common core hypothesis,” *Exerc Sport Sci Rev.*, vol. 33, no. 1, pp. 54–60, 2005.
- [67] E. Zehr and J. Duysens, “Regulation of arm and leg movement during human locomotion.” *Neuroscientist*, vol. 10, no. 4, pp. 347–361, 2004.
- [68] G. Taga, “Emergence of bipedal locomotion through entrainment among the neuro-musculo-skeletal system and the environment,” *Physica D*, vol. 75, no. 1-3, pp. 190–208, 1994.
- [69] A. Frigon, D. Collins, and E. Zehr, “Effect of rhythmic arm movement on reflexes in the legs: modulation of soleus H-reflexes and somatosensory conditioning.” *J Neurophysiol*, vol. 91, pp. 1516–1523, 2004.
- [70] E. P. Zehr, J. E. Balter, D. P. Ferris, S. R. Hundza, P. M. Loadman, and R. H. Stoloff, “Neural regulation of rhythmic arm and leg movement is conserved across human locomotor tasks.” *J Physiol*, vol. 582(1), pp. 209–27, 2007.

BIBLIOGRAPHY

- [71] T. Klarner, T. Barss, Y. Sun, C. Kaupp, and E. Zehr, “Preservation of common rhythmic locomotor control despite weakened supraspinal regulation after stroke.” *Front Integr Neurosci.*, vol. 8, no. 95, pp. 1–9, 2014.
- [72] G. Schöner, “Timing, clocks, and dynamical systems.” *Brain Cogn*, vol. 48, pp. 31–51, 2002.
- [73] D. P. Hanes and J. D. Schall, “Neural control of voluntary movement initiation.” *Science*, vol. 274, pp. 427–430, 1996.
- [74] P. Simen, F. Balci, L. deSouza, J. D. Cohen, and P. Holmes, “A model of interval timing by neural integration.” *J Neurosci*, vol. 31(25), pp. 9238–9253, 2011.
- [75] S. G. Carver, E. S. Fortune, and N. J. Cowan, “State-estimation and cooperative control with uncertain time,” in *Proc Amer Control Conf.* IEEE, 2013, pp. 2990–2995.
- [76] B. H. Repp, “Sensorimotor synchronization: A review of the tapping literature.” *Psychon Bull Rev*, vol. 12(6), pp. 969–992, 2005.
- [77] A. M. Wing, “Voluntary timing and brain function: An information processing approach,” *Brain Cogn*, vol. 48, pp. 7–30, 2002.
- [78] S. M. Rao, D. L. Harrington, K. Y. Haaland, J. A. Bobhold, R. W. Cox, and

BIBLIOGRAPHY

- J. R. Binder, “Distributed neural systems underlying the timing of movements,” *J Neurosci*, vol. 17(4), pp. 5528–5535, 1997.
- [79] D. J. O’Boyle, J. S. Freeman, and F. W. J. Cody, “The accuracy and precision of timing of self-repetitive movements in subjects with parkinsons disease.” *Brain*, vol. 119, pp. 51–70, 1996.
- [80] M. Fernandez Del Olmo, B. Cheeran, G. Koch, and J. C. Rothwell, “Role of the cerebellum in externally paced rhythmic finger movements,” *J Neurophysiol*, vol. 98, pp. 145–152, 2007.
- [81] R. Spencer, H. Zelaznik, J. Diedrichsen, and R. Ivry, “Disrupted timing of discontinuous but not continuous movements by cerebellar lesions,” *Science*, vol. 300, pp. 1437–1439, 2003.
- [82] B. Conrad and V. B. Brooks, “Effects of dentate cooling on rapid alternating arm movements.” *J Neurophysiol*, vol. 37, no. 4, pp. 792–804, 1974.
- [83] D. Durstewitz and J. K. Seamans, “The computational role of dopamine D1 receptors in working memory,” *Neural Netw*, vol. 15, pp. 561–572, 2007.
- [84] W. H. Meck, T. B. Penney, and V. Pouthas, “Cortico-striatal representation of time in animals and humans,” *Curr Opin Neurobiol*, vol. 18(2), pp. 145–152, 2008.
- [85] K. I. Bakhurin, V. Goudar, J. L. Shobe, L. D. Claar, D. V. Buonomano, and

BIBLIOGRAPHY

- S. C. Masmanidis, “Differential encoding of time by prefrontal and striatal network dynamics,” *J Neurosci*, vol. 37(4), pp. 854–870, 2017.
- [86] J. Wang, D. Narain, E. A. Hosseini, and M. Jazayeri, “Flexible timing by temporal scaling of cortical responses,” *Nat Neurosci*, vol. 21, no. 1, p. 102, 2018.
- [87] S. Schaal, D. Sternad, R. Osu, and M. Kawato, “Rhythmic arm movement is not discrete.” *Nat Neurosci*, vol. 7, no. 10, pp. 1136–1143, 2004.
- [88] H. Merchant and B. B. Averbeck, “The computational and neural basis of rhythmic timing in medial premotor cortex,” *J Neurosci*, vol. 37(17), pp. 4552–4564, 2017.
- [89] S. Donnet, R. Bartolo, J. M. Fernandes, J. P. S. Cunha, L. Prado, and H. Merchant, “Monkeys time their pauses of movement and not their movement-kinematics during a synchronization-continuation rhythmic task,” *J Neurophysiol*, vol. 111, no. 10, pp. 2138–2149, 2014.
- [90] D. Marr and T. Poggio, “From understanding computation to understanding neural circuitry,” *Massachusetts Institute of Technology, A.I. Memo 357*, 1976.
- [91] W. H. Warren, “The dynamics of perception and action,” *Psychol Rev*, vol. 113(2), pp. 358–389, 2006.

BIBLIOGRAPHY

- [92] B. R. Fajen, M. A. Riley, and M. T. Turvey, “Information, affordances, and the control of action in sport,” *Int J Sport Psychol*, vol. 40, no. 1, p. 79, 2009.
- [93] R. Goebel, R. G. Sanfelice, and A. R. Teel, “Hybrid dynamical systems,” *IEEE Control Syst Mag*, vol. 29, no. 2, pp. 28–93, 2009.
- [94] S. Schaal, C. Atkeson, and D. Sternad, “One-handed juggling: A dynamical approach to a rhythmic movement task,” *J Motor Behav*, vol. 28, pp. 165–183, 1996.
- [95] M. H. Raibert, H. B. B. Brown, M. Chepponis, E. Hastings, J. Koechling, K. N. Murphy, S. S. Murthy, and A. J. Stentz, “Dynamically stable legged locomotion,” The Robotics Institute and Department of Computer Science, Carnegie–Mellon University, Tech. Rep., 1983.
- [96] M. Bühler, D. Koditschek, and P. Kindlmann, “A family of robot control strategies for intermittent dynamical environments,” *IEEE Control Syst Mag*, vol. 10, no. 2, pp. 16–22, Feb 1990.
- [97] F. C. Anderson and M. G. Pandy, “Dynamic optimization of human walking,” *J Biomech Eng*, vol. 123, pp. 381–390, 2001.
- [98] C. E. Shannon, *Collected Papers*. Wiley-IEEE, 1993.
- [99] P. Beek and A. Lewbel, “The science of juggling,” *Sci Am*, vol. 273, no. 5, pp. 92–97, 1995.

BIBLIOGRAPHY

- [100] V. L. Veitz and I. S. Beilin, “Dynamics of transportation of a material particle with stochastic characteristic along a horizontal plane,” *Mech Mach Theory*, vol. 7, no. 2, pp. 155–165, 1972.
- [101] L. A. Wood and K. P. Byrne, “Analysis of a random repeated impact process,” *J Sound Vib*, vol. 78, no. 3, pp. 329–345, 1981.
- [102] P. J. Holmes, “The dynamics of repeated impacts with a sinusoidally vibrating table.” *J Sound Vib*, vol. 84, no. 2, pp. 173–189, 1982.
- [103] T. L. Vincent and A. I. Mees, “Controlling a bouncing ball,” *Int J Bifurc Chaos*, vol. 10, no. 3, pp. 579–592, 2000.
- [104] R. Ronsse, K. Wei, and D. Sternad, “Optimal control of a hybrid rhythmic–discrete task: the bouncing ball revisited,” *J Neurophysiol*, vol. 103, pp. 2482–2493, 2010.
- [105] M. Buehler, D. E. Koditschek, and P. J. Kindlmann, “Planning and control of robotic juggling and catching tasks,” *Int J Rob Res*, vol. 13, no. 2, pp. 101–118, 1994.
- [106] A. A. Rizzi and D. E. Koditschek, “Further progress in robot juggling: Solvable mirror laws,” in *Proc IEEE Int Conf Robot Autom*, 1994, pp. 2935–2940.
- [107] J. Guckenheimer and P. Holmes, *Nonlinear Oscillations, Dynamical Systems, and Bifurcation of Vector Fields*. Springer-Verlag, 1983.

BIBLIOGRAPHY

- [108] N. B. Tufillaro, T. Abbott, and J. Reilly, *An Experimental Approach to Non-linear Dynamics and Chaos*. Addison-Wesley Redwood City, CA, 1992.
- [109] A. Lamperski and A. D. Ames, “Lyapunov theory for Zeno stability,” *IEEE Trans Autom Control*, vol. 58, no. 1, pp. 100–112, 2013.
- [110] E. W. Aboaf, “Task-level robot learning: MIT artificial intelligence laboratory technical report 1079,” Master’s thesis, Massachusetts Institute of Technology, 1988.
- [111] M. Kawato, “Internal models for motor control and trajectory planning.” *Curr Opin Neurobiol*, vol. 9, no. 6, pp. 718–727, 1999.
- [112] E. W. Aboaf, S. M. Drucker, and C. G. Atkeson, “Task-level robot learning: Juggling a tennis ball more accurately,” in *Proc IEEE Int Conf Robot Autom*, 1989, pp. 1290–1295.
- [113] R. Huys and P. J. Beek, “The coupling between point-of-gaze and ballmovements in three-ball cascade juggling: the effects of expertise, pattern and tempo,” *J Sports Sci*, vol. 20, no. 3, pp. 171–186, 2002.
- [114] P. N. Kugler, J. A. S. Kelso, and M. T. Turvey, “On the control and coordination of naturally developing systems,” in *The Development of Movement Control and Coordination*. Wiley, 1982.

BIBLIOGRAPHY

- [115] S. Schaal and C. G. Atkeson, “Open loop stable control strategies for robot juggling,” in *Proc IEEE Int Conf Robot Autom*, 1993, pp. 913–918.
- [116] A. A. Rizzi and D. E. Koditschek, “An active visual estimator for dexterous manipulation,” *IEEE Trans Rob Autom*, vol. 12(5), pp. 697–713, 1996.
- [117] P. Kulchenko and E. Todorov, “Policy gradient methods with model predictive control applied to ball bouncing,” *IEEE Adaptive Dynamic Programming and Reinforcement Learning*, 2011.
- [118] R. Ronsse, P. Lefevre, and R. Sepulchre, “Rhythmic feedback control of a blind planar juggler,” *IEEE Trans Robot*, vol. 23, no. 4, pp. 790–802, 2007.
- [119] T. McGeer, “Passive dynamic walking,” *Int J Rob Res*, vol. 9, no. 2, pp. 62–82, 1990.
- [120] P. Reist and R. D’Andrea, “Design and analysis of a blind juggling robot,” *IEEE Trans Robot*, vol. 28, no. 6, pp. 1228–1243, 2012.
- [121] T. L. Vincent, “Control using chaos,” *IEEE Control Sys Mag*, vol. 17, no. 6, pp. 65–76, 1997.
- [122] A. Kini, T. L. Vincent, and B. Paden, “The bouncing ball apparatus as an experimental tool,” *J Dyn Syst Meas Control*, vol. 128, no. 2, pp. 330–340, 2006.

BIBLIOGRAPHY

- [123] P. Reist and R. D’Andrea, “Control of nonlinear systems with symmetries using chaos,” in *Proc IEEE Int Conf on Decision Control*, 2012, pp. 997–1002.
- [124] M. S. Madhav and R. W. Nickl, “Mimicry or scrutiny? striking a partnership between engineering design and biological research,” *IEEE Potentials*, vol. 34, no. 2, pp. 26–32, 2015.
- [125] T. Dijkstra, H. Katsumata, A. de Rugy, and D. Sternad, “The dialogue between data and model: Passive stability and relaxation behavior in a ball bouncing task,” *Nonlinear Studies*, vol. 11(3), pp. 319–344, 2004.
- [126] K. Wei, T. M. H. Dijkstra, and D. Sternad, “Passive stability and active control in a rhythmic task,” *J Neurophysiol*, vol. 98, pp. 2633–2646, 2007. [Online]. Available: <http://jn.physiology.org/content/103/5/2482.short>
- [127] R. Huys, A. Daffertshofer, and P. J. Beek, “Multiple time scales and multiform dynamics in learning to juggle,” *Motor Control*, vol. 8, no. 2, pp. 188–212, 2004.
- [128] A. M. van Santvoord and P. J. Beek, “Spatiotemporal variability in cascade juggling,” *Acta Psychologica*, vol. 91, no. 2, pp. 131–151, 1996.
- [129] R. Huys, A. Daffertshofer, and P. J. Beek, “Learning to juggle: on the assembly of functional subsystems into a task-specific dynamical organization,” *Biol Cybern*, vol. 88, no. 4, pp. 302–318, 2003.

BIBLIOGRAPHY

- [130] E. Todorov and M. I. Jordan, “Optimal feedback control as a theory of motor coordination,” *Nat Neurosci*, 2002.
- [131] M. Zago, I. Pacifici, N. Lovecchio, M. Galli, P. A. Federolf, and C. Sforza, “Multi-segmental movement patterns reflect juggling complexity and skill level,” *Hum Mov Sci*, vol. 54, pp. 144–153, 2017.
- [132] I. A. Siegler, C. Bazile, and W. H. Warren, “Mixed control for perception and action: timing and error correction in rhythmic ball-bouncing,” *Exp Brain Res*, vol. 226, pp. 603–615, 2013.
- [133] G. Avrin, I. A. Siegler, M. Makarov, and P. Rodriguez-Ayerbe, “Model of rhythmic ball bouncing using a visually controlled neural oscillator,” *J Neurophysiol*, vol. 118, no. 4, pp. 2470–2482, 2017.
- [134] H. A. Austin, “A computational theory of physical skill.” *Unpublished doctoral dissertation, Department of Electrical Engineering, Massachusetts Institute of Technology, Cambridge, MA*, 1976.
- [135] A. A. M. van Santvoord and P. J. Beek, “Phasing and the pickup of optical information in cascade juggling,” *Ecol Psychol*, vol. 6, no. 4, pp. 239–263, 1994.
- [136] J. C. Dessing, F. P. Rey, and P. J. Beek, “Gaze fixation improves the stability of expert juggling,” *Exp Brain Res*, vol. 216, no. 4, pp. 635–644, 2012.

BIBLIOGRAPHY

- [137] M. E. Huber and D. Sternad, “Implicit guidance to stable performance in a rhythmic perceptual-motor skill,” *Exp Brain Res*, vol. 233, pp. 1783–1799, 2015.
- [138] H. Katsumata, V. Zatsiorsky, and D. Sternad, “Control of ball-racket interactions in rhythmic propulsion of elastic and non-elastic balls,” *Exp Brain Res*, vol. 149, no. 1, pp. 17–29, 2003.
- [139] M. Buehler, D. E. Koditschek, and P. J. Kindlmann, “A simple juggling robot: Theory and experimentation,” in *Experimental Robotics I, The First International Symposium*. Springer, 1990.
- [140] J. Brown and B. Martin, “How fast is fast enough? choosing between xenomai and linux real-time applications,” in *Twelfth Real-Time Linux Workshop*, 2010.
- [141] M. Quigley, B. Gerkey, K. Conley, J. Faust, T. Foote, J. Leibs, E. Berger, R. Wheeler, and A. Ng, “ROS: an open-source Robot Operating System,” in *Proc. Open-Source Software workshop of the IEEE Int Conf Robot Autom (ICRA)*, 2009.
- [142] H. Bruyininckx, “Open robot control software: the OROCOS project,” in *Proc IEEE Int Conf Robot Autom*, 2001, pp. 2523–2528.
- [143] M. Ernst and M. Banks, “Humans integrate visual and haptic information in a statistically optimal fashion,” *Nature*, vol. 415, pp. 429–433, 2002.

BIBLIOGRAPHY

- [144] R. C. Oldfield, “The assessment and analysis of handedness: The edinburgh inventory,” *Neuropsychologia*, vol. 9, pp. 97–113, 1971.
- [145] R. Pintelon and J. Schoukens, *System Identification: A Frequency Domain Approach*, 2nd ed. Hoboken, New Jersey: Wiley, 2012.
- [146] S. Revzen and J. M. Guckenheimer, “Estimating the phase of synchronized oscillators,” *Phys Rev E*, vol. 78, no. 5, p. 051907, 2008.
- [147] J. S. Bendat and A. G. Piersol, *Engineering Applications of Correlation and Spectral Analysis*. New York: Wiley-Interscience, 1980.
- [148] R. Sigrist, G. Rauter, R. Riener, and P. Wolf, “Augmented visual, auditory, haptic, and multimodal feedback in motor learning: a review,” *Psychon Bull Rev*, vol. 20, pp. 21–53, 2013.
- [149] A. V. Oppenheim, R. W. Shafer, and J. R. Buck, *Discrete-time Signal Processing*, 2nd ed. Upper Saddle River, NJ: Prentice–Hall, 1999.
- [150] E. Roth, M. B. Reiser, M. H. Dickinson, and N. J. Cowan, “A task-level model for optomotor yaw regulation in drosophila melanogaster: a frequency-domain system identification approach,” in *Proc IEEE Int Conf on Decision Control*, 2012.
- [151] R. Scheidt, J. Dingwell, and F. Mussa-Ivaldi, “Learning to move amid uncertainty,” *J Neurophysiol*, vol. 86, pp. 971–985, 2001.

BIBLIOGRAPHY

- [152] M. Smith, A. Ghazizadeh, and R. Shadmehr, “Interacting adaptive processes with different timescales underlie short-term motor learning,” *PLoS Biol*, vol. 4(6), pp. 1035–1043, 2006.
- [153] D. Vorberg and H. H. Schulze, “Linear phase-correction in synchronization: predictions, parameter estimation, and simulations,” *J Math Psychol*, vol. 46, pp. 56–87, 2002.
- [154] C. Bazile, N. Benguigui, and I. A. Siegler, “Development of information–movement couplings in a rhythmical ball–bouncing task: from space- to time-related information.” *Exp Brain Res*, vol. 234, pp. 173–183, 2016.
- [155] P. Bertelson and G. Aschersleben, “Temporal ventriloquism: crossmodal interaction on the time dimension: 1. evidence from auditory–visual temporal order judgment,” *Int J Psychophysiol*, vol. 50, no. 1, pp. 147–155, 2003.
- [156] B. H. Repp and A. Penel, “Rhythmic movement is attracted more strongly to auditory than to visual rhythms,” *Psychol Res*, vol. 68, no. 4, pp. 252–270, 2004.
- [157] S. E. Guttman, L. A. Gilroy, and R. Blake, “Hearing what the eyes see: auditory encoding of visual temporal sequences,” *Psychol Sci*, vol. 16, no. 3, pp. 228–235, 2005.
- [158] F. Crevecoeur, D. Munoz, and S. Scott, “Dynamic multisensory integration:

BIBLIOGRAPHY

- somatosensory speed trumps visual accuracy during feedback control,” *J Neurosci*, vol. 36, no. 33, pp. 8598–8611, 2016.
- [159] W. Fujisaki, S. Shimojo, M. Kashino, and S. Nishida, “Recalibration of audio-visual simultaneity,” *Nat Neurosci*, vol. 7, no. 7, pp. 773–778, 2004.
- [160] E. Roth, R. Hall, T. Daniel, and S. Sponberg, “Integration of parallel mechanosensory and visual pathways resolved through sensory conflict,” *Proc Nat Acad Sci U S A*, vol. 113, pp. 12 832–12 837, 2016.
- [161] S. Ohmae, J. Kunimatsu, and M. Tanaka, “Cerebellar roles in self-timing for sub- and supra-second intervals,” *J Neurophysiol*, vol. 37, no. 13, pp. 3511–3522, 2017.
- [162] C. J. Chang and M. Jazayeri, “An integral role for timing in interception,” *bioRxiv*, 2017.
- [163] D. Narain, E. D. Remington, C. I. De Zeeuw, and M. Jazayeri, “A cerebellar mechanism for learning prior distributions of time intervals,” *Nature Commun*, vol. 9, no. 1, p. 469, 2018.
- [164] A. Schurger, “Specific relationship between the shape of the readiness potential, subjective decision time, and waiting time predicted by an accumulator model with temporally autocorrelated input noise,” *eNeuro*, pp. ENEURO–0302, 2018.
- [165] H. Geyer, A. Seyfarth, and R. Blickhan, “Compliant leg behaviour explains

BIBLIOGRAPHY

- basic dynamics of walking and running,” *Proc R Soc Lond B Biol Sci*, vol. 273, no. 1603, pp. 2861–2867, 2006.
- [166] H. Merchant, O. Perez, W. Zarco, and J. Gamez, “Interval tuning in the primate medial premotor cortex as a general timing mechanism,” *J Neurosci*, vol. 33(21), pp. 9082–9096, 2013.
- [167] C. E. Bauby and A. D. Kuo, “Active control of lateral balance in human walking,” *J Biomech*, vol. 33, no. 11, pp. 1433–1440, 2000.
- [168] D. Logan, T. Kiemel, and J. Jeka, “Using a system identification approach to investigate subtask control during human locomotion,” *Front Comput Neurosci*, vol. 10, no. 146, 2017.
- [169] J. M. Finley, A. J. Bastian, and J. S. Gottschall, “Learning to be economical: the energy cost of walking tracks motor adaptation,” *J Physiol*, vol. 591, no. 4, pp. 1081–1095, 2013.
- [170] J. Ahn and N. Hogan, “Walking is not like reaching: evidence from periodic mechanical perturbations,” *PLoS One*, vol. 7, no. 3, p. e31767, 2012.
- [171] I. Uyanik, M. M. Ankarali, N. J. Cowan, O. Morgul, and U. Saranlı, “Toward data-driven models of legged locomotion using harmonic transfer functions,” in *Int Conf on Advanced Robotics*, 2015.
- [172] S. N. Simic, S. Sastry, K. H. Johansson, and J. Lygeros, “Hybrid limit cycles

BIBLIOGRAPHY

and hybrid Poincaré-Bendixson,” *IFAC Proc Vol*, vol. 35, no. 1, pp. 197–202, 2002.

- [173] E. R. Westervelt, J. W. Grizzle, C. Chevallereau, J. H. Choi, and B. Morris, *Feedback Control of Dynamic Bipedal Robot Locomotion*. CRC press, 2007, vol. 28.

CURRICULUM VITAE FOR Ph.D. CANDIDATES

The Johns Hopkins University School of Medicine

Robert W. Nickl

Last Updated: March 22, 2018

EDUCATIONAL HISTORY

| | | | |
|----------------|------|----------------------------|----------------------------------|
| Ph.D. expected | 2018 | Biomedical Engineering | Johns Hopkins School of Medicine |
| | | Mentor: Noah J. Cowan, PhD | |
| B.S.E.E. | 2006 | Electrical Engineering | University of Pittsburgh |
| Minor | | Bioengineering | |
| B.A. | 2006 | German | |

OTHER PROFESSIONAL EXPERIENCE

Extracurricular Training

| | | |
|------------|--------------------------|---|
| 9-10/2017 | Johns Hopkins University | Bootcamp for Technology Entrepreneurs (Team placed co-1st out of 10 teams in final “shark tank” competition) |
| 11-12/2013 | Stanford University | Introduction to Haptics (Instructor: Prof. Alison Okamura). Admitted by competitive application process to initial run of online course. Awarded certificate of accomplishment. |

Peer Review

Reviewer: IEEE Potentials Magazine, Journal of Neurophysiology
Assistant reviewer: IEEE Transactions on Biomedical Engineering; Journal of Neurophysiology, PLOS One

Employment Prior to Graduate School

| | | | |
|--------------------------------|-----------|---|--|
| Research Assistant | 2003-2006 | Laboratory of Dr. J. Robert Boston, Dept. of Electrical and Computer Engineering | University of Pittsburgh |
| Teaching Assistant / Counselor | 2003 | Teaching Assistant for two courses in mathematics; Supervisor for team project in computer science. | Pennsylvania Governor’s School for the Sciences (Carnegie-Mellon University) |
| Research Assistant | 2002 | Laboratory of Dr. Marlin H. Mickle, Dept. of Electrical and Computer Engineering | University of Pittsburgh |

SCHOLARSHIPS, FELLOWSHIPS, OR OTHER EXTERNAL FUNDING

Link Foundation Fellowship in Simulation and Training (7/1/2017-6/30/2018). Amount: \$29,000. Stipend for final year of PhD studies.

Travel Grant, Graduate Representative Organization (GRO) (Summer 2016). Amount: \$300.

National Science Foundation Graduate Research Fellowship (GRFP) (2006; Tenure completed in 2013), Graduate student stipend for 3 years.

Brackenridge Undergraduate Research Fellow (Summer 2003, Summer 2004). Amount: \$3000 each. Stipend to fund undergraduate summer research at University of Pittsburgh.

Chancellor's Scholarship, University of Pittsburgh (2001-2006). Amount: Full tuition, room, board. Competitive merit-based scholarship awarded to incoming University of Pittsburgh freshmen.

ACADEMIC AND OTHER HONORS

2006 Graduation Department of Electrical and Computer Engineering, University of
summa Pittsburgh
cum laude

2006 Graduation Department of German, University of Pittsburgh
summa
cum laude

2000 Pennsylvania Governor's School for the Sciences (Carnegie-Mellon University
and PA Dept. of Education)

1998 Eagle Scout, Boy Scouts of America

Honor Societies: Phi Beta Kappa, Tau Beta Pi, Eta Kappa Nu

PUBLICATIONS (PEER REVIEWED)

Nickl RW, Ankarali MM, Cowan NJ. Human rhythmic arm movements involve complementary spatial- and timing-based control. *Manuscript submitted for publication.*

Nickl RW. The medial premotor cortex as a bridge from internal timekeeping to action. *J Neurosci* 37(37), 8860-8862, 2017.

Madhav MS and **Nickl RW**. Mimicry or scrutiny? Striking a partnership between engineering design and biological research. *IEEE Potentials*, March/April 2015. (*Co-first authors)

Campbell BR and **Nickl RW**. The Impact of STEM Enrichment Opportunities on Secondary School Students. 4th First Year Engineering Experience (FYEE) Conference. August 9-10, 2012, Pittsburgh, PA

Shin HC, Jia X, **Nickl R**, Geocadin RG, and Thakor NV (2008). A Subband-based Information Measure of EEG During Brain Injury and Recovery After Cardiac Arrest. *IEEE Trans Biomed Eng* 55(8): 1985-90.

Jia X, Koenig MA, **Nickl R**, Zhen G, Thakor NV, and Geocadin RG. (2008) Early Electrophysiologic Markers Predict Functional Outcome Associated with Temperature Manipulation after Cardiac Arrest in Rats. *Crit Care Med* 36(6) 1909-1916.

POSTERS AND ABSTRACT PRESENTATIONS

Nickl RW, Ankarali MM, and Cowan NJ. Complementary roles of spatial- and timing-based control during rhythmic arm movements. Neuroscience Meeting Planner. Washington, DC: Society for Neuroscience, 2017.

Nickl RW, and Cowan NJ. Proportional—integral control in paddle juggling. Omega Psi Cognitive Science Society regional conference. Baltimore, MD. April 1, 2017.

Nickl RW, and Cowan NJ. Proportional—integral control in paddle juggling. In *Dynamic Walking* 2016.

Samson EW, **Nickl RW**, Ankarali MM, and Cowan NJ. “Time” as a sensorimotor control problem: performance limits of human auditory-motor entrainment. Neuroscience Meeting Planner. Chicago, IL: Society for Neuroscience, 2015.

Nickl RW, Ankarali MM, and Cowan NJ. Sensory Weighting in a Rhythmic Ball Bouncing Task. In *Dynamic Walking* 2015.

Nickl RW, Izawa J, Shadmehr R. Cost of motor commands in the Parkinsonian brain. Program No. 354.7. 2009 Neuroscience Meeting Planner. Chicago, IL: Society for Neuroscience, 2009.

Nickl RW, Izawa J, Shadmehr R. Motor costs in the healthy and Parkinsonian brains. Program No. 379.2. 2008 Neuroscience Meeting Planner. Washington, DC: Society for Neuroscience, 2008.

Jia X, Koenig MA, Zhen G, **Nickl R**, Thakor NV, Geocadin RG. Unnormalized Quantitative EEG predicts benefit of therapeutic hypothermia after Cardiac Arrest within Rats. International Society for Heart Research 2008 North American Section Meeting. June 17-20, 2008. Cincinnati, OH.

Koenig MA, Jia X, **Nickl R**, Thakor NV, Geocadin RG. Intraventricular Injection of Orexin-A Elicits Earlier Arousal in Rats after Cardiac Arrest. 37th Critical Care Congress 2008. Critical Care Medicine annual meeting. Feb 2-6, 2008. Honolulu, HI.

Jia X, Koenig MA, **Nickl R**, Zhen G, Wang Y, Thakor NV, and Geocadin RG. Early Electrophysiologic Markers of Functional Outcome After Cardiac Arrest with Temperature Manipulation in Rats. 37th Critical Care Congress. Critical Care Medicine Annual Meeting. Feb 2-6, 2008. Honolulu, HI.

Jia X, Koenig MA, **Nickl R**, Zhen G, Wang Y, Hanley DF, Thakor NV, Geocadin RG.
Electrophysiologic Monitoring Of Neurological Recovery with Temperature Manipulation After
Cardiac Arrest in Rats. American Heart Association 2007 Annual Meeting. Nov 3-7, 2007.
Orlando, FL.

SERVICE AND LEADERSHIP

Teaching (Johns Hopkins University)

Locomotion in Mechanical and Biological Systems Lab (Fall 2012 – pres.)

- Lead mentor or co-mentor of 8 undergraduate students, including 2 semester projects for research credit.
- Accomplishments of lead-mentored undergraduate students include:
 - Sophomore awardee of small project grant from Johns Hopkins Robotics Club (Spring 2018).
 - Honorable mention honoree for NSF Graduate Research Fellowship Program (2016)
 - First author and poster presenter at Society for Neuroscience Annual Meeting (2015)

EN.580.456: Introduction to Rehabilitation Engineering

- Role: Guest lecturer, “Telerehabilitation and rehabilitation robotics”
 - Dates: 9/10/2015; 11/29/2016; 11/28/2017. Originated and developed majority of materials for lecture (duration 90 min).
- Role: Judge, final project presentations
 - Dates: 12/3/2015; 12/7/2017

EN.580.457: Rehabilitation Engineering Design Lab (Spring 2016 – Spring 2018)

- Role: Judge for team project presentations
 - Dates: 4/28/2016; 3/9/2017; 3/6/2018

EN.530.343 Design and Analysis of Dynamical Systems.

- Role: Guest lecturer, Discrete-time dynamical system analysis and identification (overview and case study). Originated lecture materials (duration ~35 min)
- Date: 5/3/2017

Laboratory for Computational Sensing and Robotics (LCSR) skill workshop

- Role: Led workshop on Linux operating system basics and shell scripting. Originated lecture materials (duration ~45 min)
- Date: 1/24/2017

EN.580.491/691 Learning Theory

- Role: Teaching Assistant
- Date: Spring semester 2010

EN.580.111: Biomedical Engineering Modeling & Design

- Role: Teaching Assistant
- Date: Fall semester 2009

Leadership Positions

2014-2015 Co-Director of Careers, BME EDGE

- Co-organized Graduate Networking and Career Fair at Johns Hopkins School of Medicine (with Johns Hopkins Graduate Student Association and Postdoctoral Association).
- Organized satellite event at Homewood Career Fair to showcase graduate student research to exhibitors (with Johns Hopkins University Career Center).

2013-2014 Co-Director of Professional Development, BME EDGE

- Co-organized Entrepreneurship Week (with Medical Engineering Perspectives and Innovation Factory)
- Co-organized Professional Skills Day (with Johns Hopkins University Career Center and Professional Development Office).

IEEE University of Pittsburgh Chapter

- 2005-2006: Branch Mentor
- 2004-2005: Chairman
- 2003-2004: Promotions Chair

Tau Beta Pi, PA Lambda Chapter, University of Pittsburgh

- 2004-2006: President

Eta Kappa Nu, Beta Delta Chapter, University of Pittsburgh

- 2004-2005: Corresponding Secretary

Outreach and Other Service

Laboratory Safety Captain and Member of Laboratory Safety Captain Committee, Locomotion in Mechanical and Biological Systems Laboratory and Dept. of Mechanical Engineering, Johns Hopkins University.

2014 - 2016 : **Judge, Johns Hopkins Robo Challenge (various events)**

2013 - pres.: **Various laboratory and research demonstrations** (campus tours, incoming and prospective students, industry representatives, Research Experience for Undergraduates (REU) students).

2013-2016: **Volunteer mentor, SABES** (NSF afterschool STEM program for Baltimore area children from underrepresented backgrounds)

2011-2012: **Volunteer, PGSS Campaign, Inc.** (Alumni association and science education advocacy group for Pennsylvania Governor's School for the Sciences)

- Roles: Alumni surveying and data mining; Grant writing